MONTANA
Department of Transportation
Research

USE OF FIBER-REINFORCED POLYMER COMPOSITES FOR BRIDGE REPAIRS IN MONTANA

FHWA/MT-26-001/10337

Final Report

March 2026

prepared for

THE STATE OF MONTANA DEPARTMENT OF TRANSPORTATION

in cooperation with

THE U.S. DEPARTMENT OF TRANSPORTATION
FEDERAL HIGHWAY ADMINISTRATION

March 2026

prepared by

Emtiaz Ahmed, PhD Graduate Research Assistant

Kirsten Matteson, PhD Associate Professor

Michael Berry, PhD Professor

Montana State University
Bozeman, Montana

TECHNICAL REPORT DOCUMENTATION PAGE

1. Report No. FHWA/MT-26-001/10337	**2. Government Accession No.**	**3. Recipient's Catalog No.**
4. Title and Subtitle Use Of Fiber-Reinforced Polymer Composites for Bridge Repairs in Montana		**5. Report Date** March 2026
7. Author(s) Emtiaz Ahmed, Ph.D https://orcid.org/0009-0005-4411-0011 Kirsten Matteson, PhD https://orcid.org/0000-0001-9367-6867 Michael Berry, PhD https://orcid.org/0000-0003-2134-9335		**6. Performing Organization Code** **8. Performing Organization Report No.**
9. Performing Organization Name and Address Montana State University PO Box 172470 Bozeman, MT 59717-2470		**10. Work Unit No.** **11. Contract or Grant No.** MDT Project # 10337
12. Sponsoring Agency Name and Address Research Program Montana Department of Transportation (SPR) 2701 Prospect Avenue PO Box 201001		**13. Type of Report and Period Covered** Final Report (January 2023-March 2026) **14. Sponsoring Agency Code** 5401

15. Supplementary Notes

Conducted in cooperation with the U.S. Department of Transportation, Federal Highway Administration. This report can be found at https://doi.org/10.21949/1529573

Recommend Citation: Ahmed, E., Matteson, K.,& Berry, M. (2026). Use Of Fiber-Reinforced Polymer Composites for Bridge Repairs in Montana (FHWA-MT-26-001/10337). Montana Department of Transportation. https://doi.org/10.21949/1529573

16. **Abstract:** Montana's timber bridge inventory includes over 600 state and county owned bridges, many more than 80 years old and showing visible deterioration. Traditional girder repair methods, such as steel hangers and timber or steel sister girders, are heavy, labor-intensive, and often lack well-documented performance verification. Fiber-reinforced polymer (FRP) composites offer a lightweight, corrosion-resistant alternative with strong potential for timber bridge rehabilitation, yet their application to timber bridges remains relatively underexplored, particularly at full scale and under field conditions. This report investigates the use of pultruded FRP composites to repair and strengthen deteriorated timber bridge girders to restore capacity and extend service life. Full-scale laboratory testing was conducted on 22 salvaged Douglas-fir/Larch beams from bridges across Montana. Beams were categorized as control, repaired (with pre-existing or induced splits and cracks), or strengthened (intact), and retrofitted using carbon–glass hybrid strips, glass FRP channels, or a combination of both. The channel–strip configuration showed the most robust performance, increasing moment capacity significantly compared to control specimens, while strip-only repairs also improved performance, particularly for moderately damaged beams. To validate the laboratory findings, selected FRP repair techniques were implemented on two in-service timber bridges near Toston, Montana. Installation was completed rapidly using standard tools, demonstrating the constructability of the repair systems under field conditions. A seven-month follow-up inspection indicated no visible deterioration or issues. Overall, this work provides a validated, field-tested approach for rehabilitating timber bridge girders using pultruded FRP composites, offering transportation agencies a practical strategy to extend the service life of aging timber infrastructure.

Key Words	**18. Distribution Statement**
Fiber Reinforced Polymer (FRP) Composites, Timber Bridge Rehabilitation, Timber Girder Repair/Strengthening, Field Implementation	No restrictions.

19. Security Classif. (of this report)	**20. Security Classif. (of this page)**	**21. No. of Pages**	**22. Price**
Unclassified	Unclassified	178	

Form DOT F 1700.7 (8-72) Reproduction of completed page authorized

Disclaimer Statement

Alternative Format Statement

USE OF FIBER-REINFORCED POLYMER COMPOSITES FOR BRIDGE REPAIRS IN MONTANA

Final Report

Prepared By:
Emtiaz Ahmed, PhD
Graduate Research Assistant,

Kirsten Matteson, PhD
Associate Professor,

and
Michael Berry, PhD
Professor

Civil Engineering Department
College of Engineering
Montana State University – Bozeman

Prepared for the
MONTANA DEPARTMENT OF TRANSPORTATION
in cooperation with the
U.S. DEPARTMENT OF TRANSPORTATION
FEDERAL HIGHWAY ADMINISTRATION

February, 2026

Disclaimer Statement:

This document is disseminated under the sponsorship of the Montana Department of Transportation (MDT) and the United States Department of Transportation (USDOT) in the interest of information exchange. The State of Montana and the United States assume no liability for the use or misuse of its contents.

The contents of this document reflect the views of the authors, who are solely responsible for the facts and accuracy of the data presented herein. The contents do not necessarily reflect the views or official policies of MDT or the USDOT.

The State of Montana and the United States do not endorse products of manufacturers.

This document does not constitute a standard, specification, policy or regulation.

Alternative Format Statement:

Alternative accessible formats of this document will be provided on request. Persons who need an alternative format should contact the Office of Civil Rights, Department of Transportation, 2701 Prospect Avenue, PO Box 201001, Helena, MT 59620. Telephone 406-444-5416 or Montana Relay Service at 711.

Acknowledgements:

The authors would like to acknowledge the financial support for this project provided by the Montana Department of Transportation (MDT). The authors would also like to recognize and thank the MDT Research Section and the technical panel for their participation in this project.

Table of Contents

List of Figures

List of Tables

1. INTRODUCTION

1.1 Background

New methodologies are needed to repair and strengthen aging and failing transportation infrastructure. The use of fiber-reinforced polymer (FRP) composites as a construction and repair material for bridges in the United States has gained popularity since the early 1970s [1]. The Federal Highway Administration (FHWA) and the National Science Foundation (NSF) increased funding for research on FRP materials for infrastructure applications in the late 1980s after observing the growing acceptance of advanced composite materials in various fields (e.g., sporting goods and aerospace industries) [2]. Since then, increased research and development have led to the introduction of FRP materials being used in pedestrian and vehicular bridges. FRPs offer several advantages over conventional building materials, such as high strength-to-weight ratios, increased durability and corrosion resistance, and being more environmentally friendly in terms of embodied energy [3, 4]. Additionally, the application processes require less installation time, resulting in minimal road closures. Research also suggests that a bridge can remain functional during the repair process, as traffic loading does not affect the strength of the FRP bond [5, 6]. As a result of this initial research and the known benefits of this material, several state departments of transportation (DOTs) have started investigating the use of FRPs as a bridge repair method in recent years.

1.2 Motivation

Over the past three decades, FRP has been used to strengthen bridges in the U.S. However, this methodology is still relatively new, and the application methods, specifications, and design criteria are still evolving. Several state DOTs have recently explored the use of FRPs to strengthen and repair/replace structural elements on bridges. They have documented their own design criteria and specifications to meet their unique requirements.

Timber bridge beams have significant potential for FRP repair, as timber bridges are the largest critical findings category. In Montana alone, there are over 600 timber bridges owned by the state and counties, many of which were built several decades ago and are now showing signs of deterioration due to age, environmental exposure, and increased traffic demand. There is limited information on timber beam repair with FRP. Additionally, the solution must be lightweight, safe, and easy to install for the maintenance crew.

To close this gap, this project explored various repair and strengthening techniques using pultruded FRP sections for Montana's bridges, focusing on full-scale testing of salvaged timber beams originally used in bridges from the 1950s and 1960s. An implementation phase followed, and selected repair techniques were applied to two in-service timber bridges in Montana. This research is crucial to fully understand the benefits of using FRP on timber bridge beams, ultimately contributing to improved performance and extended lifespans of Montana's bridge infrastructure.

1.3 Objectives

This research aims to improve the understanding of using FRP for repairing and strengthening timber structures, with a specific focus on bridge rehabilitation. The approach includes comprehensive literature review, experimental testing, and field implementation. The key objectives of this research are as follows:

- Conduct a thorough review of FRP applications in timber and RC bridge repair/strengthening, focusing on surface preparation, application techniques, and performance in extreme environments to guide experimental design.
- Design and conduct experimental tests to assess the performance of different repair and strengthening techniques applied to salvaged timber beams, including detailed analysis of materials, test setup, and FRP application methods.
- Implement the selected FRP repair techniques on two in-service timber bridges and document the process to guide future applications.

1.4 Organization

A literature review of previous research is included in Chapter 2, covering FRP application techniques such as external wrapping, NSM systems, and pultruded sections, repair and strengthening of reinforced concrete and timber bridge elements, and mechanical fastener design for connecting FRP to structural members. Chapter 3 describes the experimental program, including timber beam damage assessment, selected FRP materials, repair and strengthening techniques, and test setup. Chapter 4 presents test results for flexural- and shear-controlled beams, comparing the performance of control, repair, and strengthened configurations. Chapter 5 presents the field implementation of FRP repairs on two in-service timber bridges in Montana, including installation procedures, equipment, site conditions, and results from a post-implementation inspection. Chapter 6 summarizes conclusions and key findings from the experimental testing and field implementation.

2. LITERATURE REVIEW

This chapter reviews various application techniques for fiber-reinforced polymer (FRP), including external wrapping, near-surface mounted (NSM) systems, laminates, FRP strips, and anchoring systems. It also examines the use of FRP for repairing reinforced concrete and timber bridge elements, with particular focus on beams, piles or columns, and pile caps. An extensive search of the MDT bridge database was conducted to identify bridges that have undergone FRP repairs and to evaluate their inspection status. The chapter further explores the use of pultruded FRP sections for strengthening timber elements. The review also includes research on the mechanical connection between FRP and structural elements, emphasizing the required fastener number, spacing, and patterns to ensure reliable load transfer and structural performance.

2.1 FRP application techniques

There are several techniques available for applying FRP to structural elements, such as external wrapping, Near Surface Mounted (NSM) bars, FRP laminates, and mechanically fastened FRP strips. Each of these techniques has its own benefits and shortcomings. A brief overview of the techniques and some research performed with these methods is included in the following sub-sections.

2.1.1 External wrapping

External wrapping with epoxy resin is one of the most common methods of using FRP for strengthening and repairing. There are three main processes of applying FRP externally for strengthening: wet layup systems, prepreg systems, and precured systems [7, 8]. Among these methods, the wet layup method is most popular because of its easy application process and smaller time requirement [8-10]. The process can be briefly described with the following four steps: 1) prepare the surface of the existing structure, 2) apply the epoxy resin to the surface, 3) place fiber fabrics on the structure surface, and 4) apply the epoxy resin on the fiber fabrics [10]. The process of applying FRP by the wet layup method is further detailed in ACI (American Concrete Institute) 440.2R-17 [11].

2.1.2 Near Surface Mounted (NSM) bars

NSM bars are another form of FRP strengthening and are a comparatively newer technique among the FRP application methods. Aiswarya and Prabhakaran described the NSM technique as cutting a series of shallow channels on concrete or masonry surfaces in the desired direction and then placing reinforcements into the channels after partially filling with epoxy mortar [12]. This technique has been used for strengthening beams [13-15], columns [16], and beam-column connections [17].

2.1.3 Laminates

The method of strengthening existing concrete structures with FRP laminates includes preparing the concrete surface and attaching FRP laminates to the concrete with an epoxy resin system. Significant works using the lamination method have been focused on strengthened beams [18-20] and columns [9, 21].

2.1.4 FRP strips

FRP strips, which are fastened mechanically to the surface of the structure, is another method of using FRP to strengthen/repair deteriorating structures. FRP strips require less installation time compared to other FRP strengthening techniques and do not require skilled labor. FRP strips are commercially available in varied

sizes. Researchers describe the following application process of FRP strips: 1) predrill or mark the fastener location on the FRP strip, 2) clean the surface of the structure, 3) place and clamp the FRP strip on the structure surface, and 4) fasten the FRP strip to the structure with bolts [22, 23]. Selecting bolts is critical while strengthening with FRP strips. Many smaller bolts distribute the loads more evenly than fewer numbers of larger bolts [22]. FRP strips have been used to increase flexural capacity of concrete girders [22, 23] and to improve composite action of timber double caps [24].

2.1.5 Anchorage systems

Debonding is one of the main concerns when applying FRP techniques; however, this risk can be mitigated by providing anchorage. Examples of different anchorage systems are shown in Figure 1 – Figure 4. Kalfat [25] discussed several anchorage systems for different FRP applications techniques including U-wrap, mechanical fastener, nailed metal plates, concrete embedment, and fiber spike anchorage. Figure 1 shows an example U-wrap layout. Pham and Hao [26] showed that applying additional layering in the transverse direction can help mitigate debonding. They also described eliminating stress concentrations and thus improving the strengthening effectiveness and delaying premature debonding. Their researchers used longitudinal FRP for flexural resistance and transverse FRP for resistance to premature debonding. This same strategy was also employed in the past research at MSU previously discussed in the proposal of the current project. Lee mentioned that the angle and number of transverse wraps are two of the key parameters for mitigating longitudinal FRP debonding [27]. This study also showed that multiple 90º U-wraps provide better ductility, whereas 45º U-wraps can maximize overall capacity. Researchers also discussed the FRP spike anchorage (Figure 2), a comparatively newer anchorage system [25, 28]. This anchorage system has two parts: the anchor dowel that is inserted into a predrilled hole, and the fan that is fanned out and epoxied over the external wrapping. This technique is more flexible than U-wrapping, in that it can be easily applied on wide elements such as walls and slabs [25]. Anchorage is required at the ends of FRP NSM bar applications (Figure 3) to prevent slippage of the FRP bar. Anchorage is also necessary for prestress NSM systems to reduce the prestress loss [29]. Anchorage (bolts) is often used at various locations (primarily at the ends, Figure 4) to grip the FRP laminates [8, 30]. Al-Mahaidi and Kalfat presented two types of anchorage systems for FRP laminates to strengthen the web flange interface and combined shear and torsional strengthening [31]. To prevent the brittle failure of structures strengthened with FRP strips, several researchers recommended providing mechanical anchorage at the ends [22, 32].

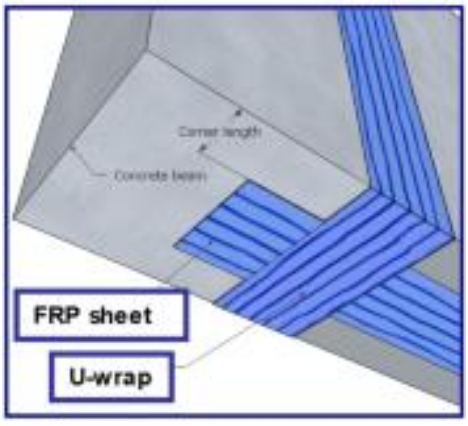

Figure 1: Example U-wrap FRP anchorage system [27]

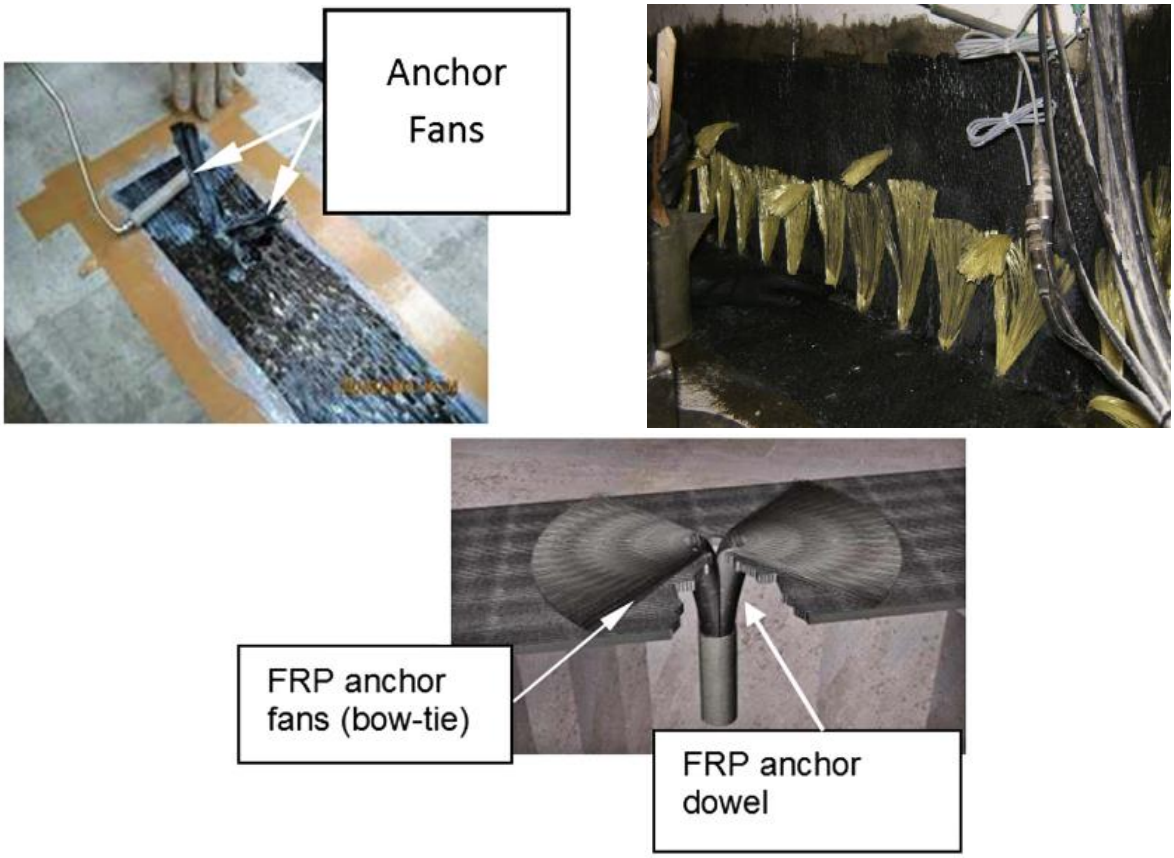

Figure 2: Example FRP spike anchorage systems [25, 28]

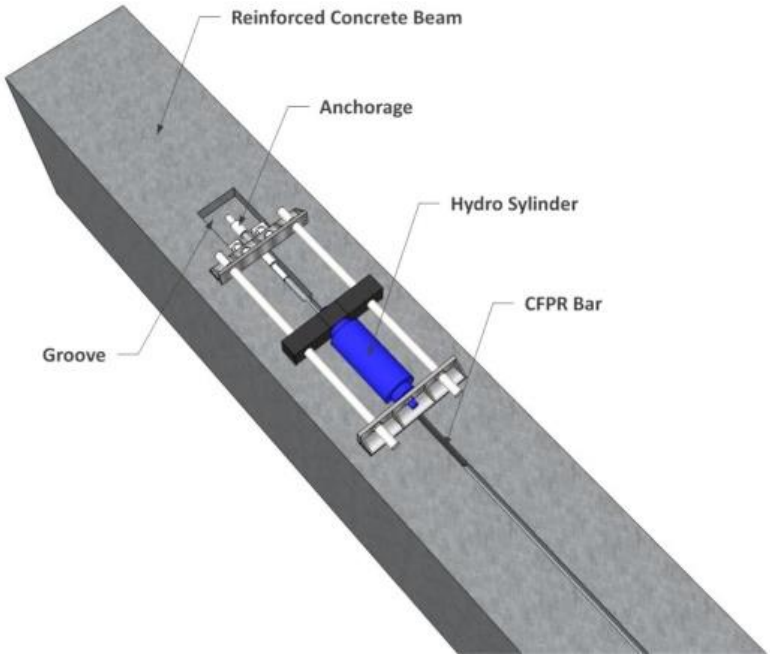

Figure 3: Example anchorage system for NSM bar [29]

Figure 4: Example mechanical anchorage system [25]

2.2 Timber bridge repair with FRP

This section summarizes the application of FRP in timber bridge projects. Specifically, this section discusses the FRP repair of several timber bridge elements including girders, piles, and pile caps.

2.2.1 Girder Applications

This section specifically discusses three timber bridge projects that used FRP strengthening techniques to repair timber girders. Specifically, this section discusses (1) a timber bridge in Washington County, Colorado, (2) a covered wooden bridge in Sins, Switzerland, and (3) a timber railroad bridge in Moorefield, West Virginia. This section also includes an example of a new build bridge with FRP located in Delaware County, Iowa.

2.2.1.1 Timber bridge, Washington County, Colorado

The superstructure of the F-22-V bridge, located in Washington County, Colorado, was rated 4 (Poor Condition, FHWA 1995) in 2019 due to aging and deterioration [33]. The Colorado Department of Transportation (CDOT) sponsored a program to rehabilitate the deteriorated bridge. The three-span, 83-year-old timber bridge is supported by 14 Douglas-Fir girders (Figure 5). The design load used at the time of construction was H15. This program had three major aspects: (1) laboratory testing, (2) field application and finite element model evaluation, and (3) load ratings.

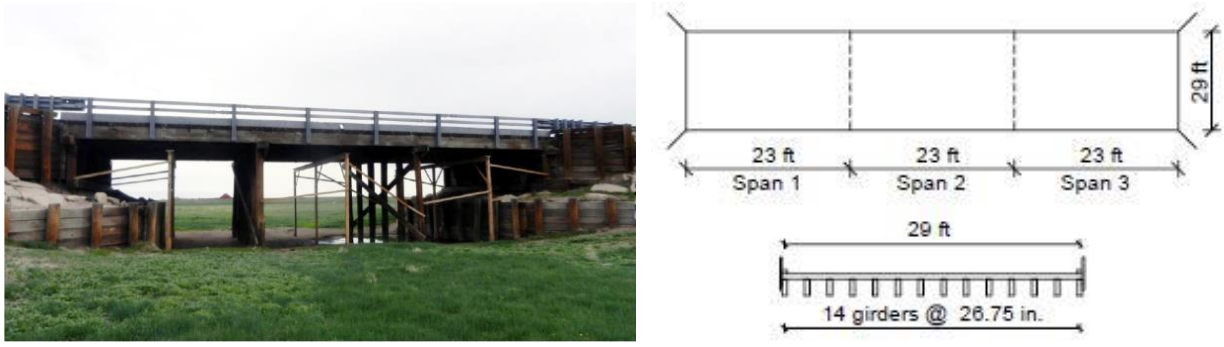

Figure 5: F-22-V bridge, Washington County, Colorado [33]

Three retrofitting techniques were evaluated in the laboratory testing section which included lag bolts, CFRP sheets, and hollow structural section (HSS), shown in Figure 6. The timber girder specimens were obtained from a decommissioned bridge that had similar characteristics to the retrofitted bridge. The girders were scaled down (6 in. x 6.7 in. x 130 in. long) by saw cut to match the testing space and actuator capacity. Each retrofitting technique was tested three times, and the responses of the 12 girders (Table 1) were evaluated.

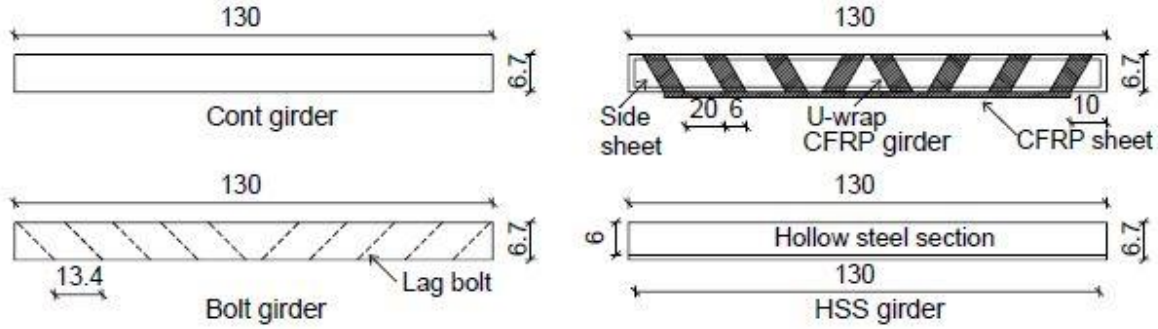

Figure 6: Control and strengthened girder specimens [33]

Table 1: Girder configurations [33]

Girder	Retrofit	Ultimate load (kip)		Modulus of rupture (psi)	
		Individual	Average	Individual	Average
Cont-1	None	9.26	8.72	5,482	5,154
Cont-2	None	8.00		4,728	
Cont-3	None	8.88		5,250	
Bolt-1	Lag bolts	6.68	7.01	3,945	4,143
Bolt-2	Lag bolts	7.06		4,177	
Bolt-3	Lag bolts	7.28		4,307	
CFRP-1	CFRP	9.33	9.55	5,526	5,647
CFRP-2	CFRP	10.07		5,961	
CFRP-3	CFRP	9.24		5,453	
HSS-1	Steel beam	22.41	22.35	13,256	13,223
HSS-2	Steel beam	20.30		12,009	
HSS-3	Steel beam	24.35		14,402	

A unidirectional CFRP sheet with a thickness of 0.013 in. was used for the CFRP strengthening technique. The CFRP sheet has a yield strength of 109 ksi. An epoxy resin consisting of a resin and hardener mixture was used at a mass ratio of 4:1 as the adhesive. The application process of the CFRP sheet to the girders includes cleaning the bottom and the side of the girders with a wet towel and fully drying them before the epoxy application. A single layer of the CFRP sheet (4 in. wide) was attached at the tension phase. U-wrap CFRP sheets (6 in. width) at an angle of 30^o and one more layer of side sheets was applied to prevent premature debonding failure. The retrofitted girders were cured at room temperature for 7 days before testing. Lag bolts (0.75-in-diameter) were used for the bolt-strengthened girders. The bolts were placed at an angle of 45^o in the predrilled hole on the girders, and the extra portion of the bolts was cut off. For the HSS strengthened girders, the 2 in. x 6 in. x 0.25 in. thick HSS sections were precut to 130 in. and predrilled in the middle and near the ends. Then they were attached to timber girders with washers and nuts. The girders underwent a four-point bending test and were loaded at a rate of 0.039 in./min until they failed. The test setup is shown in Figure 7. To monitor the strain, transducers were positioned 0.8 in. from the top and bottom of the girders. Additionally, a digital image correlation (DIC) technique was used to visually track

the damage progression. The capacities of the CFRP and HSS strengthened girders exceeded the control girder's capacity by 9.5% and 156.2%, respectively. However, the bolts initiated local failure, resulting in the bolt-strengthened girder having a 19.6% lower capacity compared to the control girder. The amount of dissipated energy increased in all retrofitted girders.

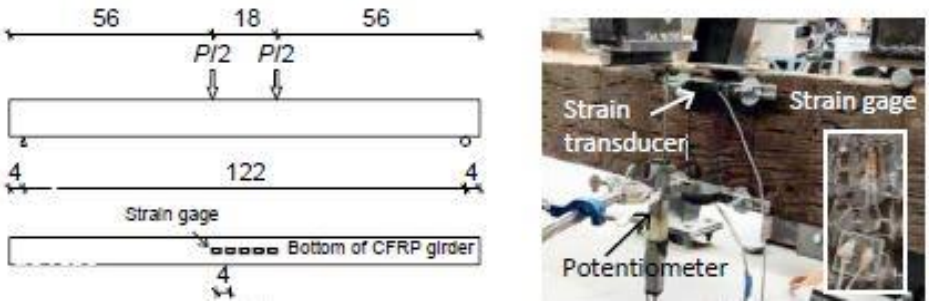

Figure 7: Test setup [33]

The next section of this report focused on strengthening several girders of the F-22-V bridge with CFRP sheets, lag bolts, and HSS (Figure 8). The bridge was load tested with a truck, and its responses were recorded and compared with the responses from three-dimensional finite element models. The strengthening processes were similar to those tested in the lab. Two layers of 4-in. wide unidirectional CFRP sheets were bonded with an epoxy adhesive on the bottom of the girders after cleaning and drying the girder surface. CFRP U-wrap (6 in. wide) was provided at a spacing of 20 inches. The GFRP sheet was also bonded to the sides of the girders to prevent premature debonding. ASTM A500 Grade C HSS beams (12 in. x 8 in. x 5/16 in.) were mechanically fastened with the timber at both ends and midspan using threaded rods. ASTM A354 Grade BC threaded bolts were embedded through 45o predrilled holes with an impact wrench. A Type 3 legal truck was used for the load testing, and there were two scenarios: a) unloaded truck (28 kips), and b) loaded truck (60 kips). The truckload was applied to a location near the exterior girder (the distance between the inside curb face and the rear axle outside tire was 25.4 in.) where the maximum bending moment would be generated. LVDTs were placed underneath the girders to monitor the girders' downward deflections.

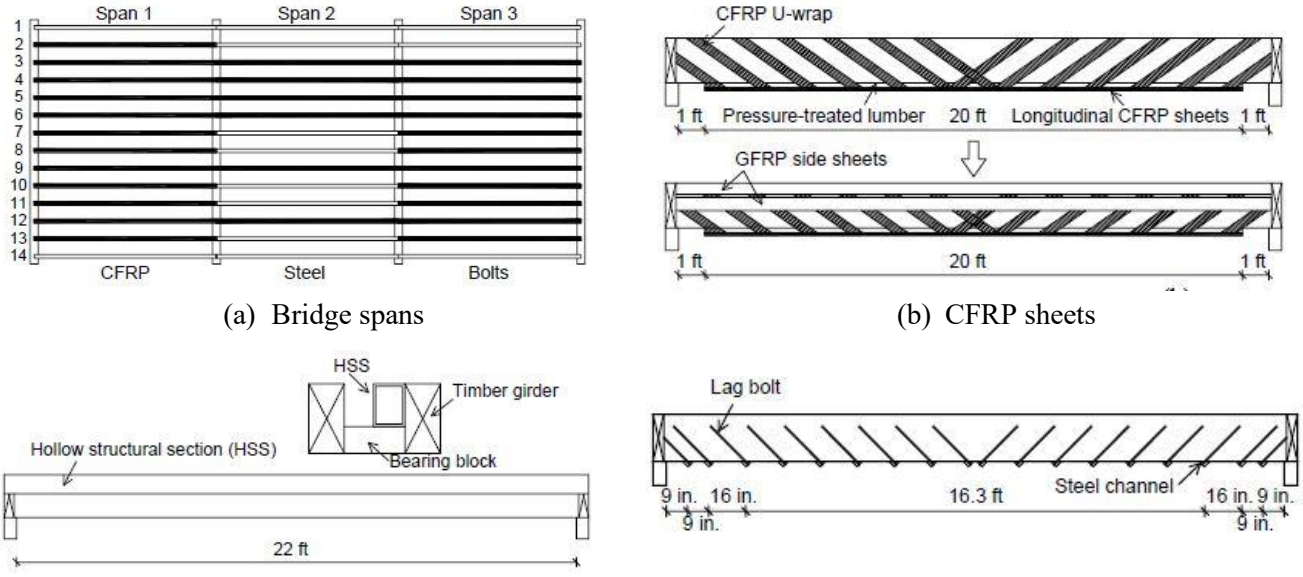

(a) Bridge spans (b) CFRP sheets

(c) HSS (d) Lag bolts

Figure 8: Bridge strengthening [33]

Three-dimensional finite element models were constructed using ANSYS to represent the F-22-V bridge with and without strengthening (Figure 9). In this analysis, the timber was modeled using eight-node structural solid elements (SOLID185). The transverse bracings of the bridge superstructure, the steel strips connected with lag bolts, the HSS beams, the unidirectional CFRP sheets, and the pressure-treated lumber strips were simplified using spar elements (LINK180). Properties of timber (Table 2) and CFRP (Table 3) from several previous studies were used to validate the model.

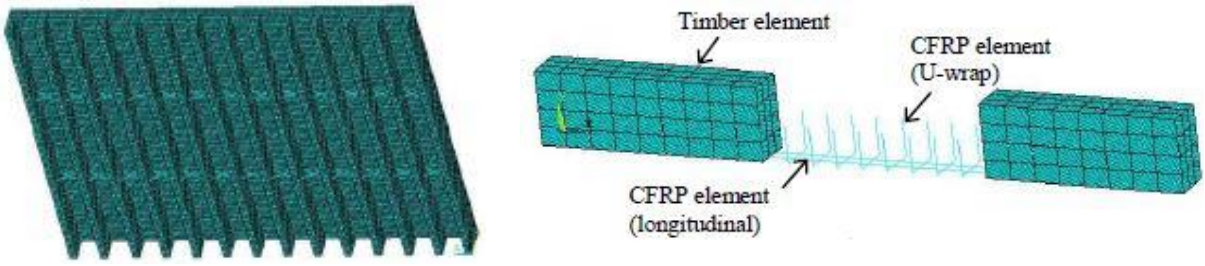

(a) Full-scale bridge model. (b) Girder model.

Figure 9: Model development [33]

Table 2: Properties of timber girders for model validation [33]

Reference	Dimension			Material properties						
	Width (in.)	Depth (in.)	Length (ft)	E_L (ksi)	E_T (ksi)	E_R (ksi)	G_{LT} (ksi)	G_{TR} (ksi)	G_{LR} (ksi)	MOR (ksi)
Gentile	4	12	14.1	1,100	55	75	86	7.7	70.6	2.87
Yang	3	12	19.7	1,560	78	106	122	10.9	99.9	4.48
Rescalvo	3	6	4.3	1,740	86	118	135	12.2	111	4.32
Nziengui	2.3	7	13.3	2,850	142	193	222	19.9	182	N/A*
Halicka	5.5	8	11.2	1,190	60	81	93	8.4	76	N/A**

Gentile = Gentile et al. (2002); Yang = Yang et al. (2016); Rescalvo = Rescalvo et al. (2017); Nziengui = Nziengui et al. (2019); Halicka = Halicka and Slosarz (2021)
*: test was ceased at a load of 4.59 kN
**: average test capacity of 19.8 kips was given

Table 3: Properties of CFRP for model validation

Reference	t_f (in.)	f_{fu} (ksi)	ε_{fu} (%)	E_f (ksi)	v
Rescalvo et al. (2017)	0.047	320	1.22	26,110	0.3
Halicka and Slosarz (2021)	0.047	410	1.35	24,700	0.3

t_f = thickness; f_{fu} = tensile strength; ε_{fu} = rupture strain; E_f = elastic modulus; v = Poisson's ratio

Several key findings were obtained. The increased magnitude of the truckload resulted in greater dispersion in girder deflections and discrepancies between measured and predicted responses due to load placement above the girders. The probability of exceeding deflection limits per AASHTO standards was significantly reduced after strengthening the bridge. Among the three methods, the stiffening efficiency of the HSS option was higher at the system level while the use of CFRP was most efficient at the member level. The computational model's predicted live load distribution factors closely matched the measured factors, suggesting the use of the approach proposed by Fanous et al. (2011) as an alternative to AASHTO distribution methods [34].

The final portion of this project focused on the load ratings of two timber bridges retrofitted with HSS. Finite element models were formulated and validated under 17 live load specifications from the manual of a transportation agency and proposed a mechanics-based rating approach. The repair significantly improves girder capacity and timber allowable stress, reducing failure probability by up to 99.2% and emphasizing the importance of steel beam configuration and placement for enhancing repair system efficacy. No additional details are discussed here, as they are outside of the FRP application scope of the current project.

2.2.1.2 Covered wooden bridge, Sins, Switzerland

A covered wooden bridge near Sins, Switzerland, constructed in 1807, was initially designed for horse-drawn vehicles [35]. The bridge's western side was supported by arches strengthened with suspended and trussed members. The supporting structure on the eastern side consists of suspended and trussed members with interlocking tensioning transoms. The cross beams were constructed by placing two solid oak beams on top of each other. The lower beams were 14.6 inches (37 cm) deep and 11.8 inches (30 cm) wide; the upper beams were 11.8 inches (30 cm) deep and 11.8 inches (30 cm) wide. Twenty-ton vehicles were permitted for the bridge.

In 1992, the bridge required repairs. The Swiss Federal Laboratories for Materials Testing and Research (EMPA) worked on strengthening the beams using carbon fiber reinforced epoxy strips. They used two

types of strengthening to reinforce the crossbeams: 0.04 inch (1 mm) thick, high-modulus M46J fibers carbon FRP (CFRP) strips, and 0.04 inch (1 mm) thick, high-strength T700 fibers CFRP strips. The M46J strips had a width of 9.8 inches (250 mm) at the top and 7.9 inches (200 mm) at the bottom, while the T700 strips were 11.8 inches (300 mm) wide at the top and 7.9 inches (200 mm) wide at the bottom. The properties of the strengthening materials are shown in Table 4.

Table 4: Properties of the CFRPs used in strengthening the Sins bridge, Switzerland [35]

Property	Strip type no.				
	1	2	3	4	5
Fibre type	66% T 300 34% E-glass	Carbon T 300	Carbon	Carbon T 700	Carbon M 46 J
Fibre volume fraction [%]	–	70	51	50	70
Longitudinal strength [MPa]	960	2000	1900	2100	2600
Longitudinal elastic modulus [GPa]	80	147.5	129	130	305
Strain at failure [%]	1.15	1.36	1.47	1.62	0.85
Density [g/ccm]	–	1.58	1.46	–	–

Prior to application of the strengthening technique, the surface was prepared with a portable system. Strain measurement devices were installed in selected crossbeams for post monitoring. Pulse infrared thermography was also installed to observe the bonding between the structure and the CFRP strips. Figure 10 shows pictures of the strengthened girder.

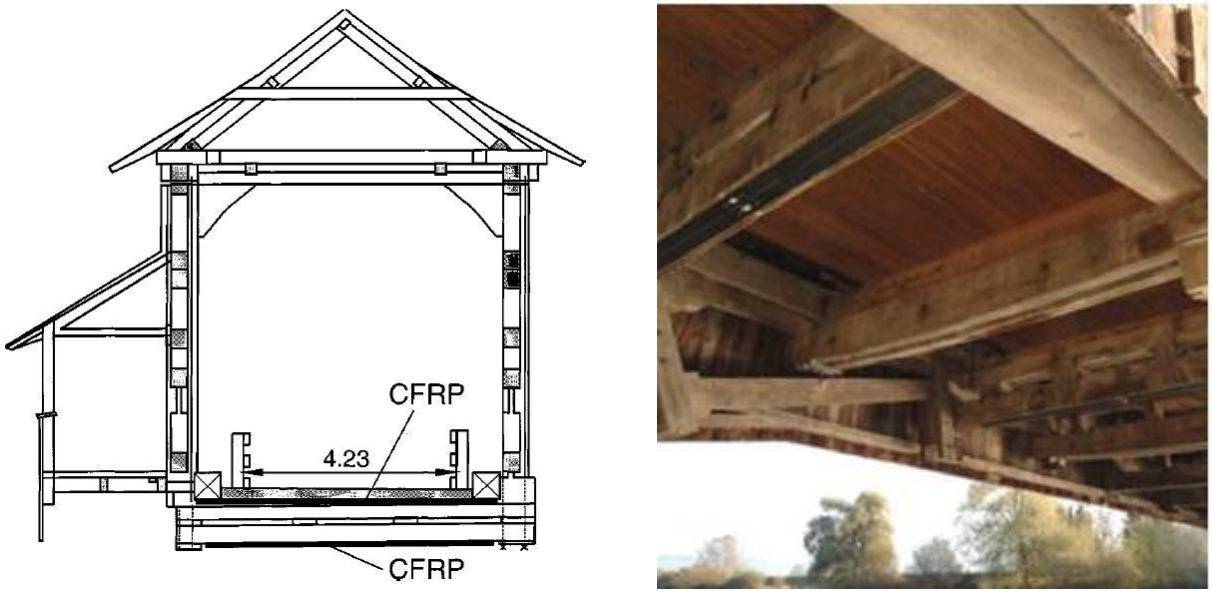

Figure 10: Strengthened girder in Sins bridge, Switzerland [35, 36]

The performance of the Sins bridge was satisfactory as of the year 2000. No significant damage was observed. Figure 11 depicts a photo of post monitoring.

Figure 11: Post monitoring of Sins bridge, Switzerland [36]

2.2.1.3 Timber Railroad bridge, Moorefield, West Virginia

West Virginia University worked on load testing and rehabilitating two 50+ year old open deck timber railroad bridges located on the South Branch Valley Railroad (SBVR), Moorefield, WV [37]. The bridge consists of seven spans on eight pile bents. Each span length is approximately 12 ft (3.6 m) center to center of the supports and contains two main chords. The chords are supported by pile bents which consist of one pile cap and four piles. Figure 12 shows a photograph of one of the bridges.

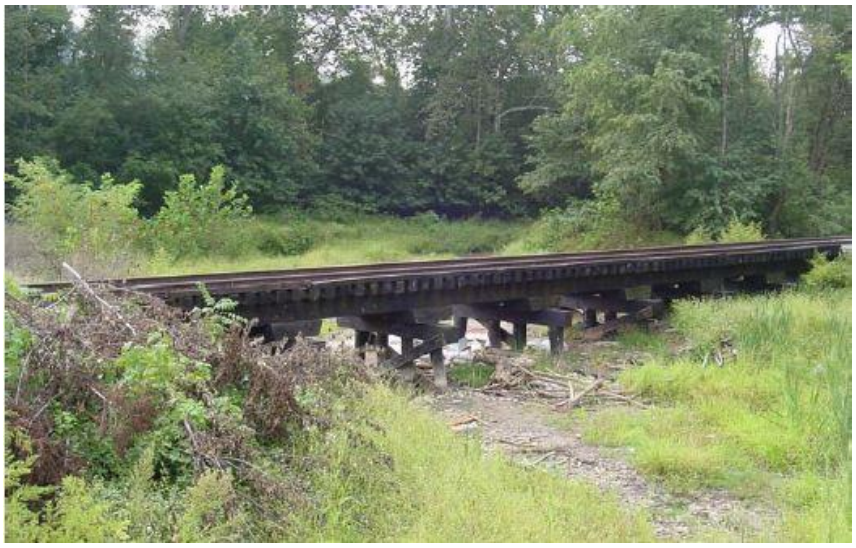

Figure 12: Photograph of timber railroad bridge in Moorefield, West Virginia [37]

The rehabilitation process of the bridges involved repairing the piles and pile caps with Glass FRP (GFRP) composite wraps, in combination with phenolic formaldehyde adhesives. To verify the strength and bonding capabilities of the repaired structure, a series of lab tests were performed before applying this in the field. Four full-scale, 8 inch x 16 inch x 12 ft (20.3 cm x 40.6 cm x 3.6 m) timber stringers were tested following the four-point bending configuration. Two control specimens were tested for failure in bending (Figure 13) and a second pair for shear failure (Figure 14). The specimens were then repaired in the maximum moment

and maximum shear areas, respectively, using GFRP materials and phenolic-based adhesives. All the repaired beams were then retested in four-point bending.

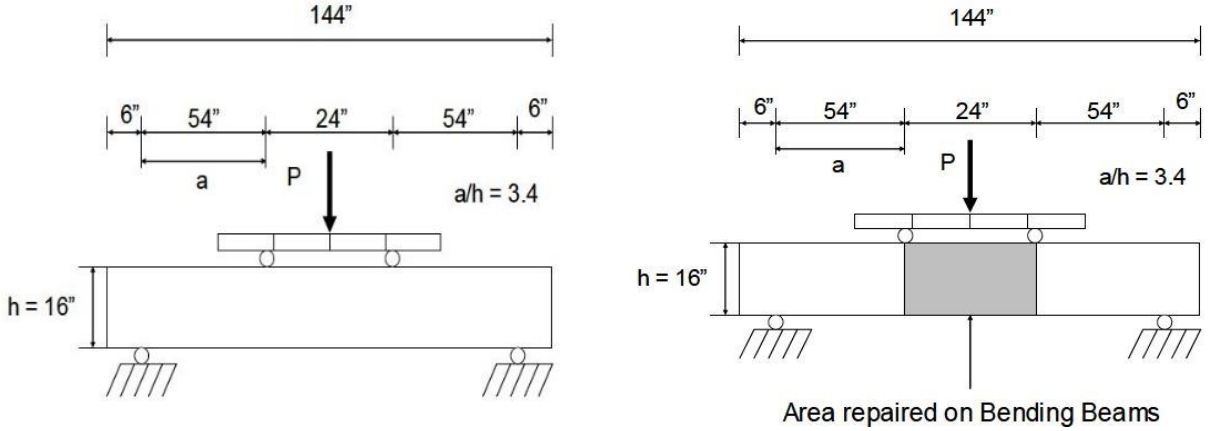

(a) Before repair (b) After repair

Figure 13: Bending test setup for the railroad bridge project, Moorefield, West Virginia [37]

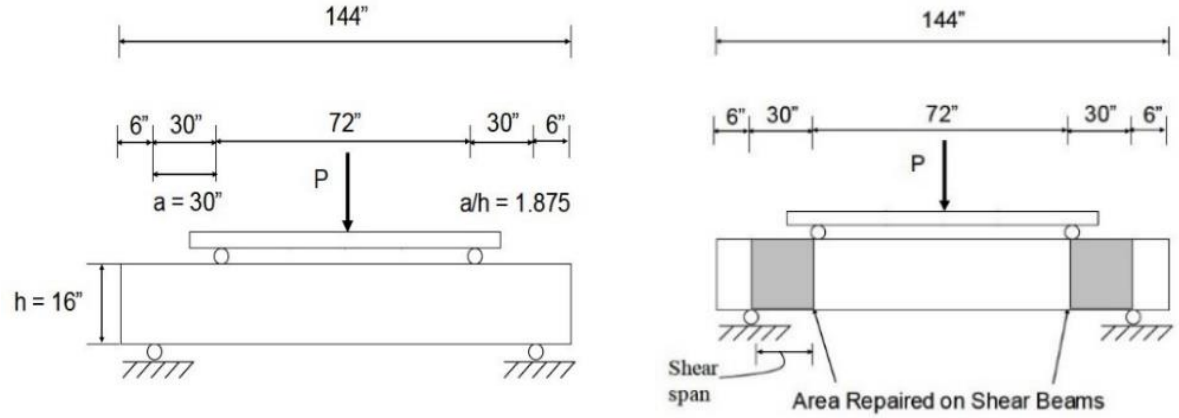

(a) Before repair (b) After repair

Figure 14: Shear test setup for the railroad bridge project, Moorefield, West Virginia [37]

These laboratory tests validated the effectiveness of phenolic adhesives in combination with GFRP when applied to creosote-treated beams and evaluated the load-carrying capacity of the repaired beams. The repaired beams performed well and regained reasonable shear and bending strength.

The field load testing was done before and after repairing the pile cap, stringer, and pile. The phenolic resin and formaldehyde hardener ratio used was 5:1 by weight. The pile cap and stringer repairing process involved removal of decayed material, rounding and sanding, priming the structure surface, coating of GFRP fabric with resin, and applying the GFRP wrap. The pile repairing process followed similar steps including removal of decayed material, construction of molding, placing of bulk filler, sanding, GFRP fabric application, applying pressure, and sealing. Load testing was done using a General Electric 80-ton locomotive (Figure 15) provided by SBVR. Tests were done using the locomotive at three different speeds (5, 10, and 15 mph) and dynamic responses were recorded. Static loading was performed by positioning the test locomotive at a specific place.

Figure 15: 80-TON SBVR Locomotive used for the Moorefield bridge field testing, West Virginia [37]

The GFRP composite with phenolic formaldehyde adhesives performed well. The GFRP composite material and timber bonds were adequate and overall, the strain distribution within the substructure of a timber railroad bridge was improved.

2.2.1.4 Example of a new build bridge with FRP (Delaware County Bridge), Iowa

Delaware County, Iowa, constructed a bridge comprised of FRP-reinforced glued-laminated timber girders and a transverse glued-laminated timber deck [38]. This system was chosen because it was economical, durable, and required less installation time. This bridge had a simple 64-ft (19.5 m) span with two lanes, and was 29 ft 7.5 inch (9 m) wide. It is located in Lime Creek, east of Ryan, Iowa. The superstructure is comprised of eight glued-laminated timber girders strengthened with FRP plates, and a transverse glued laminated timber deck (cross-section shown in Figure 16). The substructure consists of timber piles, timber abutment caps, and a timber plank abutment back wall.

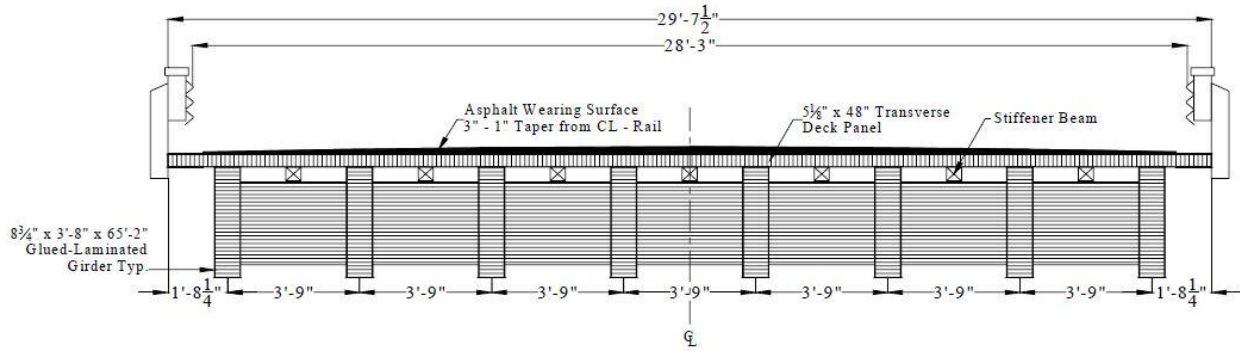

Figure 16: Cross-section of the Delaware county bridge [38]

After a preliminary inspection at the Alamco Wood Products, Inc. plant, Albert Lea, MN, the girders were planed, drilled, routed, and prepared for FRP applications. The FRP plates were 0.50 inch (12.7 mm) thick. There were no complications during the application of FRP. Standard deck panels were used for this bridge

construction. After construction and prior to testing, another inspection was made. One girder (G1) bumped while handling, and there was a delamination of the first foot (30.5 cm) of the FRP plate. No significant defects were found during the inspection. The decks were well seated, but there were gaps in several locations between adjacent decks ranging between 0.25 inch (6.35 mm) to 0.5 inch (12.7 mm). The asphalt-wearing surface was also inspected before load testing. Some key points from the inspection include that no moisture-blocking membrane was installed between the glued-laminated deck, the wearing surface did not cover the entire deck, and small transverse cracks formed at each panel joint and at the abutments.

The bridge was instrumented (Figure 17) and the structural performance was evaluated through a series of loading tests conducted over a three-year period. Girder and deck deflections were accurately measured at critical locations using an Optim Megadec data acquisition system. Transducers were installed underside of all the girders and deck panel to measure the global and localized deflections, respectively.

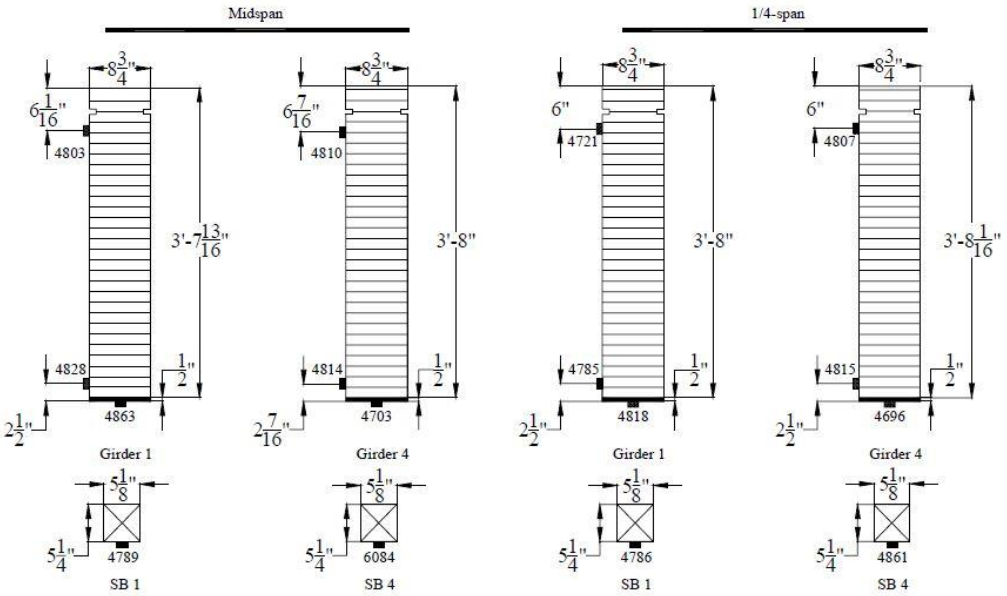

Figure 17: Position of the transducers on the Delaware county bridge girders [38]

The Delaware County Secondary Roads Department provided a fully loaded (51,560 lb.) tandem axle dump truck which was used for load testing. Four load cases (Figure 18) were investigated and two sets for each case were performed.

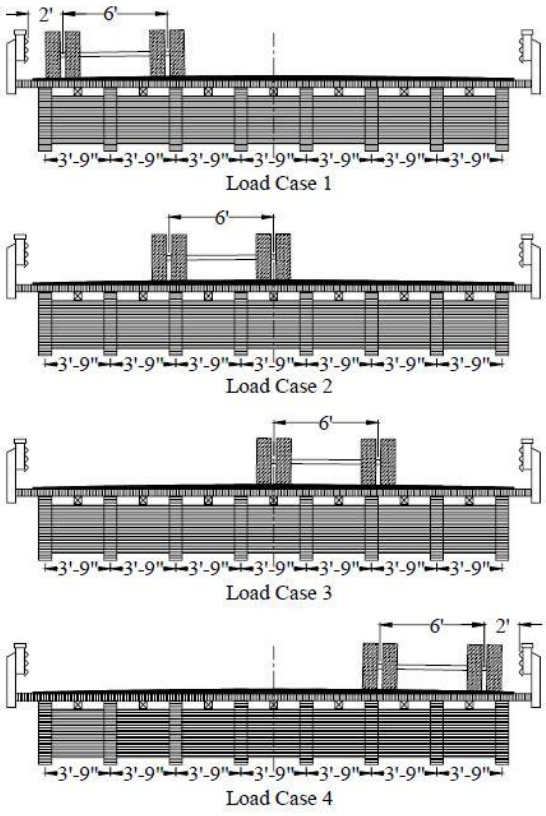

Figure 18: Load cases for Delaware county bridge [38]

The overall bridge performance was adequate and within the limit for static load testing. The global deflection of the bridge was within AASHTO 1996 limits. All girders performed as intended and the girder ends showed good bearing during the tests. Girder G1, which was damaged prior to testing, showed no noticeable stiffness reduction. As of a 2006 (2 years after construction) inspection, all the girders were in good condition and the FRP/timber bonds showed no signs of deterioration.

2.2.2 Pile Applications

This section briefly discusses FRP repair of biologically deteriorated timber piles and an evaluation of FRP repaired wood piles subjected to a bending test.

2.2.2.1 Deteriorated timber pile rehabilitation, Louisiana

The Southern Plains Transportation Center sponsored a program to evaluate the capacity of deteriorated timber piles strengthened with FRP under concentric and eccentric loads with different deterioration configurations [39]. The timber piles of Louisiana bridges are experiencing biological degradation in the wet-dry zone. An example of a biologically degraded pile is shown in Figure 19. Since complete replacement of the piles is not economically feasible, in situ repair of the piles with FRP was explored, which eliminates the need for shoring the superstructure and road closure.

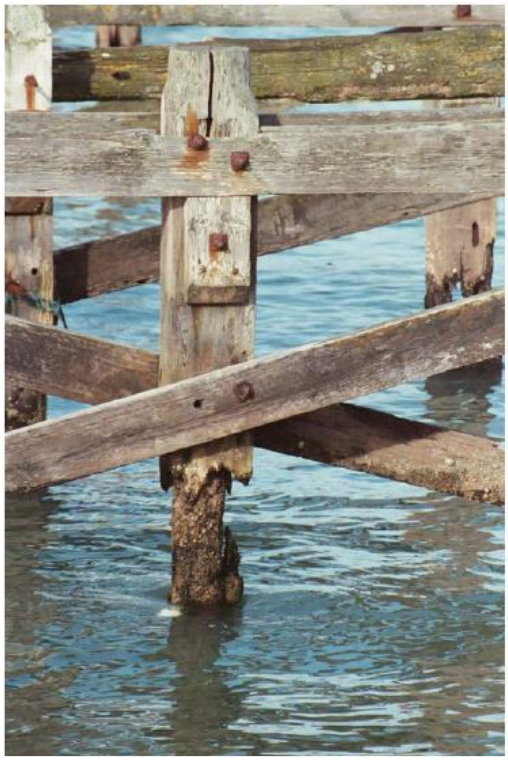

Figure 19: Biologically degraded pile [39]

In this study, the observed damaged condition in the wet-dry zone was mimicked. An hourglass shaped reduction of the cross-sectional area was implemented using a table saw and five different damage types were introduced for the test program (Figure 20). The test program consists of a total 42 monotonic tests, with 21 tests on concentrically loaded piles and 21 tests on eccentrically loaded piles (Figure 21). A self-contained loading frame was used to test all piles, with a capacity of 400 kips. Linear variable differential transducers (LVDTs) were used at the top and bottom of the piles to measure the axial deformation. The aim of these tests was to assess the efficiency of different repair techniques in restoring the original capacity of the piles. Three different commercially available repair techniques from three different companies (Denso North America, Simpson Strong Tie, and Pilemedic) were investigated in this study (Figure 22).

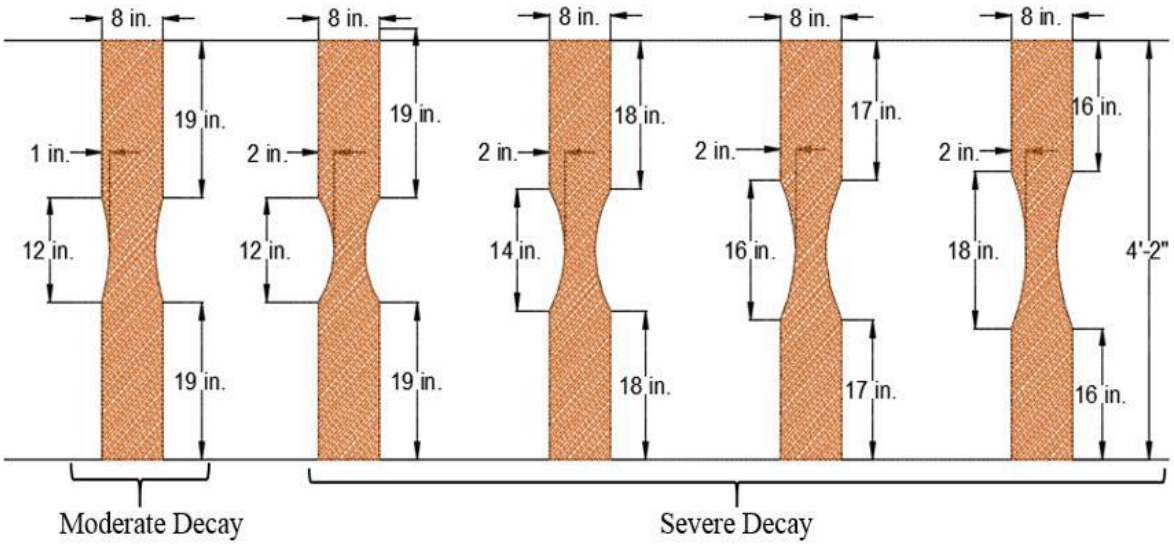

Figure 20: Configuration of induced damage piles for Louisiana test program [39]

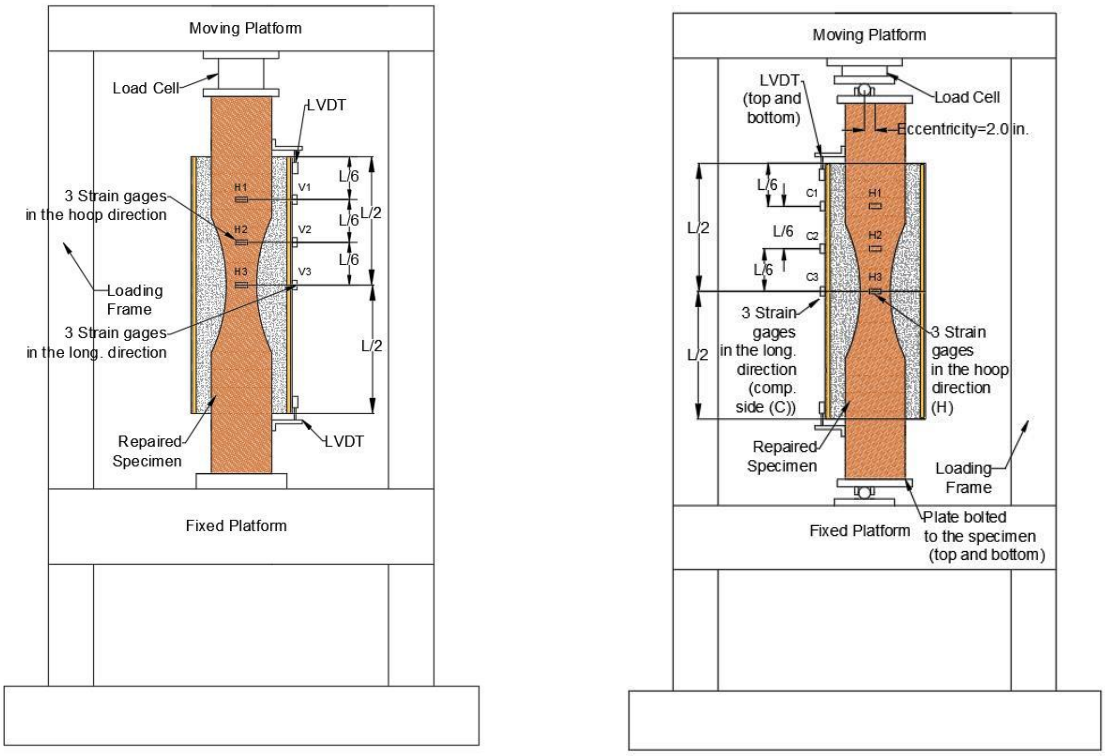

(a) Concentrically loaded (b) Eccentrically loaded

Figure 21: Test setup for Louisiana test program [39]

(a) Denso (b) Simpson Strong Tie (c) Pilemedic

Figure 22: Repaired timber piles for Louisiana test program [39]

All repaired piles exhibited higher concentric load carrying capacities than the damaged piles and surpassed the axial capacity of the reference undamaged pile. Both the concentric and eccentric load carrying capacities of the damaged piles increased significantly after repairing them with FRP composites, regardless of the repair technique. No slip was observed at the pile-fill interface during the testing. They concluded that all investigated repair techniques are efficient and can be used to restore the capacity of damaged timber piles.

2.2.2.2 FRP repaired wood pile evaluation under bending tests, University of Maine

Wood piles in the marine area deteriorate from marine borers, crustaceans, fungi, and other sources, causing them to lose capacity [40], and therefore require restoration to regain strength. This project focused on repairing pre-damaged wood piles with a specially developed FRP composite shield and investigated their responses in bending.

Southern yellow pine class B wood piles were selected as test specimens (details listed in Table 5). The damaged piles were achieved by reducing approximately 62% of the diameter of the cross-section over a segment of 35.4 inches (900 mm) from the center span toward the pile tip. Then unidirectional woven E-glass fabric with an underwater curing epoxy adhesive, named Hydrobond 500 were selected as the reinforcing materials for the two repaired piles. Two types of load-transfer mechanisms were investigated between the wood pile and the FRP composite: (1) cement-based structural grout between the FRP wrap and the wood pile and (2) steel shear connectors with an expanding polyurethane chemical grout between the wood and the FRP wrap.

Table 5: Wood pile system configurations [40]

System	Wood pile	FRP Composite shield	Grout	Shear connectors	Pile length, L (m)	Span length, L_s (m)
Intact reference (IW)	Intact	N.A.	N.A.	No	9.14	8.84
Damaged control (DW)	Pre-damaged	N.A.	N.A.	No	9.14	8.84
Repair system B	Pre-damaged	Yes	Cement-based	No	9.14	8.84
Repair system C	Pre-damaged	Yes	Poly urethane	Yes	9.14	8.84

The specimens were tested under a three-point bending test procedure (Figure 23). Vertical deflections were measured at mid-span, and the two ends of the FRP composite using LVDTs. Horizontal movement between the wood pile and the FRP composite shield was also measured on the top and bottom at the ends of the FRP composite using LVDTs. Moreover, the load deformation response, strain distribution, ultimate bending moment capacity and failure mode were evaluated.

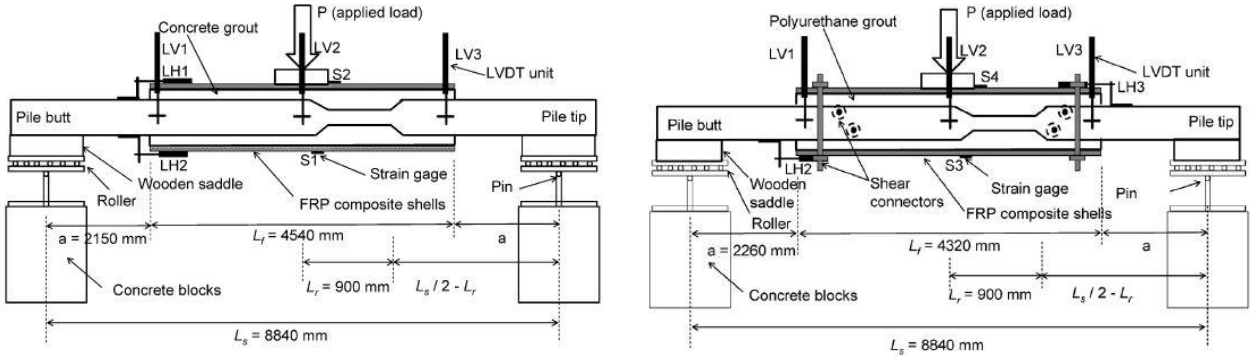

(a) System B (b) System C

Figure 23: Three-point bending test setup for piles [40]

The repaired piles with FRP composite shield and cement-based grout exceeded the bending capacity of the reference wood pile. However, the repair system using the FRP composite shield with steel shear connectors and polyurethane grout did not restore the bending capacity to the capacity of the reference wood pile.

2.2.3 Pile Cap Applications

This section briefly discusses the investigation of the feasibility of a timber double cap with mechanically fastened FRP strips. Most of the railroad timber bridges in Wisconsin are over 50 years old and are experiencing deterioration due to increased traffic loads. One viable solution to address this problem is to enhance the stiffness of the pile cap and enable better load distribution [24]. The Wisconsin Department of Transportation (WisDOT) sponsored an investigation that focused on exploring mechanically fastened fiber

reinforced polymer (MF-FRP) strips fastened to timber with screws to create composite action between two beams. All tests were performed at the Forest Products Laboratory in Madison, WI.

Douglas Fir rough sawn lumber and Douglas Fir creosote treated timber wood specimens were used in this study. The moisture contents of Douglas Fir rough sawn lumber range from 9% to 13% and their grading was Select Structural. The grade of Douglas Fir creosote treated timbers was Grade No. 1. The composite material used in this study was SAFSTRIP manufactured by Strongwell. SAFSTRIP (Figure 24) consists of carbon tows surrounded by layers of glass fiber mats, impregnated with a vinyl ester resin, and has dimensions of 4 inches (102 mm) wide and 0.13 inch (3.2 mm) thick. The design tensile strength and modulus are 92.9 ksi and 9020 ksi, respectively.

Figure 24: SAFSTRIP [24]

In this study, several test series were conducted, including deep beams over short spans and full-scale specimens, to determine if and how FRP strips improved the member's performance. Tests were conducted over various widths of beams and lengths of spans to investigate how the geometry affected the strengthening's ability to create composite action. The testing for this project was divided into two phases. For phase 1, beams were tested over two span lengths (126 inches and 60 inches) and there were two series of testing beams: width series and depth series. Four strengthening configurations were explored for the width series beams (Table 6) and five strengthening configurations were tested for depth series beams (Table 7). This phase's objectives were (1) to investigate the influence of beam width and depth on the composite behavior of MF-FRP and (2) to assess the impact of the distance between supports. The test setup for Phase 1 was a typical three-point bending test for wood specimens (Figure 25). LVDTs were used to collect deflection data, and strain gauges were utilized on the FRP. Data was collected using LabView.

Table 6: Phase 1 - Width series beam configurations [24]

Beam Width	Beam Depth	Configuration	Description
4" 8" and 12"	4"	Single Beam	A single member
4" 8" and 12"	4"	Stacked Beams	One beam on top of the other – no composite action
4" 8" and 12"	4"	Epoxied Beams	Simulates fully composite section between two members
4" 8" and 12"	4"	FRP X-Braced Beams	FRP fastened to outer surface on either side, achieving some composite action

Table 7: Phase 1 - Depth series beam configurations [24]

Beam Width	Beam Depth	Configuration	Description
4"	14"	Single Beam	A single member
4"	14"	Stacked Beams	One beam on top of the other – no composite action
4"	14"	Epoxied Beams	Simulates fully composite section between two members
4"	14"	FRP V-Braced Beams	FRP fastened to outer surface on either side, achieving some composite action
4"	14"	FRP X-Braced Beams	FRP fastened to outer surface on either side, achieving some composite action

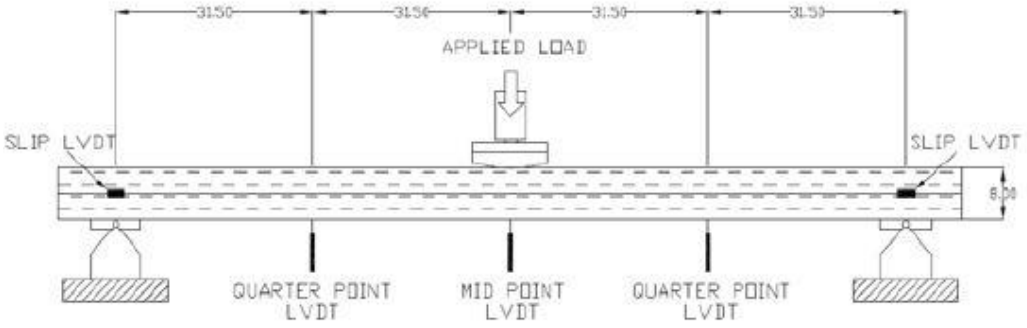

Figure 25: Test setup of Phase 1 [24]

Phase 2 tests were conducted on full-sized specimens provided by Wisconsin & Southern Railroad (WSOR), which were typical of the in-situ condition of a timber railroad bridge. Five supports were used to replicate the support condition of the piles. Static testing was completed on various MF-FRP configurations (Table 8), and then one configuration was subjected to 1 million cycles of dynamic testing. The objectives of this phase were (1) to determine the applicability of the MF-FRP method in continuous deep beams over multiple short spans, (2) to investigate the potential of MF-FRP strips in redistributing loads, and (3) to examine the behavior of the beam and determine whether it acts in accordance with design equations. A custom designed test setup (Figure 26) was used for phase 2 testing, with unique parts designed to fit the existing test area at the Forest Products Lab. Cyclic loading was set at 0.75 cycles per second, and the load varied between approximately 8 kips and 45 kips during each cycle. LVDTs were used to measure deflections, and strain gauges were placed on the FRP. All data was collected using LabView.

Table 8: Phase 2 beam configuration [24]

Specimen Name	Description	Test Load (lbs)
Prescribed Spacing 33" – 30" – 30" – 33"		
NB12-1	Single pile cap	30,000
NB12-2	Single pile cap	30,000
NB12-3	Single pile cap	30,000
NB12-4	Single pile cap	30,000
NB12-2 over NB12-1	Double pile cap	40,000
NB12-3 over NB12-2	Double pile cap	40,000
NB12-3 over NB12-4	Double pile cap	40,000
Worst Spacing 27" – 36" – 36" – 27"		
NB12-3 over NB12-4	Double pile cap	40,000
NB12-2 over NB12-3	Double pile cap	40,000
NB12-1 over NB12-4	Double pile cap	40,000
NB12-1 over NB12-4 FRP	Double pile cap with MF-FRP strips in various configurations	40,000
NB12-2 over NB12-3 FRP	Double pile cap with MF-FRP strips in various configurations	40,000 and 150,000

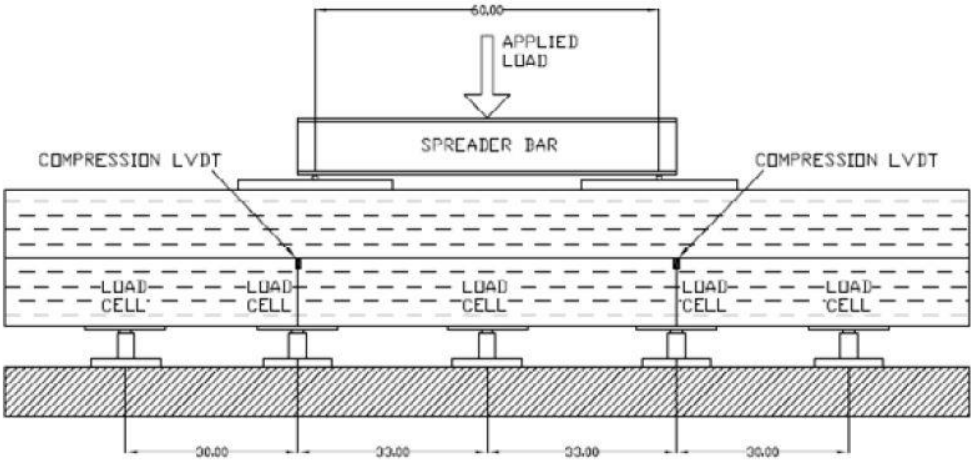

Figure 26: Test setup of Phase 2 [24]

One main finding from this study was that composite action between two timber members can be achieved with mechanically fastened FRP strips, and this method showed great potential for creating composite, stiffer double pile caps. MF-FRP strips also increase the flexural stiffness of timber beams in bending with large span-to-depth ratios. However, MF-FRP strips did not significantly improve load distributions to piles.

2.3 RC bridge repair with FRP

The RC (Reinforced Concrete) bridge repair with FRP section summarizes the application of FRP in RC bridge projects. Specifically, this section discusses the FRP repair of several RC bridge elements including girders, piles/columns, and pier caps.

2.3.1 Girder Applications

This section summarizes three RC bridge girder FRP repair/strengthening including Louisa-Fort Gay bridge, Kentucky, Uphapee Creek bridge, Alabama, and Route 378 Bridge, New York.

2.3.1.1 Retrofit of the Louisa-Fort Gay bridge, Kentucky

The Louisa-Fort Gay is a 12-span continuous bridge structure consisting of composite concrete deck-steel girder span and reinforced concrete middle span and is located in Lawrence County, Kentucky. Flexural cracks (Figure 27) were found in the positive bending regions of the bridge girders because of excess traffic loading that exceeded the legal weight limit specified by the American Association of State and Highway Transportation Officials (AASHTO) [41].

Figure 27: Cracks in Louisa Fort Gay bridge [41]

FHWA and the Kentucky Transportation Cabinet sponsored a program to repair and strengthen the bridge. CFRP laminates were selected as the strengthening material (Figure 28). Before applying the CFRP laminates, surface preparation was performed, including cleaning, and removing loose concrete particles, debris, and other contaminants. The CFRP laminate application process included applying the epoxy on the concrete surface, placing the laminates to the structure surface, pressing the laminates, and removing excess adhesives.

Figure 28: Repaired Louisa Fort Gay bridge girders [41]

For the post monitoring of the bridge performance, crack gauges were installed during the strengthening process. After 3 years of monitoring, no cracks were recorded.

2.3.1.2 Repair of the Uphapee Creek bridge, Alabama

The Uphapee Creek, three span, continuous bridge was identified insufficient to carry modern traffic loads. To strengthen the bridge, the Auburn University Highway Research Center conducted a study that was

sponsored by the Alabama Department of Transportation (ALDOT) and FHWA. The bridge was designed following the H-15 traffic loading, but the minimum design specification required AASHTO HS 20-44 for the bridges carrying heavy traffic loading. Significant flexural cracks were also identified in the positive moment regions of the bridge girders [42].

The Tyfo UC Composite Laminate Strip System from Fyfe Company, LLC was selected as the strengthening material (Table 9). Tyfo TC epoxy was used as the adhesive, primed with Tyfo S Epoxy. The strengthening process included surface preparation, epoxy injection to the cracks, epoxy application to the structure surface, and placing the FRP to the surface (Figure 29). Figure 30 shows the strengthened girders.

Table 9: Tyfo UC composite laminate properties [42]

Property	Nominal Value
Ultimate tensile strength in primary fiber direction	405,000 psi
Ultimate tensile strength 90° to primary fiber direction	0 psi
Tensile Modulus	22.5 x 10^6 psi

Figure 29: Application of FRP strip to the Uphapee Creek bridge girder [42]

Figure 30: FRP-strengthened Uphapee Creek bridge girders [42]

Static and dynamic tests were performed before and after the FRP composite installation. Field live load tests were performed with two identical load test trucks (LC-5 and LC-6, Figure 31) owned and operated by ALDOT. Electrical resistance strain gauges (ERSGs) and deflectometers were used to measure live load deflections. MEGADAC 3415AC high-speed data acquisition system, manufactured by OPTIM Electronics, was employed for data acquisition.

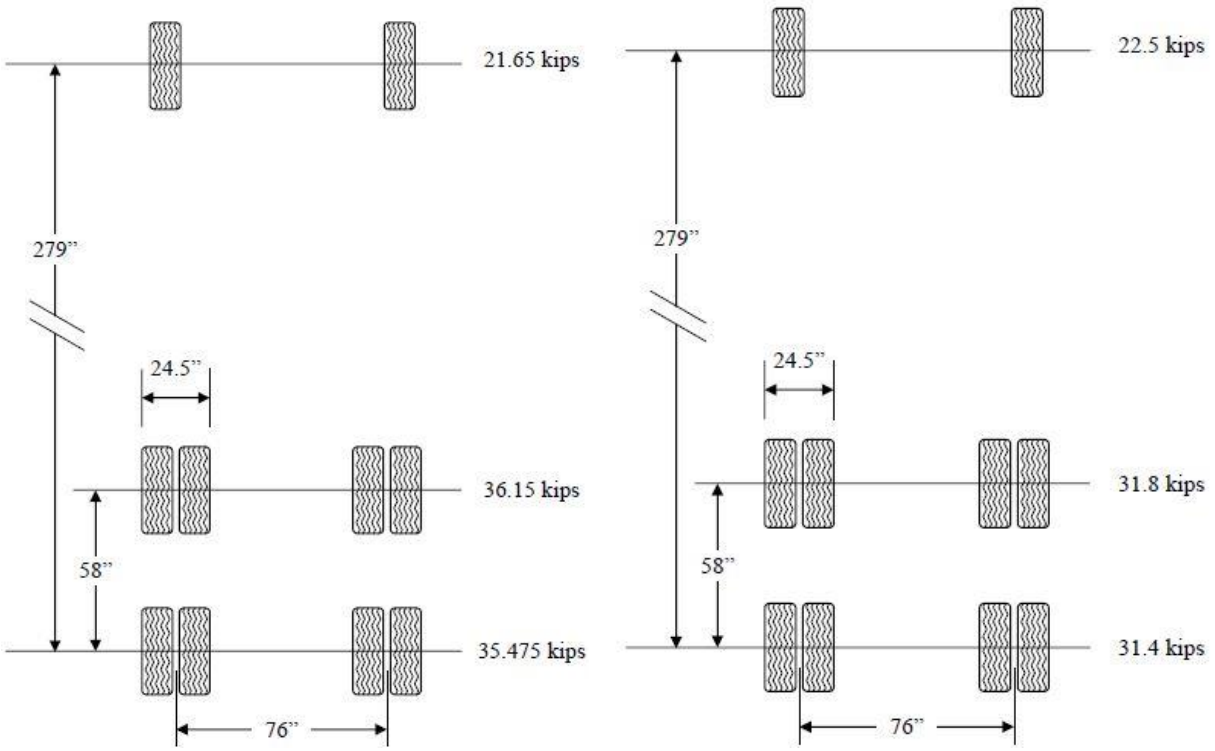

(a) LC-5. (b) LC-6.

Figure 31: Truck configuration for Uphapee Creek bridge field test [42]

In conclusion, the strengthened girders performed as predicted. No major problems were found in post monitoring after 6 months. A tap test was also performed, and no delamination was found in the FRP bond. It was also mentioned that road closures were not required while applying the externally bonded FRP strengthening techniques.

2.3.1.3 Repair of Route 378 Bridge, New York

A 40-ft (12.19 m) long bridge carries State Route 378, located in the City of South Troy, Rensselaer County, New York. During a routine inspection, freeze-thaw cracking, concrete delamination, and efflorescence were found at several locations of the bridge beams [43]. The New York State Department of Transportation (NYSDOT) decided to repair the bridge with FRP laminates. Replark 30 unidirectional carbon fiber was selected as the strengthening material, which was manufactured by Mitsubishi Chemical Corporation in Japan. The surface was cleaned, and the loose concrete was removed. Cement-based grout material was injected into the cracks, and then the surface was smoothed by sandblasting. The laminates were placed on the structure surface after applying epoxy. After drying, the structure was repainted to match the original structure (Figure 32). Load testing was done before and after strengthening the bridge girder with a 44-kip

(196 kN) truck (Figure 33). Conventional strain gauges were used to measure the deflection, which were manufactured by Measurements Group, Raleigh, North Carolina.

Figure 32: FRP-strengthened girder of State Route 378 bridge, New York [43]

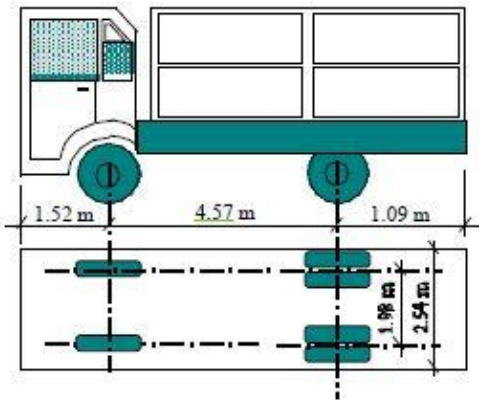

Figure 33: Load truck configuration for field test of State Route 378 bridge, New York [43]

The load distribution to bridge beam was improved with the girder repairing. It was also discussed that the rehabilitation process was cost effective since road closure was minimal.

2.3.2 Pile/Column Applications

This section briefly discusses FRP-repair of corrosion damaged RC bridge columns in Michigan and FRP-repair of corrosion damaged submerged concrete piles of the Friendship trail bridge, Florida.

2.3.2.1 Repair of corrosion damaged columns, Michigan

Chloride contamination has significantly damaged numerous bridge columns in Michigan, such as corrosion of the steel reinforcement and swelling and spalling of the concrete [44]. The Michigan Department of Transportation (MDOT) sponsored a program to investigate the effectiveness of FRP wrap to address the problem. Michigan State University (MSU) conducted several tests to explore freeze-thaw durability of FRP-wrapped specimen subjected to an internal expansive force, the effect of wrapping on the rate of corrosion, the impact resistance of FRP, and the effect of elevated temperature on wraps. MSU fabricated a 4-ply composite Tyfo-S fiber glass/epoxy sheet and a 2-ply Tonen carbon/epoxy sheet which

were used for all lab testing. Lab testing results indicated that freeze-thaw cycles did not significantly impact the compressive strength of glass and carbon fiber, and both fibers effectively slowed down the corrosion rate. Carbon and glass fiber performed well during the impact test. However, the epoxy in the FRP deteriorated when exposed to temperatures exceeding 200°C, resulting in the ineffectiveness of the FRP.

The next phase of the program was the field application of the strengthening technique. Six columns were selected for this program which were located under the I-96 overpass, Lansing, Michigan. The columns had surface spalling and exposed rebar at several locations (Figure 34). The strengthening configurations were: two reference columns, two columns wrapped with two layers of carbon fiber, and two columns wrapped with three layers of glass fiber. Figure 35 shows one of the repaired columns.

Figure 34: Deteriorated column of I-96 overpass bridge, Michigan [44]

Figure 35: Repaired I-96 overpass bridge columns [44]

The repaired columns were monitored twice a month for 10 months. There were some drifts in the post monitoring readings, but no significant problems were found.

2.3.2.2 Corrosion repair of submerged concrete piles of Friendship trail bridge, Florida

High concentrations of chloride ions in seawater causes severe corrosion damage to the submerged concrete piles [45]. Additionally, the wet/dry cycles and high humidity can deteriorate concrete structures rapidly. To address this problem, this project investigated FRP repairing techniques for several corrosion-damaged

underwater concrete piles. The 2.6-mile-long Friendship trail bridge is located in Tampa Bay, Florida, and was selected for the project. Two types of FRP strengthening systems were introduced in the study: 1) Aquawrap, a uni-directional/bi-directional carbon FRP repair system with water-activated urethane resin, and 2) Tyfo SEH-51, a weave, uni-directional glass fabric with Tyfo-S underwater epoxy. A total of eight piles were selected for the study (Table 10). A pressure washer was used to remove all the dust and loose concrete from the pile surface above the water. A quick-setting hydraulic cement was injected into the cracks and any discontinuities. Four piles were wrapped following the wet lay-up process, and the other four piles were wrapped following the prepreg system. A boat was used to wrap the piles above water, and divers wrapped the piles under water, shown in Figure 36. A scaffolding system was also introduced to have easy access to the pile.

Table 10: Pile configuration of Friendship trail bridge project [45]

Pier number	Repair system	Specimen type	Pile name	Instrumentation
Pier 99	None	Control	99-N	Yes
	None	Control	99-S	Yes
Pier 100	Aquawrap®	Carbon 1 + 2 layers[a]	100-N	Yes
		Carbon 1 + 2 layers	100-N*	No
		Glass 2 + 4 layers	100-S*	No
		Glass 2 + 4 layers	100-S	Yes
Pier 101	Tyfo® SEH-51A	Glass 2 + 4 layers	101-N	Yes
	Tyfo Zinc Cathodic Protection	Glass 2 + 4 layers	101-S	Yes

(a) Using a boat (b) Using divers

Figure 36: FRP wrapping of Friendship trail bridge pile [45]

It was concluded that the prepreg system was more convenient than the wet lay-up process. However, the wet lay-up system performed better. Bond tests were also performed after two years of repair. The repaired piles performed as intended during the post-monitoring.

2.3.3 Pile Cap Applications

This section discusses the FRP jacket repair deteriorating pier caps of Silver Spring Cove Bridge, Rhode Island using the vacuum bagging process and the FRP-repair of the Morganza Spillway bridge pile cap located in Louisiana.

2.3.3.1 FRP jackets for deteriorating pier cap of Silver Spring Cove Bridge, Rhode Island

The Rhode Island Department of Transportation sponsored a program to repair the deteriorating RC pier cap of the Salt Pond Road bridge in South Kingstown, Rhode Island. The pier caps showed severe spalling and cracking, and the reinforcements were exposed at several locations [46] (Figure 37). The bridge is located near the ocean, and the constant exposure to contaminated water flowing over the pier caps was identified as the cause of the severe deterioration.

Figure 37: Deteriorated pier cap of Salt Pond Road Bridge [46]

The vacuum-assisted impregnation technique, commonly known as "vacuum bagging" in the aerospace industry, was employed to fabricate a composite jacket for repairing the pier caps and prevent further deterioration. E-glass fiber from the Saint Gobain Company was chosen for the strengthening material. This specific fabric was selected due to its lightweight and high tensile and flexural strength properties. A low-viscosity resin was necessary for this application technique to flow better. Pot life was also critical since this process required time to vacuum. Three epoxy resins were selected: Tyfo S, Sikadur Hex 300, and Sikadur 35. A rotary vane high vacuum pump with a 0.5 horsepower capacity was selected, which ran at a speed of 1725 RPM with a frequency of 60 Hz.

Before field application, Rutgers University in New Jersey performed lab tests on full-scale specimens to ensure the feasibility of the repairing techniques. The testing procedure includes cleaning the concrete surface with a pressure washer to remove all loose debris, applying a thin layer of epoxy resin, impregnating E-glass fiber with resin on top, placing the wet fabric on the structure surface, attaching the vacuum bag, and running it for 4 hours. The lab test went well, and it was concluded that the resin system and vacuum bagging were feasible for the actual application.

The faculty and students at Rutgers University and the University of Rhode Island carried out the field application with the help of professional staff. Scaffolding and surface preparation were complete before the actual application (Figure 38). E-glass fabric with Sikadur Hex 300 resin was selected as the strengthening material for field application. After the concrete surface was completely dry, the FRP composite was placed. The vacuum bagging process (Figure 39) began after 16 hours of placing the FRP.

Figure 38: Scaffolding and safety measures for repairing the Salt Pond Road Bridge [46]

Figure 39: Vacuum bagging system adopted in repairing the Salt Pond Road Bridge [46]

The post-monitoring of the repaired bridge included visual inspection, chloride level tests, and compressive strength tests of the repaired pier cap. The repaired area performed as intended, and the compressive strengths were higher than the design strength.

2.3.3.2 FRP-repair of the Morganza Spillway bridge pile cap, Louisiana

The pile cap of the Morganza Spillway bridge in Louisiana needed repairing, as the previous repair method of patching the damaged area with structural grade high-adhesive material epoxy concrete was ineffective and resulted in delamination (Figure 40) [47]. The Louisiana Department of Transportation and

Development sponsored a program to repair the damaged pile cap and Louisiana State University conducted the project. CFRP was used as the strengthening material, with Young's modulus of 90 million psi. After placing the FRP on the concrete surface, the bent surface was coated with an inorganic polymer coating reinforced with short carbon fiber (Figure 41). The coating formulation, originally developed for use in aircraft structures, was used to prevent deterioration and provide UV-protection, and had self-cleaning properties.

Figure 40: Delamination under the bearing plate of the Morganza Spillway bridge, Louisiana [47]

Figure 41: Repaired pile cap of the Morganza Spillway bridge, Louisiana [47]

No significant problems were found during the two years of monitoring and the repair zone of the pile cap performed as intended.

2.4 MDT bridge repair with FRP

This section briefly discusses the Montana bridge projects in which FRP has already been used to repair and strengthen different bridge elements. According to an extensive search through MDT's bridge inventory database [48], nine reinforced concrete bridges (Table 11) have been repaired in Montana using FRP wrap. The repairs include two girder repairs, six cap repairs, one pile repair, and four column repairs. According to the most recent inspection, the FRP repaired bridges #01044, #01490, #01491, #05868, #05972, and #07011 were in good condition. However, bridge #02096 showed some random delamination in the FRP repair area.

Table 11: FRP-repaired reinforced concrete bridges in Montana

MDT Bridge Number	Construction Year	Location	Repairing Year	Repaired Area	Last Inspection Year	Last Noted Condition
#01044	1965	8M N Clark Canyon Dam, Beaverhead, Butte	2021	Girder, Span 1.	2021	Good
#01490	1979	1.2M S Garrison, Powell, Butte	2003	Top portion of cap, Bent 2 and 3.	2022	Good
#01491	1979	1.2M S Garrison, Powell, Butte	2003	Top portion of cap, Bent 2 and 3.	2022	Good
#02096	1964	0.6M W Butte, Silver Bow, Butte	2020	Cap faces and Column.	2022	Some random delamination at spalls in column.
#05868	1960	16M NE Wisdom, Deer Lodge, Butte	2020	Cap.	2022	No significant defects noted.
#05972	1971	1M N Hobson, Judith Basin, Billings	2021	4 inside girders at abutment 4.	2023	No defects noted.
#06860	1972	Columbia Falls, Flathead, Missoula	-	Column cap.	2022	Good
#06982	1936	Havre- 7th Ave N, Hill, Great Falls	2021	Caps at Bent 15, 16, and 21.	2022	2016 inspection showed some cracks and spalls. Repairs were made.
#07011	1962	Missoula-S Higgins Ave, Missoula	2022	Bent 2, Column 2, full height FRP wrap. Bent 3, Column 2, 3.5 ft (1.1 m) high FRP wrap at the top of the column.	2022	Good

A thorough search of the same database [48], revealed that FRP has been more extensively applied to timber bridges in Montana, with jacket repairs made to piles on 56 bridges. The FRP wrap was applied to piles at various heights as needed. Appendix A presents a detailed summary table of all FRP-repaired timber bridges located in Montana. Most repairs were made between 2020-2021 and were inspected one year later. As of the most recent inspection, no deterioration/damage has been reported for most of the bridges and they were performing as expected.

2.5 Pultruded FRP

The use of FRP for timber girder repair holds significant potential, especially since aging timber bridges are a major concern, and there is limited information available on effective FRP repair techniques for girders. The most common method, external wrapping using wet lay-up, is challenging to apply to timber girders due to bonding and installation complexities. A solution that is lightweight, safer, and easier for

maintenance crews is needed. Following an extensive literature review and consultations with the MDT Technical Panel, it was decided to explore pultruded FRP sections and FRP strips attached with mechanical fasteners to repair and strengthen damaged timber girders and beams. This section discusses two research projects that used pultruded FRP sections to strengthen timber beams, including Beech Wood Beams with Pultruded GFRP Profiles [49] and Wooden Beams Reinforced with Pultruded GFRP Elements [50].

The Beech Wood Beams with Pultruded GFRP Profiles study tested 24 beams, including 20 strengthened with flat, U-shaped, and L-shaped GFRP profiles and four control specimens. The three-point bending tests (Figure 42) revealed significant improvements in the strengthened beams, with an average increase of 61% in modulus of rupture, 59% in flexural rigidity, 79% in ductility, and 209% in energy absorption. The U and L-shaped profiles proved superior to the flat ones, enhancing load capacity and reducing debonding.

Figure 42: Timber beams strengthened with pultruded glass FRP profiles [49]

The Wooden Beams Reinforced with Pultruded GFRP Elements (Figure 43) experiment assessed the stiffness and strength of seven white fir and six chestnut beams reinforced with either H or I-section GFRP elements. The beams were tested using four and three-point bending tests, and results showed that the I-section GFRP strengthening increased flexural stiffness by 188%, with no significant difference between fir and chestnut. The H-section GFRP strengthening resulted in stiffness gains of 83% for fir and 58% for chestnut. This method was also applied in a real-world setting to strengthen a timber floor in Palazzo Collicola, Italy, demonstrating enhanced stiffness and strength.

Figure 43: Fir and chestnut timber beams reinforced with GFRP pultruded elements [50]

These studies provide promising insights into the use of pultruded FRP sections for effective timber girder repair, offering a practical and efficient alternative to traditional methods.

2.6 Fastener design

The study on FRP strips applied to the Vermont bridge, along with the use of different bolts, focused on assessing the effectiveness of a repair method using FRP strips for concrete structures [23]. The goal was to enhance load capacity by externally bonding high-strength FRP strips to concrete beams, leading to an immediate improvement in live load capacity. It evaluated the performance of various screws and bolts, their installation process, patterns, and the connection between the FRP strips and the concrete. A key aspect of the study involved determining the appropriate number of fasteners required to securely attach the FRP strips, ensuring full load transfer and allowing the strips to reach their full tensile capacity. The current study draws inspiration from the fastener requirement methods outlined in this research.

Figure 44: Bolt pattern used in Vermont bridge [23]

2.7 Summary of findings and future direction

Overall, FRP has been successfully implemented in various projects worldwide to strengthen and repair bridge elements. This chapter summarized key FRP application techniques, such as external wrapping, near surface mounted bars, laminates, and FRP strips, used in repairing and strengthening both reinforced concrete and timber structures. Specific examples included FRP-based repairs for girders, piles, and pile caps in bridge applications, with results generally indicating improved structural capacity and durability. Post-inspection results have shown that repaired components maintained good condition over time, supporting the long-term effectiveness of FRP systems. FRP wrap has already been used in Montana to repair reinforced concrete and timber bridges. Several reinforced concrete bridges received FRP repairs on elements including girders, caps, piles, and columns, and follow-up inspections showed good performance, with only one case of minor delamination. Additionally, FRP jackets were applied to timber piles in several bridges, and no significant post-repair damage was reported.

Recent studies have explored the use of pultruded FRP sections to overcome the limitations of conventional FRP wraps in timber girder repairs. Conventional wet lay-up systems are difficult to apply to timber due to

bonding challenges and installation complexity. Pultruded FRP sections, which are lightweight, prefabricated, and easy to install, offer a practical alternative. These studies highlighted the efficiency of pultruded profiles in enhancing timber beam performance in both laboratory and field conditions. For the mechanical connection between FRP and structural member, fastener selection and pattern play a crucial role in load transfer. A study on a Vermont bridge evaluated various bolts and screw patterns used to attach FRP strips to concrete beams. The research emphasized the importance of using sufficient fasteners to develop full tensile capacity of the FRP strips and ensure consistent bond performance. These findings guide fastener design in timber girder applications.

In summary, literature findings suggest that pultruded FRP sections combined with a well-planned fastener pattern offer a highly feasible and effective repair solution for deteriorated timber bridge girders. Compared to conventional wrap systems, pultruded profiles offer greater ease of installation, improved mechanical performance, and better compatibility with timber structures. These insights highlighted the most suitable repair techniques and guided the next phases of this research project.

3. EXPERIMENTAL PROGRAM

As part of this investigation into the rehabilitation of aging timber bridge girders in Montana, salvaged Douglas-Fir/Larch beams from bridges around the state were collected and tested to evaluate the effectiveness of various FRP based retrofitting methods. This chapter provides an overview of the timber beams, FRP materials, repair and strengthening techniques, and experimental procedures utilized in this study. The chapter begins by describing the timber beams and common types of damage observed in the beams, such as end splits and flexural cracking, followed by an introduction to the FRP materials and mechanical fasteners used in the repair and strengthening procedures, including pultruded GFRP channels and carbon glass hybrid FRP strips. Repair strategies were developed based on beam condition and geometry, and installation procedures were carried out both in the field and laboratory to ensure consistent application.

To quantify the performance of these techniques, an experimental program was designed and implemented, focusing on flexural and shear behavior. The test matrix includes undamaged control beams, beams repaired after initial damage, repaired beam with pre-existing damage, and undamaged beams strengthened with FRP prior to testing. Each beam was tested under the same loading conditions to allow direct comparison across configurations. Instrumentation and setup were selected to replicate realistic field conditions while capturing reliable and comparable data that could inform future FRP repair and strengthening applications in Montana.

3.1 Timber beams

This section provides a brief overview of the timber beams used in the study, including their origin, properties, and condition prior to testing. It also outlines the observed damage, the repair techniques adopted, and the FRP installation procedures implemented as part of this investigation.

The timber beams for this investigation were originally salvaged from bridges across the state and were collected from the MDT storage yard in Lewistown, MT. The beams include two common sizes historically used in Montana bridges, 6”x18”x20’ and 8”x18”x26’. The beams (examples shown in Figure 45) are Douglas-fir/Larch (dense No. 1) with allowable bending and shear stresses of 1.55 ksi and 0.085 ksi, from Table 13.5.1A, AASHTO [51], respectively, though some of the beams have lower values because of existing defects. The actual dimensions of the beams and pre-existing (before testing) cracks or splits are documented in Appendix B.

(a) Beam stack prior to testing

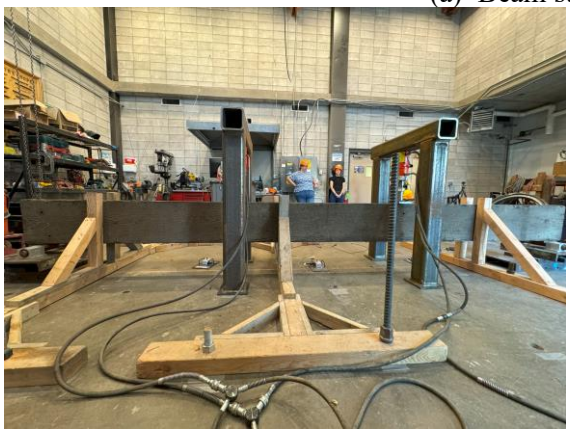

(b) 6”x18”x20’ beam

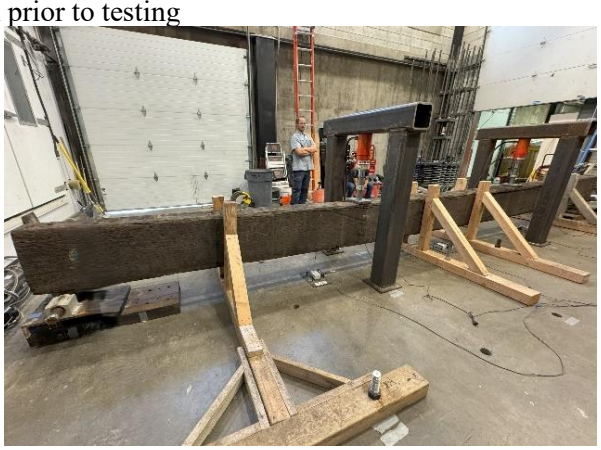

(c) 8”x18”x26’ beam

Figure 45: Example Timber Beams

3.2 Timber beam damage

This subsection provides an overview of the natural imperfections observed in the timber beams prior to testing, as well as the various failure modes documented during the experimental program.

Timber beams often have natural imperfections that can impact their performance. These imperfections, such as knots, checks, waning, and grain deviations, are not classified as damage. However, if they are significant enough, they can contribute to premature failure. Figure 46 shows a couple of examples of natural imperfections.

(a) Checks

(b) Knots

Figure 46: Examples of checks and knots

Timber beams have been observed to exhibit several failure mechanisms in the field and in this research, including tension cracking, shear splitting, compression cracking, and bearing failures. These failure mechanisms are discussed below. However, while all of these mechanisms were observed in this research, this study focused primarily on tension cracking and shear splitting as they are the most common and structurally significant damage types observed in the field.

Tension cracks are commonly formed due to flexure-induced stresses on the tension face of the beam, and extend at an angle through the member, generally along the grain of the wood (as shown in Figure 47). They often begin near mid-span (where tension stresses are greatest) and initiate at imperfections such as knots or checks, or at the site of impact or handling damage.

Figure 47: Example of a tension crack failure

Shear splitting (as observed in Figure 48), result from horizontal shear stresses induced from loading. They run parallel to the top and bottom faces and initiate near the ends of the beam where the shear forces are the greatest. Like in tension failures, these failures often initiate at imperfections in the beam.

Figure 48: Example of a shear split failure

Another failure mechanism of timber beams is longitudinal (parallel to the grain) crushing of the wood in compression zones (as observed in Figure 49). In the beams in this research this occurred at the top mid-span of the beam where the positive moments were the highest.

Figure 49: Example of a compression crushing/cracking failure

Bearing failure (crushing of the wood perpendicular to the grain) is another form of damage that can occur in timber beams. In the beams tested in this research this failure mechanism was observed under the applied loads (Figure 50-a) and at the supports (Figure 50-b).

(a) At load-bearing block (b) At the reaction-bearing plate

Figure 50: Examples of bearing failure

3.3 FRP materials and fasteners

Multiple FRP materials were selected to repair/strengthen the timber beams. This section discusses the FRP materials used in this research, including the Glass FRP channels, the Carbon/Glass hybrid FRP strengthening strips, and the fasteners. An example of the FRP materials attached to a timber beam are shown in Figure 51 and the following subsections discuss each composite in detail.

Figure 51: Example timber beam with FRP materials attached

3.3.1 GFRP channels

The glass FRP channels (Figure 52, Appendix D) used in this study are the EXTREN Series 525, manufactured by Strongwell [52]. These pultruded sections are produced using a premium general-purpose polyester resin formulated with UV inhibitors and flame-retardant additives, providing excellent corrosion resistance and improved fire performance. The inherent corrosion resistance of the resin eliminates the need for routine painting or protective coatings, reducing long-term maintenance requirements and life-cycle costs. In addition, the channels are resistant to impact and do not permanently deform under localized loading, making them non-denting and difficult to break in service. A pigmented resin system combined with a surfacing veil and UV inhibitors limits moisture absorption, prevents warping and fiber bloom, and delays surface fading, contributing to long-term durability in outdoor environments. The EXTREN Series 525 channels are supplied in a standard slate gray color.

The manufacturer-specified longitudinal tensile strength and elastic modulus of the FRP channels are 30 ksi and 2500 ksi, respectively. However, coupon testing conducted as part of this study revealed higher values. The control channel coupon exhibited a tensile strength of 53.2 ksi and an elastic modulus of 4090 ksi, representing 177% and 164% of the tabulated values, respectively. Moreover, the channel coupons extracted from full-scale tested beams (mid-span and end-region) retained high mechanical performance, with tensile strengths exceeding 150% of the tabulated values and elastic modulus values remaining above 120%. These results indicate strong durability and performance retention of the GFRP channels after beam application. Detailed procedures and results of the coupon testing are provided in Appendix C.

Figure 52: Example FRP Channels

3.3.2 SAFSTRIP

The FRP strengthening strip (SAFSTRIP®, Figure 53, Appendix D), manufactured by Strongwell [52], is a pultruded composite strip designed to increase the strength of existing structural members when mechanically fastened in place. The strip is 4 inches wide and 1/8 inch thick and is supplied in continuous rolls up to 100 feet long. SAFSTRIP is a carbon-glass hybrid composite consisting of carbon fiber tows sandwiched between layers of fiberglass mats and rovings, all bonded together with a highly corrosion-resistant vinyl ester resin. The carbon fibers provide increased stiffness, while the glass reinforcement supplies bearing strength and improves fastener performance. A synthetic surfacing veil is incorporated

into the composite to enhance resistance to corrosion, moisture, and UV degradation. In addition, the strip is designed to resist splitting and delamination when drilled, which improves constructability and long-term durability at fastener locations.

The manufacturer-specified tensile strength and longitudinal elastic modulus of the strip are 92.90 ksi and 9020 ksi, respectively. Coupon testing showed that the control strip specimens had higher measured properties, with tensile strengths of up to 133.7 ksi (107–109% of the tabulated value) and elastic moduli up to 9822 ksi (109%). The tested coupons removed from full-scale beams also performed well, maintaining tensile strengths and stiffness within ±10% of the design values. These results suggest minimal degradation and confirm the reliability of the FRP strip in structural strengthening applications. Additional details on the coupon testing procedure and results are provided in Appendix C.

Figure 53: SAFSTRIP sample in rolled/shipped condition

3.3.3 Fasteners

RSS-GRK screws [53] (Figure 54-a) were used as the fasteners in this study to attach the channels and strips to the timber beams. These screws feature a washer head design that effectively addresses potential bearing issues. For the channels, 5/16”x3-1/8” screws were used, while 1/4"x3-1/2" screws were selected for the strips. These fasteners were chosen for their specified high shear capacities of 982 lb and 754 lb, respectively. In addition, #12x6-3/8” R4-GRK screws [53] (Figure 54-b) were used to close the cracks before attaching the channels and strips to the repaired beams.

(a) RSS-GRK screws for attaching FRP to timber beams

(b) R4-GRK screws for repairing crack beams prior to FRP installation

Figure 54: Fasteners used in repair/strengthening

3.4 Repair/strengthening techniques

As stated above, the focus of this research was primarily on strengthening/repairing beams to avoid/repair tension cracking and shear splitting mechanisms. This section outlines the FRP repair and strengthening techniques used in this study. A total of four configurations were tested under either flexure- or shear-controlled loading schemes. Specifically, these techniques included (1) a combination of FRP channels and strips to improve the performance of flexure-controlled beams, (2) FRP strips used alone for flexure-controlled beams, (3) FRP channels used alone for shear-controlled beams, and (4) and FRP channels used in specific locations to repair existing splits in flexure-controlled beams.

To align with dimensions in the field on actual bridges and thereby simplify future implementation, the strips were 23.5’ in length for the 25’ span beams and 17.5’ for the 19’ span beams. The shortened strip ensures conservative test results, in case blocking or other obstacles exist on a physical bridge, hindering the strip from spanning the entire beam. Similarly, the channel lengths were 24’, 18’, and 8’ for the 25’, 19’, and 9’ span beams, respectively. Each technique is discussed in detail in the following sub-sections.

3.4.1 FRP channels and strip for flexure-controlled beams

This technique was used to strengthen undamaged beams and repair beams with tension cracks and shear splits, to be tested in a flexure-controlled manner. This technique was used for both beam sizes used in this study, and consisted of two GFRP channels screwed to the faces of the beam (either at the bottom or top) and a GFRP/CFRP strip screwed to the tension face (bottom) of the beam. Note that the location of the channels was at times dependent on existing damage within the beam. That is, the channels were installed on the bottom of the beam to repair tension cracks, while they were installed in the middle to repair shear splits. Schematics of this repair/strengthening technique are shown in Figure 55 and Figure 56, while actual beams with this technique employed are shown in Figure 57.

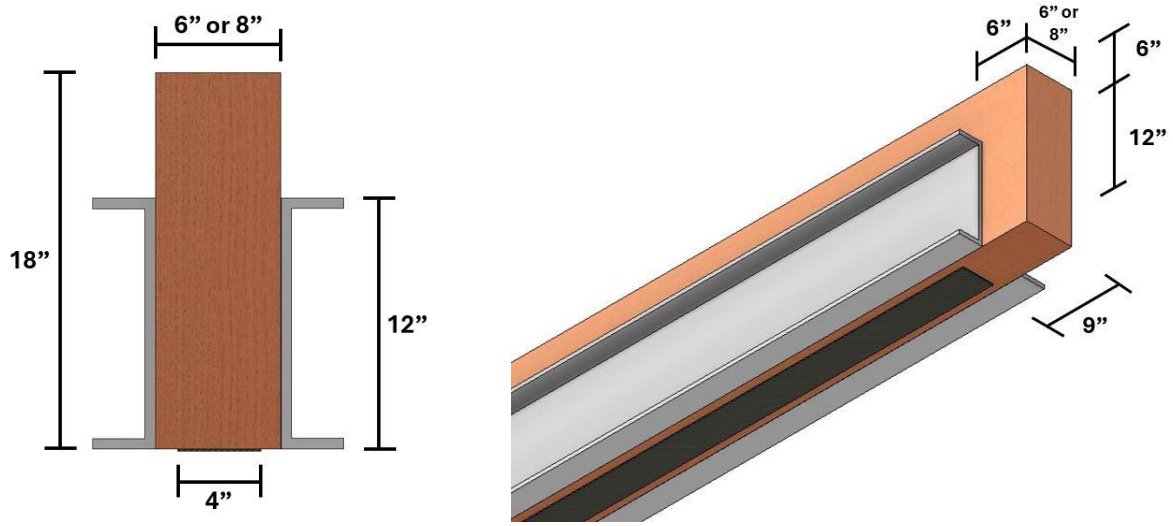

(a) Cross-section (b) Elevation

Figure 55: Schematic of FRP channels and strip repair technique (bottom channel)

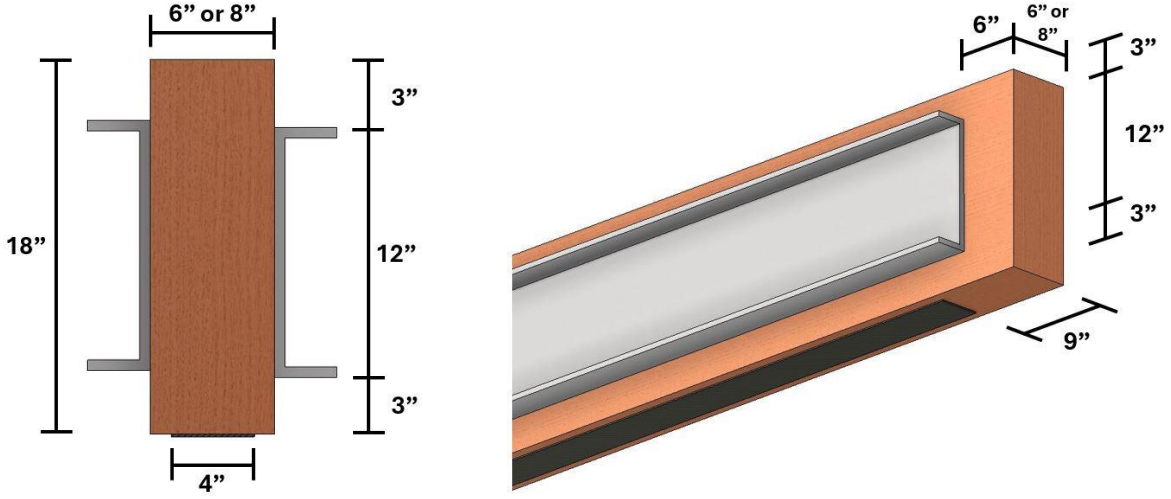

(a) Cross-section (b) Elevation

Figure 56: Schematic of FRP channels and strip repair technique (middle channel)

(a) Beam on its side with strip on bottom and channels on bottom edge

(b) Beam in testing position with channels in the mid-height of the beam

Figure 57: FRP channels and strip repair technique on test beams

3.4.2 FRP strips for flexure-controlled beams

With this technique, on beams to be tested in flexure, FRP strips were used without channels to strengthen undamaged beams and repair beams with tension cracks. Strips were screwed to the sides and bottoms of the beams, as shown in Figure 58 - Figure 60. On each side, either one or two strips were included depending on the severity and location of tension cracks.

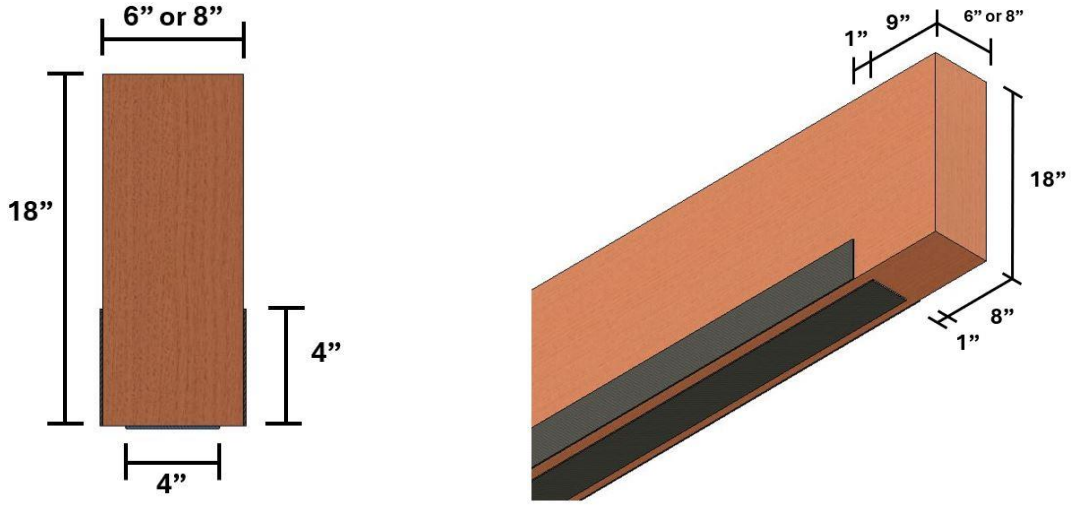

(a) Cross-section

(b) Isometric

Figure 58: Schematic of FRP strips for flexure-controlled beams – one strip per side

(a) Cross-section (b) Isometric

Figure 59: Schematic of FRP strips for flexure-controlled beams – two strips per side

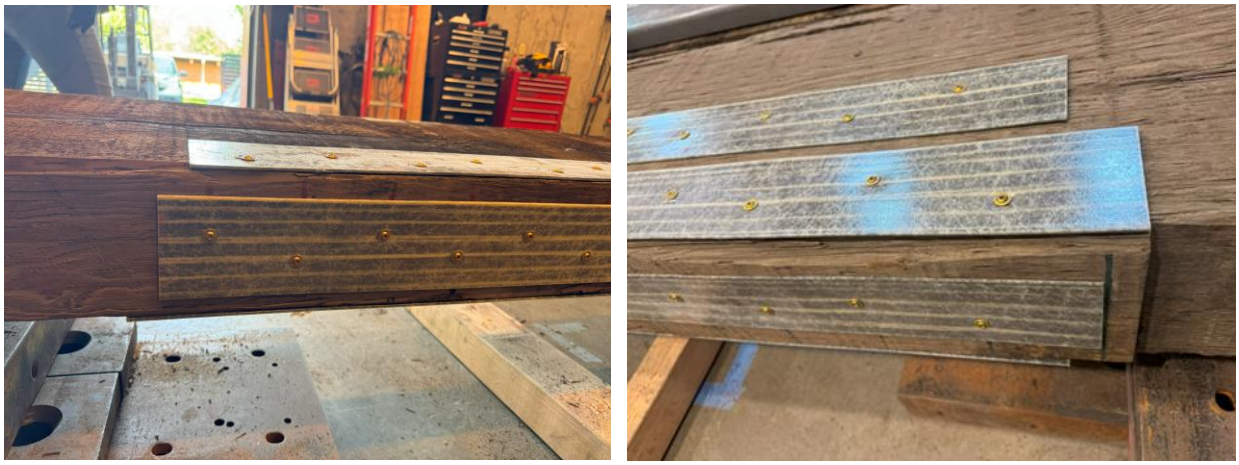

(a) Beam on its side with one strip per side (b) Beam on its side with two strips per side

Figure 60: FRP strip technique applied to test beams

3.4.3 FRP channels for shear-controlled beams

This technique was used to strengthen undamaged beams and repair shear-split beams to be tested in shear. This technique consisted of GFRP channels screwed to the sides of the beams (in the middle), as shown in Figure 61 and Figure 62.

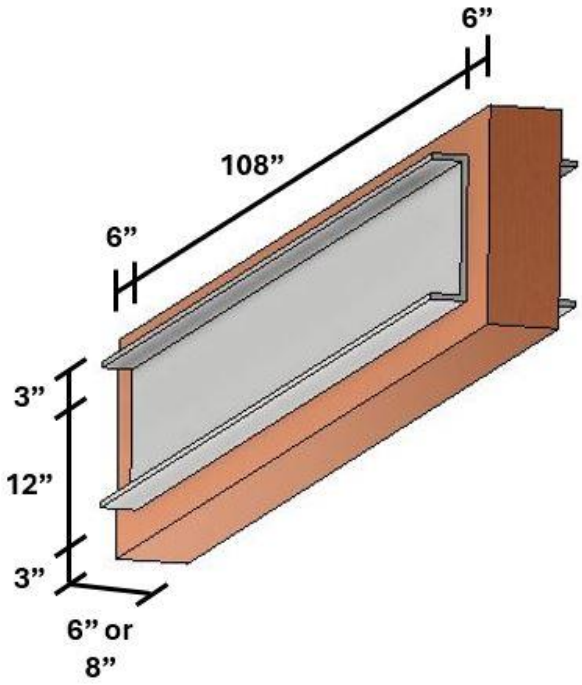

Figure 61: Schematic of FRP channels for shear-controlled beams

Figure 62: FRP channel technique applied to test beam

3.4.4 FRP channels in specific locations to repair splits in flexure-controlled beams

In some cases, the test beams had localized shear-splits near their ends, and FRP channels were used at these specific locations to repair this damage. After repair, these specimens were tested in flexure. This

technique consisted of either 3’ or 6’ channels attached to the sides of the beams (in the middle), as shown in Figure 63 and Figure 64. Two different lengths were used to evaluate the effect that this parameter has on the performance.

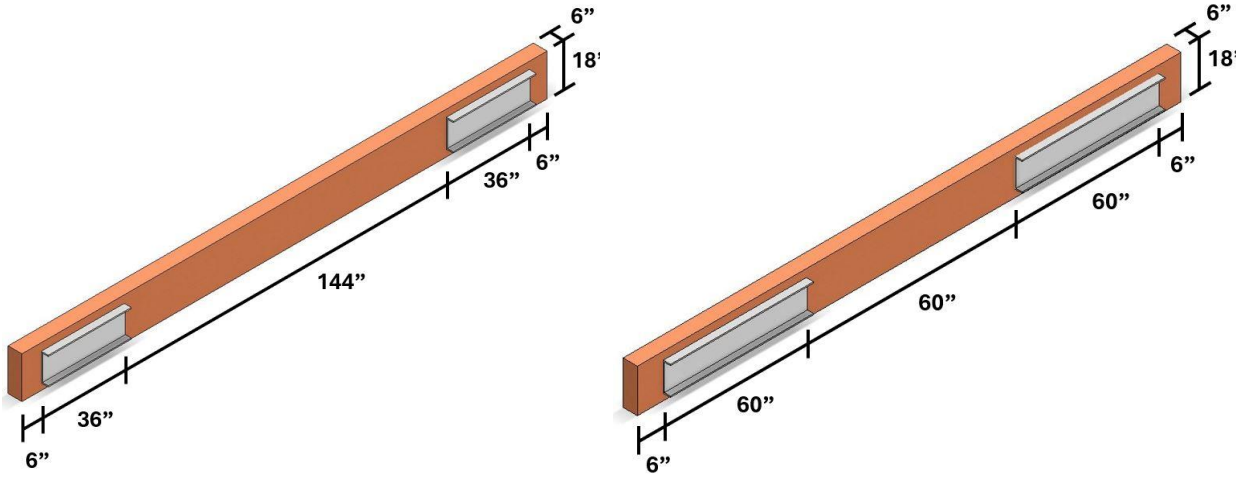

(a) 3’ channels (b) 6’ channels

Figure 63: Schematics of localized split repairs with channels

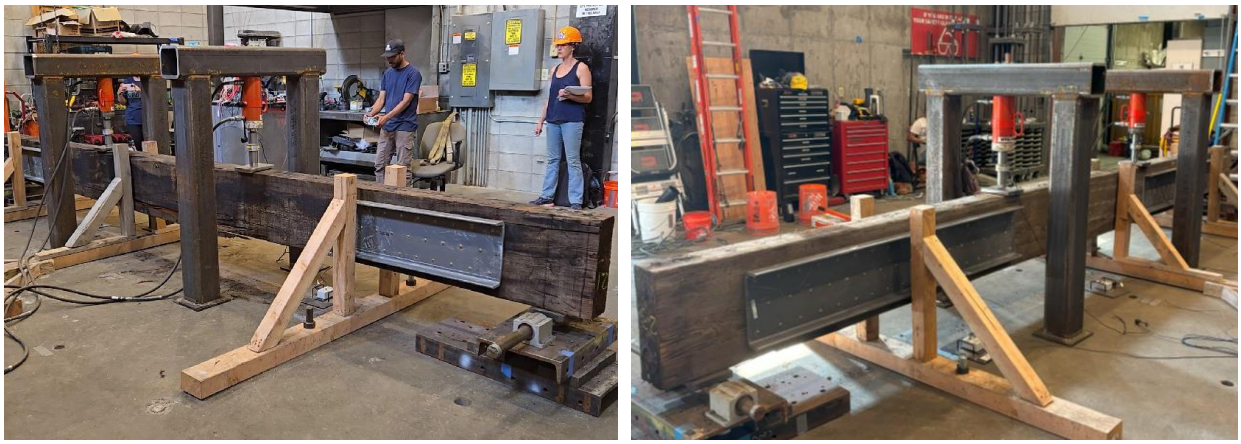

(a) 3’ channels (b) 6’ channels

Figure 64: Localized split repair technique applied to test beams

3.4.5 Example repairs

As mentioned previously, the focus of this research was on quantifying the efficacy of the above-mentioned techniques at strengthening undamaged beams and repairing damaged beams. To do this, several undamaged control beams were tested without employing the methods discussed above, giving a baseline of performance. The results from these tests were then compared to the results of tests on undamaged beams strengthened with these techniques. Additionally, the now-damaged control beams were then repaired with one of these techniques, and tested again under the same loading conditions, providing a direct comparison of the performance of the undamaged beam before testing to the performance of the same beam after repair. In some cases, the repair was quite extensive, as shown below.

Figure 65 shows a flexure-controlled beam that failed due to a large tension crack that was repaired with the FRP channel and strip method discussed above. Figure 66 shows another beam that failed due to a tension crack that was repaired with FRP strips alone. Figure 67 shows a shear-controlled beam that failed due to a shear split and repaired with FRP channels. Finally, Figure 68 shows a beam that had an existing shear split, that was repaired with FRP channels and a strip.

(a) After initial failure, before repair (b) After repair, before re-testing

Figure 65: An example of a tension-crack repair with FRP channels and strips

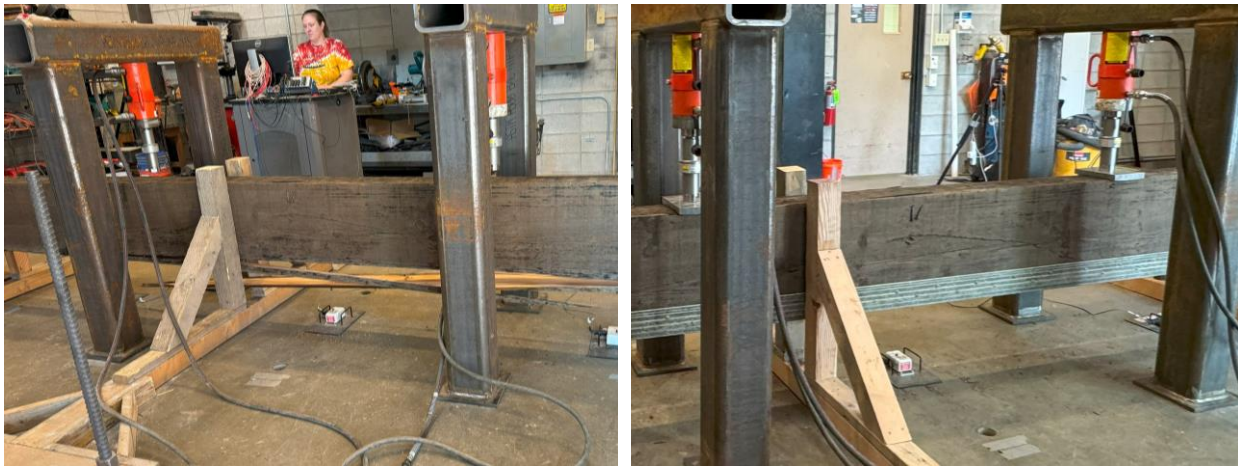

(a) After initial failure, before repair (b) After repair, before re-testing

Figure 66: An example of a tension-crack repair with FRP strips alone

(a) After initial failure, before repair

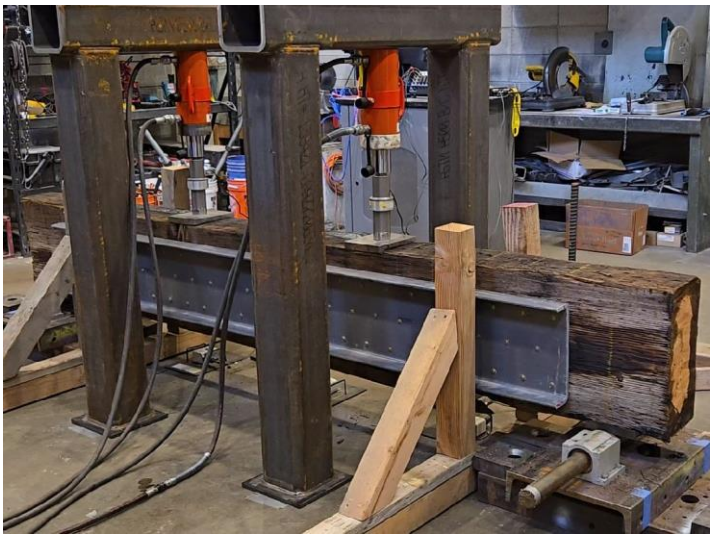

(b) After repair, before re-testing

Figure 67: An example of the shear-split repair with FRP channels

(a) Existing split, before repair

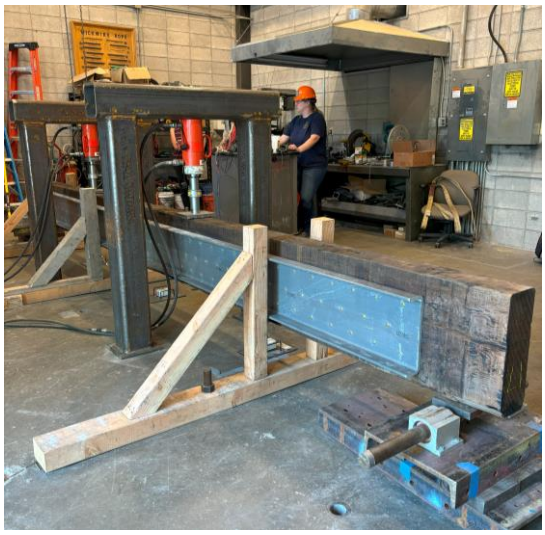

(b) After repair, before testing

Figure 68: An example of an existing shear-split repair with channels and strip

3.5 FRP Installation

Implementing the repairing/strengthening techniques discussed in the previous chapter involved several steps, including cutting the FRP strips and channels to length, predrilling the FRP section, preparing the timber beam surface for application (including closing the existing crack when applicable), and finally attaching the FRP materials to the timber beam with fasteners.

3.5.1 Cutting the FRP

The FRP strips were supplied from the manufacturer in 100’ rolls, while the FRP channels were shipped in 24’ lengths. The channels were cut to length using a reciprocating saw with a metal cutting blade (Figure 69-a). The strips were cut with a standard miter saw with a metal blade (Figure 69-b).

(a) Channel

(b) Strip

Figure 69: Cutting the FRP material

3.5.2 Pre-drilling

Strongwell recommends predrilling sections thicker than 5/16”, and therefore the channels and strips in this research were predrilled prior to installation. Details on the screw count calculations and screw pattern schematics are provided in Appendix E. The channels and strips were drilled (Figure 70) with a standard impact drill with 5/16” and 1/4” Milwaukee titanium twist metal drill bits [54], respectively.

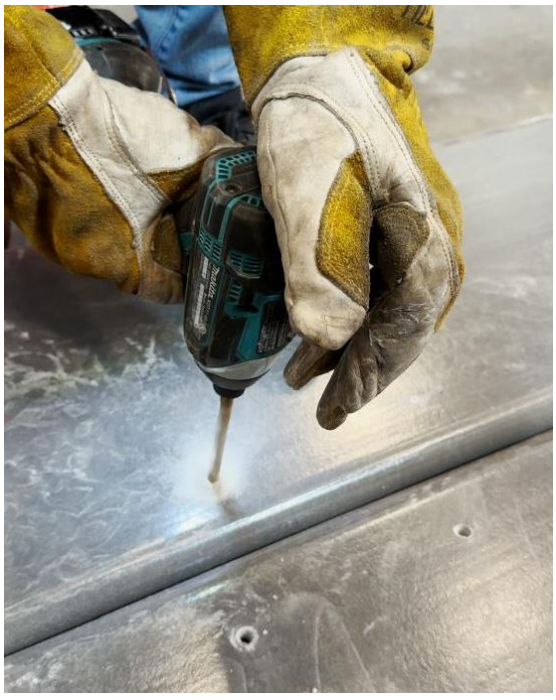

(a) Channel

(b) Strip

Figure 70: Pre-drilling the FRP

3.5.3 Surface preparation for repairs

The surface of each beam to be repaired/strengthened with the FRP methods discussed previously was first cleaned off with a broom. When applicable, existing or induced damage was repaired prior to installation. Specifically, beams with existing or induced flexure-cracks were turned upside down and secured with ratchet straps (Figure 71). The tension cracks were then closed using #12 x 6-3/8" R4-GRK screws. There was no specific screw pattern for closing the cracks, as the crack formation was different for each beam. However, care was given to avoid overlapping screws between FRP strip screws and repair screws (Figure 72). In contrast, no additional fasteners (beyond those required for the channels) were needed for the beams with existing or induced shear splits, as these beams would return to the undamaged configuration after the load was removed (shown in Figure 73).

(a) Before (b) After

Figure 71: Using ratchet straps to close any existing cracks

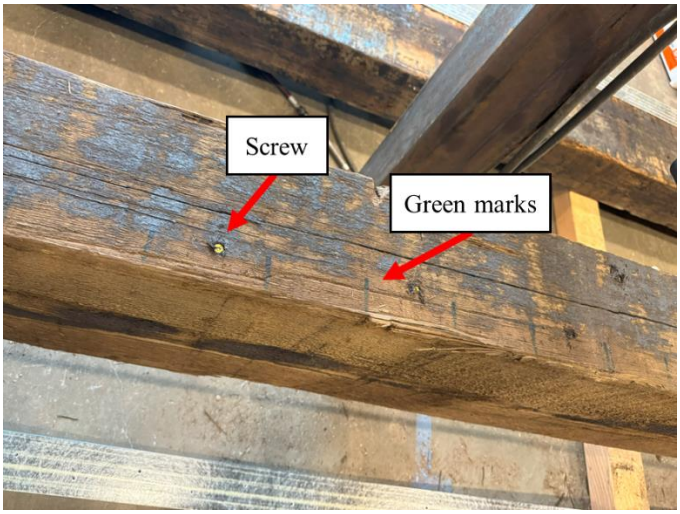

Figure 72: Marking the strip screw pattern (green marks in the photograph) and closing the crack

(a) At maximum load (b) After load removal

Figure 73: An example of a split closing after load removal

3.5.4 Attaching the FRP to the beam

The FRP strips were secured to the beams using 1/4"x3-1/2" RSS-GRK screws, starting in the center of the beam and working towards the ends, while ensuring the strip remained aligned with the beam and taught (Figure 74). Similarly, the channels were attached to the beams with 5/16”x3-1/8” RSS-GRK screws, Ratchet straps were occasionally used to align the channels with the beams, especially when the beams were not perfectly straight. The channel installation process involved securing one end of the channel with a few screws first, then aligning the channel with the beam (Figure 75-a), securing the opposite end, and then completing the screwing along the length (Figure 75-b). When used to repair shear splits, care was given to position the FRP to span across the splits.

Figure 74: Attaching strip to the beam

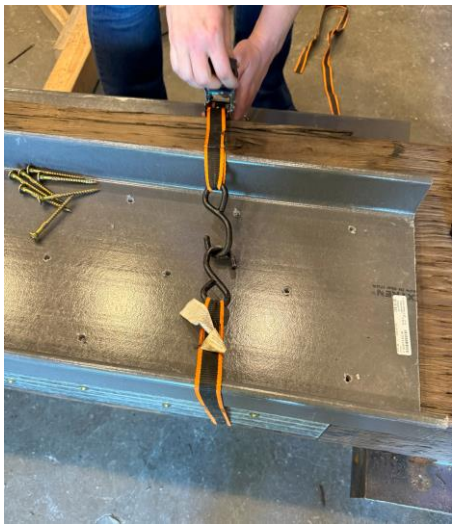

(a) Aligning the channel with the beam

(b) Screwing along the length

Figure 75: Attaching channel to the beam

3.6 Test matrix

Two standard sizes of Douglas-fir/Larch (dense No. 1) beams were tested in this study: 6”x18”x20’ and 8”x18”x26’. For each size group, the test matrix included three undamaged/unstrengthened control beams (two tested in flexure and one in shear), two flexure crack-repair beams (previously tested controls that were repaired), one shear split-repair beam (a previously tested control repaired after splitting), and three strengthened beams (undamaged beams reinforced with FRP). In addition, three 6”×18” beams and one 8”×18” beam with pre-existing splits (salvaged from bridges) were repaired and tested. An overview of all beam cases and repairing/strengthening schemes are presented in Table 12.

Throughout this report, each beam is identified by an acronym that encodes its key attributes. The first number in the acronym indicates the beam’s nominal size (6 for a 6″×18″ beam, or 8 for an 8″×18″ beam). The letters following the number denote the test setup: Sh for a shear test or Fl for a flexure test. If the acronym includes a number in parentheses immediately after (for example, 6-Fl(1)), that number identifies a specific control beam (e.g., “(1)” or “(2)” for the first or second control in that group). The final letters of the acronym indicate the repair or strengthening method, if applicable: CR for a crack-repair beam, SR for a split-repair beam, or St for a strengthened beam. Any additional parentheses at the end specify the repair/strengthening scheme used: (C-S) for a combination of FRP channels and a strip, (S) for FRP strips only, (C) for FRP channels only, (C3) for 3′-long channels on the beam ends, and (C6) for 6′-long channels on the beam ends. In Table 12, the second column lists the original beam numbers (as marked on the beams before delivery to MSU); an “(R)” following the number indicates a beam that was previously tested as a control and then repaired for a subsequent test.

Table 12: Test beam details

Acronym	Original #	Nominal cross-section	Test setup	Span length	Type	Repairing or Strengthening
6-Sh(1)	16	6" x 18"	Shear	9’	Control	None
6-Fl(1)	22	6" x 18"	Flexure	19’	Control	None
6-Fl(2)	15	6" x 18"	Flexure	19’	Control	None
6-Fl(1)-CR(C-S)	22 (R)	6" x 18"	Flexure	19’	Control - Crack Repair	Channels on the sides - Strip on the bottom
6-Fl(2)-CR(S)	15 (R)	6" x 18"	Flexure	19’	Control - Crack Repair	Strips on the sides and bottom
6-Sh(1)-SR(C)	16 (R)	6" x 18"	Shear	9’	Control - Split Repair	Channels on the sides
6-Fl-SR(C-S)	17	6" x 18"	Flexure	19’	Split Repair	Channels on the sides - Strip on the bottom
6-Fl-SR(C3)	21	6" x 18"	Flexure	19’	Split Repair	Channels (3 ft) on each ends of the sides
6-Fl-SR(C6)	23	6" x 18"	Flexure	19’	Split Repair	Channels (6 ft) on each ends of the sides
6-Sh-St(C)	13	6" x 18"	Shear	9’	Strengthened	Channels on the sides
6-Fl-St(C-S)	24	6" x 18"	Flexure	19’	Strengthened	Channels on the sides - Strip on the bottom
6-Fl-St(S)	20	6" x 18"	Flexure	19’	Strengthened	Strips on the sides and bottom
8-Sh(1)	9	8" x 18"	Shear	9’	Control	None
8-Fl(1)	7	8" x 18"	Flexure	25’	Control	None
8-Fl(2)	5	8" x 18"	Flexure	25’	Control	None
8-Fl(1)-CR(C-S)	7 (R)	8" x 18"	Flexure	25’	Control - Crack Repair	Channels on the sides - Strip on the bottom
8-Fl(2)-CR(S)	5 (R)	8" x 18"	Flexure	25’	Control - Crack Repair	Strips on the sides and bottom
8-Sh(1)-SR(C)	9 (R)	8" x 18"	Shear	9’	Control - Crack Repair	Channels on the sides
8-Fl-SR(C-S)	12	8" x 18"	Flexure	25’	Split Repair	Channels on the sides - Strip on the bottom
8-Sh-St(C)	1	8" x 18"	Shear	9’	Strengthened	Channels on the sides
8-Fl-St(C-S)	11	8" x 18"	Flexure	25’	Strengthened	Channels on the sides - Strip on the bottom
8-Fl-St(S)	8	8" x 18"	Flexure	25’	Strengthened	Strips on the sides and bottom

3.7 Test setup and instrumentation

All the beams in this investigation were tested in 4-point bending, following ASTM D198 − 22a [55], which includes both flexure and shear setups. The flexure test setup was designed to induce a flexural (bending) failure at mid-span (high moment region), whereas the shear test setup was intended to cause a shear failure at the beam ends (high shear region). Figure 76 illustrates the load configuration diagrams (free-body, shear, and moment) for the four-point bending tests.

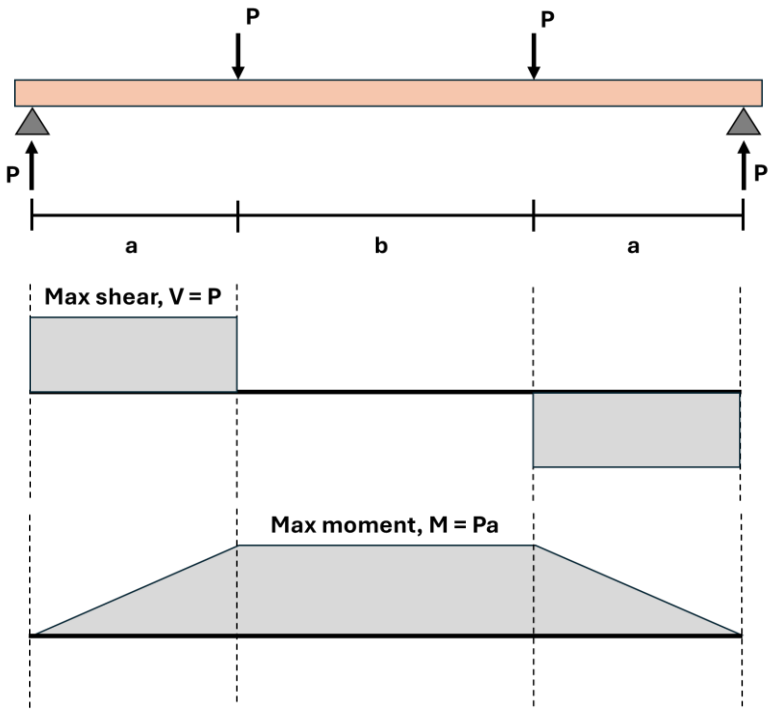

Figure 76: General 4-point bending test setup

The flexure and shear setups were geometrically similar, differing primarily in the distances between supports and loading points (dimensions "a" and "b" in Figure 76). The flexure-controlled beams had longer spans with greater moment demands, while the shear-controlled beams were shorter with increased shear demand relative to moment demand. Schematic diagrams of the flexure and shear test configurations for both beam sizes are shown in Figure 77 and Figure 78, respectively, with all key dimensions labeled.

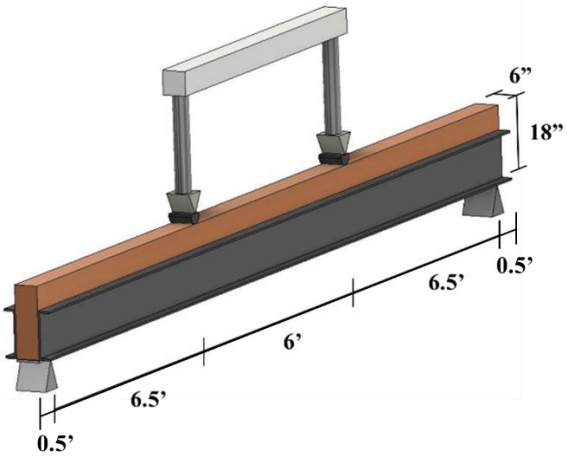

(a) 19' span (6"x18"x20') beam

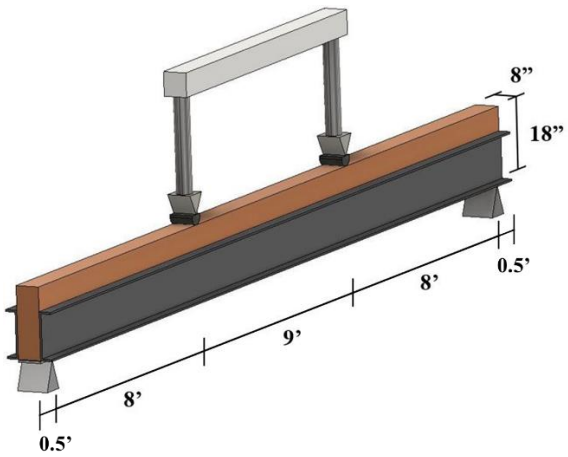

(b) 25' span (8"x18"x26') beam

Figure 77: Flexure-controlled test setup

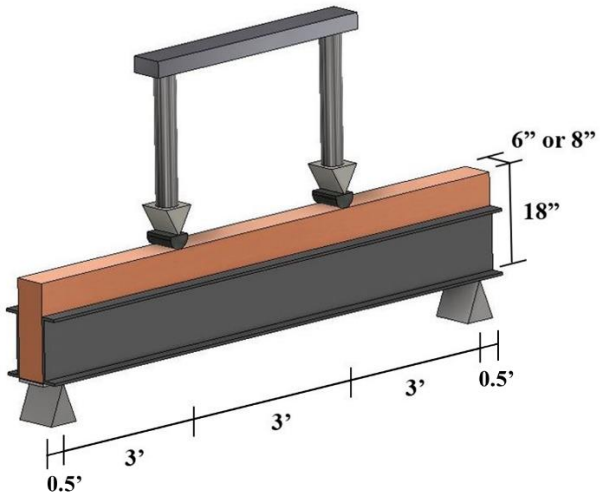

Figure 78: Shear-controlled test setup (for both 6”x18” and 8”x18”)

In the setups, the loads were applied with two power-team 110 kip hydraulic actuators on the same hydraulic line, which resulted in equal loads on each actuator. Steel bearing plates (6”x8”x1”) were included between the supports and the beams. Similarly, steel bearing plates were also included (6”x8”x1”) between the actuators and the tops of the beam specimens. It should be noted that in accordance with the ASTM specifications [55], the plates between the actuators and the top of the beam had a radius of curvature of 4’ on the loading surface of the block (Figure 79). Lateral bracings were provided at intermediate locations along the beam length to address any out-of-plane lateral instability and to prevent lateral torsional buckling.

Figure 79: Bearing plate with curvature

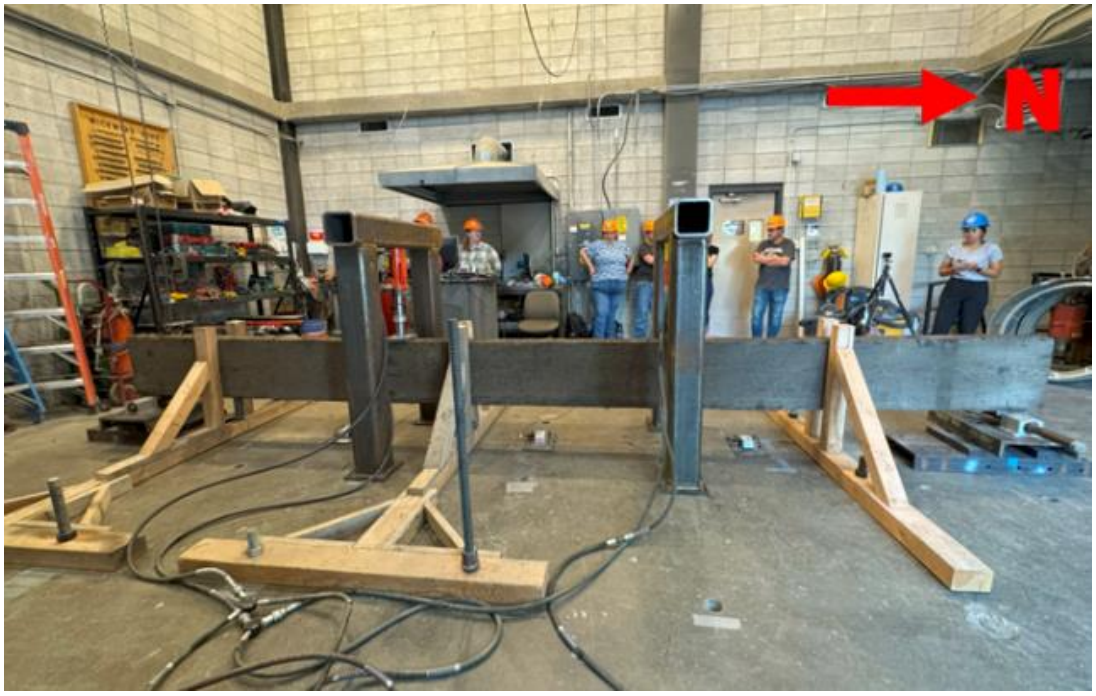

Figure 80: Flexure test setup for 19’ span beam

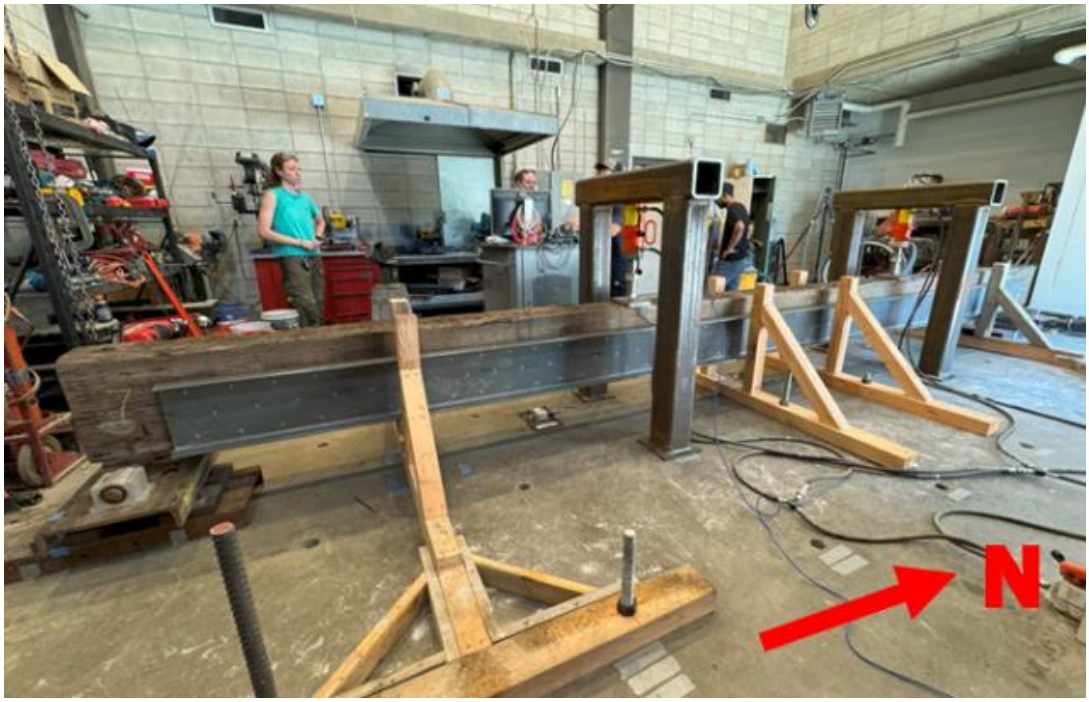

Figure 81: Flexure test setup for 25’ span beam

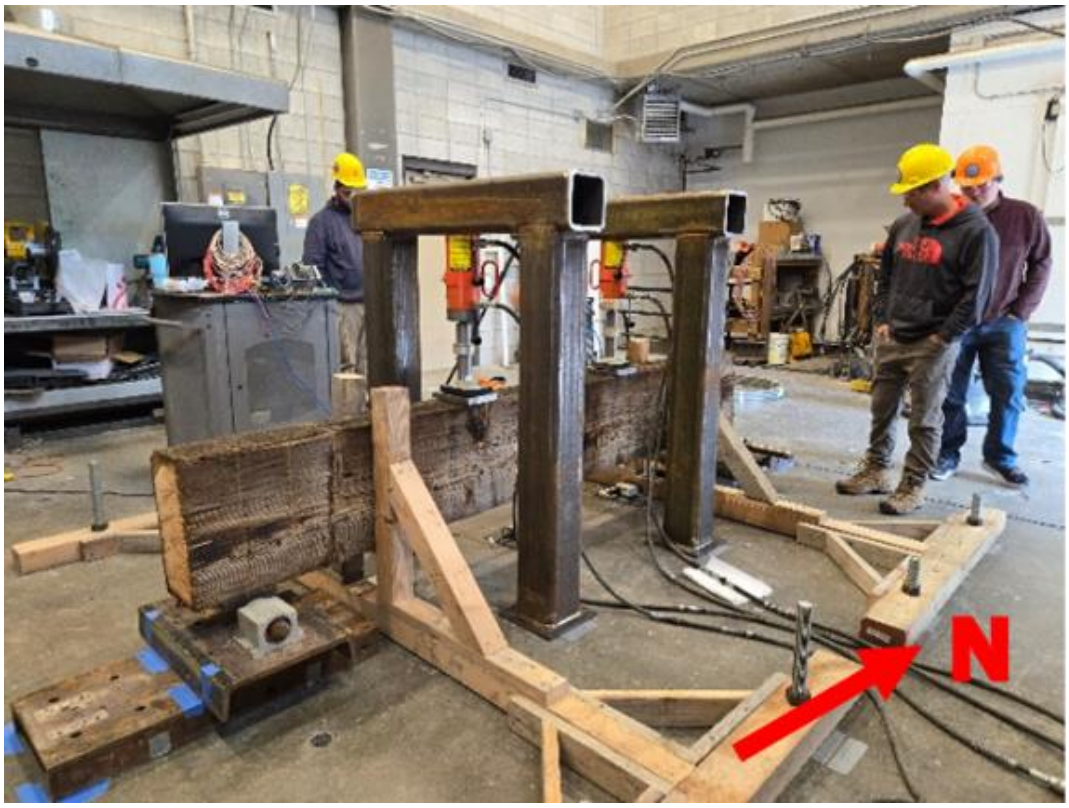

Figure 82: Shear test setup

4. TEST RESULTS

As discussed in the previous chapter, a total of twenty-two timber beams were tested in this research. These consisted of twelve 6”×18” beams and ten 8”×18” beams, encompassing various categories: control beams (tested under either flexure or shear), crack-repair beams (previously tested as controls and then repaired), split-repair beams (some initially tested as controls and others with existing splits prior to testing), and strengthened beams (which were undamaged prior to applying FRP reinforcement).

Results from this test series are summarized for the 6”x18” beams in Table 13, Table 14, and Table 15. Results for the 8”x18” beams are summarized in Table 16, Table 17, and Table 18. Note that all loads listed in the results tables are from one actuator (“P” in Figure 76) and any beams missing from the respective results tables had no data to report on that topic. The full detailed test summaries for each beam, along with the complete load–deflection plots and damage discussion, are provided in Appendix F. Common behavioral trends observed in these results are as follows.

In general, beam size had no discernible influence on qualitative behavior or repair effectiveness, aside from the expected higher absolute capacity of the larger 8” sections.

For the flexure-controlled beams, all control beams failed by fiber tension cracking near the center of the beams, with cracks often initiating at an imperfection. The repaired and strengthened beams increased ultimate capacity and postponed cracking. In most cases the FRP shifted the ultimate failure to either compressive crushing/cracking at the top of the beam, or in some cases the tests were terminated prior to failure due to instability/misalignment issues or actuator stroke limits.

For the shear-controlled beams, the controls failed abruptly when horizontal splits formed at the supports, again often initiating at imperfections. The side-channel split repairs restored/increased the shear capacity of the beams, and in several cases, redirected the governing failure to crushing of the timber from bearing at the supports and/or loading points.

Both crack- and split-repair schemes reliably restored the original strength, while preventive strengthening added 15–25% extra capacity. The combined flexure crack-repair and strengthening method, which includes FRP channels and strips (C-S) was more effective than the FRP strips alone (S).

After the summary results tables, the following sections of this chapter discuss these findings in more detail, with comprehensive data and analysis for each beam provided to support these summary observations.

Table 13: Summary of results of 6”x18” beams – Creaking and First crack/split

Beam Acronym	Creaking Load (kips)	Creaking Deflection (inch)	Creaking Location	First crack/split Load (kips)	First crack/split Deflection (inch)	First crack/split Location
6-Fl(1)	17.0	1.80"	Near South lateral bracing	20.0	2.00"	Crack near D1
6-Fl(2)	16.5	1.66"	-	-	-	-
6-Fl(1)-CR(C-S)	13.8	1.34"	South end	16.2	1.60"	-
6-Fl(2)-CR(S)	15.0	1.43"	-	21.0	2.02"	Split on the North end
6-Fl-SR(C-S)	9.0	0.89"	At the ends	10.5	1.00"	Split on the south end
6-Fl-SR(C3)	Immediately	-	-	4.0	0.58”	Crack at mid-span
6-Fl-SR(C6)	12.5	1.20"	-	12.5	1.20"	Compression crack near the top, close to the north load cell
6-Sh-St(C)	30.4	0.96"	-	30.4	0.96"	Split on the south end
6-Fl-St(C-S)	9.0	0.72"	-	25.8	2.05"	Crack at mid-span
6-Fl-St(S)	13.0	1.17"	Midspan	22.2	2.10"	Cracking under strip on the east

Table 14: Summary of results of 6”x18” beams – Bearing failure and Crushing on top

Beam Acronym	Bearing failure Load (kips)	Bearing failure Deflection (inch)	Bearing failure Location	Crushing on top Load (kips)	Crushing on top Deflection (inch)	Crushing on top Location
6-Sh(1)	21.3	0.50"	Load bearing blocks	-	-	-
6-Fl(1)-CR(C-S)	-	-	-	28.7	3.69"	North load block
6-Sh(1)-SR(C)	30.0	1.69"	Load bearing blocks	-	-	-
6-Fl-SR(C-S)	-	-	-	28.0	3.51"	Middle
6-Fl-SR(C6)	-	-	-	16.2	1.56"	Near South load cell
6-Sh-St(C)	30.5	0.97"	Load bearing blocks	-	-	-
6-Fl-St(C-S)	29.1	2.77"	North Load bearing block	-	-	-
6-Fl-St(S)	24.0	2.50"	North Load bearing block	-	-	-

Table 15: Summary of results of 6”x18” beams – Ultimate

Beam Acronym	Ultimate Load (kips)	Ultimate Deflection (inch)	Ultimate failure/End of the test
6-Sh(1)	27.0	0.89"	Shear splitting on the left end of the beam through a knot
6-Fl(1)	22.4	2.53"	Tension crack
6-Fl(2)	19.4	1.96"	Tension crack
6-Fl(1)-CR(C-S)	29.1	3.98"	Stopped loading because blocks weren't centered
6-Fl(2)-CR(S)	21.0	2.02"	Reached stroke limit
6-Sh(1)-SR(C)	30.1	1.69"	The north end leaned due to bearing failure
6-Fl-SR(C-S)	30.9	4.27"	Slight eccentricity on the load cell
6-Fl-SR(C3)	9.9	2.16"	Mid-span shot off middle string potentiometer
6-Fl-SR(C6)	21.7	2.77"	Tension crack
6-Sh-St(C)	33.2	1.10"	Eccentricity started on the north load cell
6-Fl-St(C-S)	29.1	2.77"	Bearing failure at the north load-bearing block
6-Fl-St(S)	25.4	2.81"	Shear split at the south end

Table 16: Summary of results of 8”x18” beams – Creaking and First crack/split

Beam Acronym	Creaking Load (kips)	Creaking Deflection (inch)	Creaking Location	First crack/split Load (kips)	First crack/split Deflection (inch)	First crack/split Location
8-Fl(1)	3.0	0.48"	-	16.5	2.37"	Tension crack at mid-span
8-Fl(2)	10.5	1.66"	Midspan	11.8	1.93"	Shear split at the north end
8-Fl(1)-CR(C-S)	10.4	1.53"	-	30.3	4.28"	Compression in the middle
8-Fl(2)-CR(S)	13.0	2.30"	Midspan	20.0	3.79"	Crack at the top middle through a knot
8-Fl-SR(C-S)	11.8	1.41"	-	16.7	1.99"	Bottom middle
8-Sh-St(C)	35.0	0.65"	-	-	-	-
8-Fl-St(C-S)	16.0	1.86"	-	21.5	2.47"	-
8-Fl-St(S)	14.0	1.68"	Throughout the beam	22.7	2.81"	-

Table 17: Summary of results of 8”x18” beams – Bearing failure and Crushing on top

Beam Acronym	Bearing failure Load (kips)	Bearing failure Deflection (inch)	Bearing failure Location	Crushing on top Load (kips)	Crushing on top Deflection (inch)	Crushing on top Location
8-Sh(1)	25.0	0.45"	Load bearing blocks	-	-	-
8-Fl(1)-CR(C-S)	-	-	-	31.7	4.64"	Near South load cell
8-Sh(1)-SR(C)	26.0	0.76"	North Load bearing block	-	-	-
8-Fl-SR(C-S)	-	-	-	22.9	2.86"	Top middle
8-Sh-St(C)	43.0	0.87"	Reaction bearing plates at the supports	-	-	-
8-Fl-St(C-S)	-	-	-	28.5	3.52"	Top middle
8-Fl-St(S)	25.0	4.46"	North load block	-	-	-

Table 18: Summary of results of 8”x18” beams – Ultimate

Beam Acronym	Ultimate Load (kips)	Ultimate Deflection (inch)	Ultimate failure/End of the test
8-Sh(1)	37.9	0.98"	Shear split at the end
8-Fl(1)	22.0	3.28"	Tension crack
8-Fl(2)	12.0	2.56"	Tension crack at the bottom mid-span
8-Fl(1)-CR(C-S)	33.1	5.28"	Reached stroke limit
8-Fl(2)-CR(S)	23.6	5.08"	Failed in compression through a knot at the top middle
8-Sh(1)-SR(C)	42.3	1.58"	Shear failure on the south end, propagated from the bearing failure
8-Fl-SR(C-S)	24.8	5.22"	Reached stroke limit
8-Sh-St(C)	56.3	1.45"	Shear split on the north end
8-Fl-St(C-S)	31.9	5.32"	Reached stroke limit
8-Fl-St(S)	28.8	3.76"	Tension crack propagating mid-span and compression failure at the north load block

4.1 Flexure test-setup beam results

This section discusses the performance of beams tested in the flexure test setup, including control, crack-repair, split-repair, and strengthened beams, using various repairing and strengthening techniques for 6"x18" and 8"x18" beams.

4.1.1 Control vs crack-repair and strengthened beams with FRP channels and strip

Figure 83 and Figure 84 show the three tested configurations of 6"×18" and 8”x18” timber beams, respectively: control, crack repair with C-S, and strengthened with C-S. The control beam displays the damage from testing. The repair beam is the same beam retrofitted with C-S combination, while the strengthened beam is an intact beam reinforced with C-S combination.

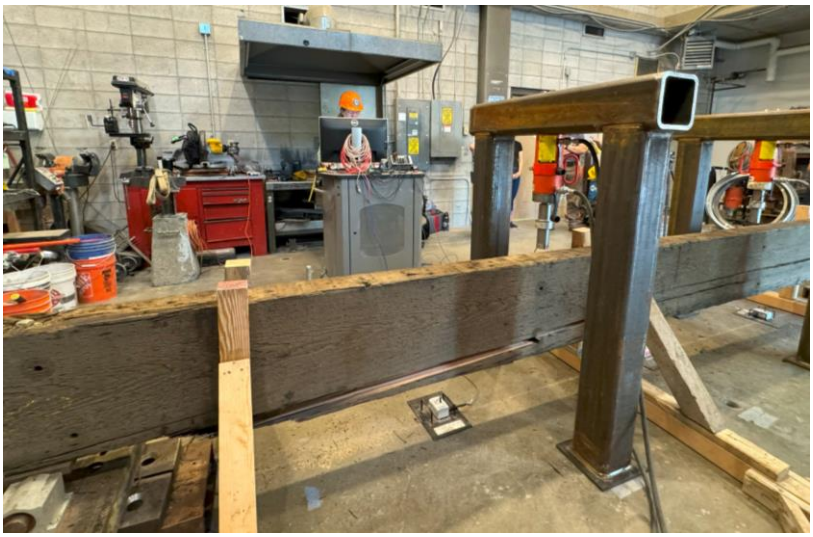

(a) Control – 6-Fl(1)

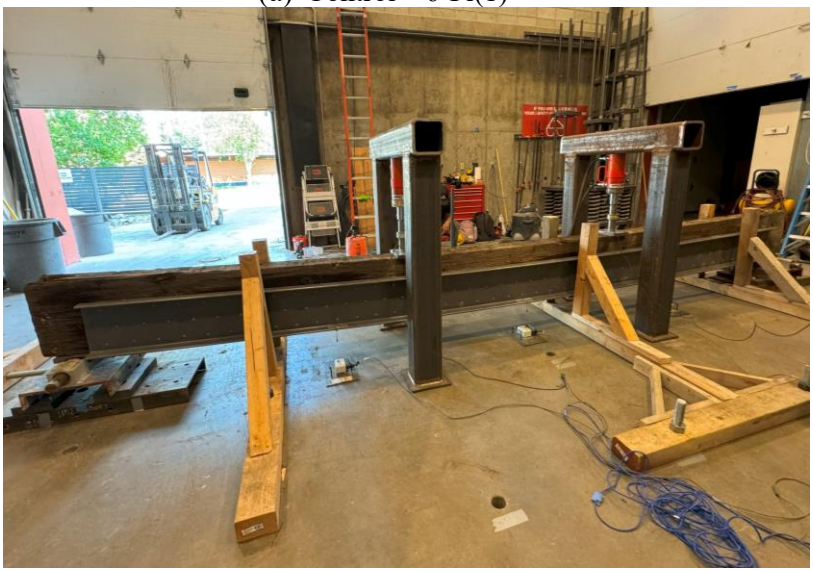

(b) Crack repair - 6-Fl(1)-CR(C-S)

(c) Strengthened - 6-Fl-St(C-S)

Figure 83: Control, crack-repair and strengthened 6”x18” beams with C-S combination

(a) Control - 8-Fl(1)

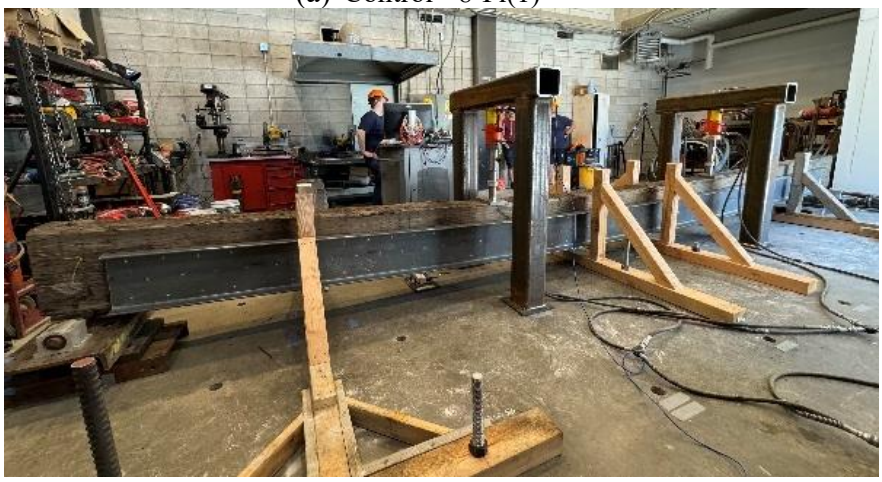

(b) Crack repair - 8-Fl(1)-CR(C-S)

(c) Strengthened - 8-Fl-St(C-S)

Figure 84: Control, crack-repair and strengthened 8”x18” beams with C-S combination

Figure 85-a compares the 6"×18" beam results, a control beam (6-Fl(1)), a crack-repair beam with FRP channels and strips (6-Fl(1)-CR(C-S)), and a strengthened beam with FRP channels and strips (6-Fl-St(C-S)). As can be observed in this plot, the control beam reached an ultimate moment of 145.6 kip-ft at a mid-span deflection of 2.53", failing abruptly due to a tension crack. The crack-repair beam – which was the previously tested control beam retrofitted with side channels and a bottom strip – achieved a higher moment capacity of 189.2 kip-ft with nearly the same initial stiffness as the control. This beam eventually failed by crushing of the wood under the north load block. The strengthened beam, which had the same FRP configuration applied to an undamaged specimen attained an ultimate moment of 189.15 kip-ft and exhibited the greatest stiffness among the three, finally failing by a bearing failure at the north load point. This demonstrates that adding the channel-and-strip reinforcement significantly increased the capacity over the unreinforced baseline.

Figure 85-b shows the analogous comparison for the 8"×18" beams. The unreinforced control beam (8-Fl(1)) carried an ultimate moment of 176.0 kip-ft at a deflection of 3.28″ before failing due to a mid-span tension crack. The crack-repair beam (8-Fl(1)-CR(C-S)), which had side channels and a strip added after its initial test, reached a higher ultimate moment of 264.0 kip-ft at 5.28″ deflection. The strengthened beam (8-Fl-St(C-S)), with similar FRP enhancements applied from the start, achieved an ultimate moment of 255.2 kip-ft at 5.32″. Both the repaired and strengthened 8" beams sustained greater loads and larger deformations than the control. The crack-repair beam's initial stiffness was similar to the control's, whereas the strengthened beam was noticeably stiffer. In terms of ultimate capacity, both FRP-enhanced beams significantly outperformed the control.

These results indicate that the FRP channel-and-strip reinforcement is highly effective: the repair technique successfully restored (and even increased) the beams' load capacities, and the strengthening approach appreciably enhanced stiffness and strength beyond the original values.

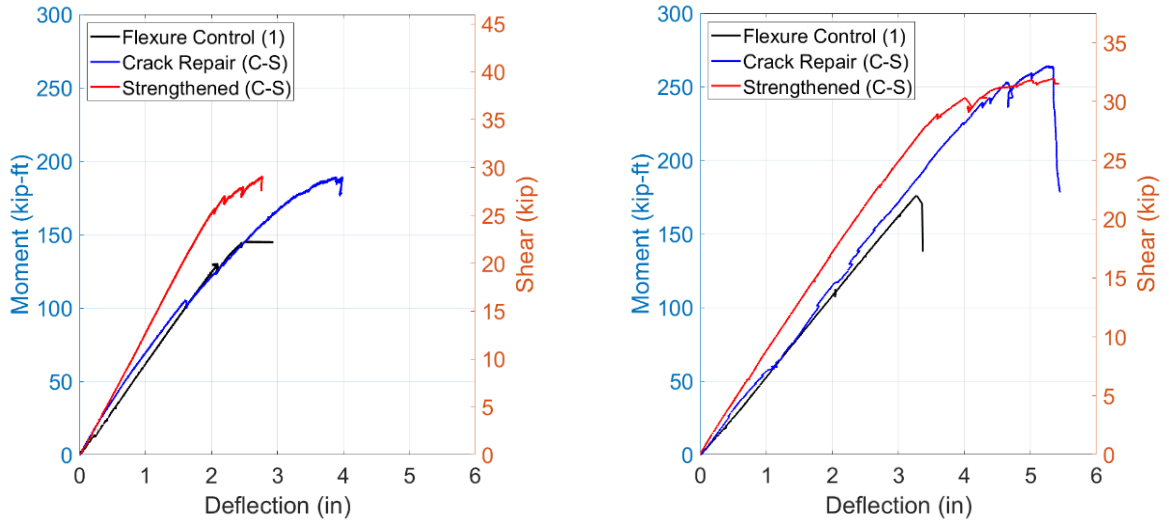

(a) 6"x18" beam data (b) 8"x18" beam data

Figure 85: Comparison of control vs crack repair and strengthened beams with channels and strip

4.1.2 Control vs crack-repair and strengthened beams with FRP strips

Figure 86 and Figure 87 show the three tested configurations of 6"×18" and 8”x18” timber beams, respectively: control, crack repair with strip only, and strengthened with strip only. The control beam displays the damage from testing. The repair beam is the same beam retrofitted with strip only, while the strengthened beam is an intact beam reinforced with strip only.

(a) Control - 6-Fl(2)

(b) Crack repair - 6-Fl(2)-CR(S)

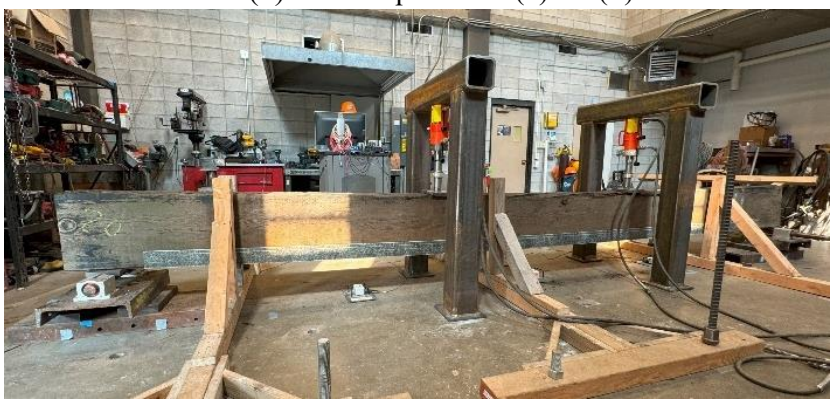

(c) Strengthened - 6-Fl-St(S)

Figure 86: Control, crack-repair and strengthened 6”x18” beams with strip only

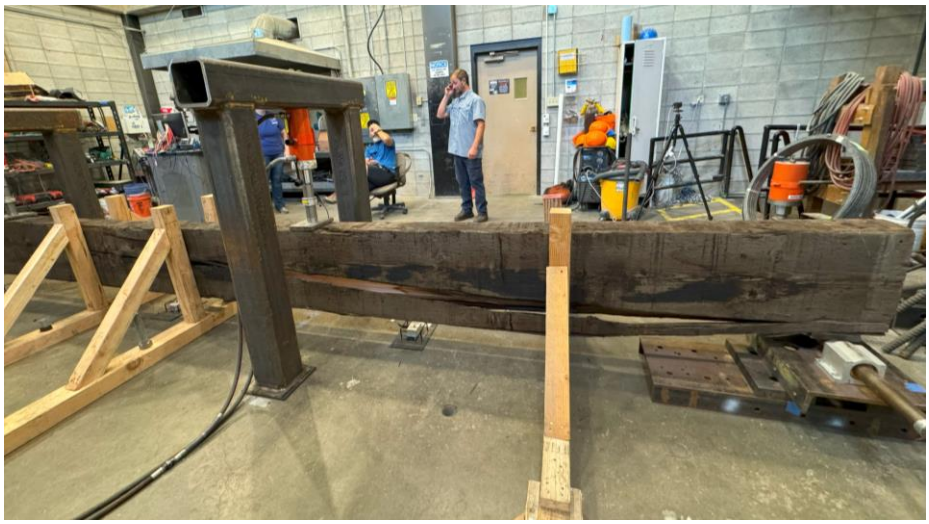

(a) Control - 8-Fl(2)

(b) Crack repair - 8-Fl(2)-CR(S)

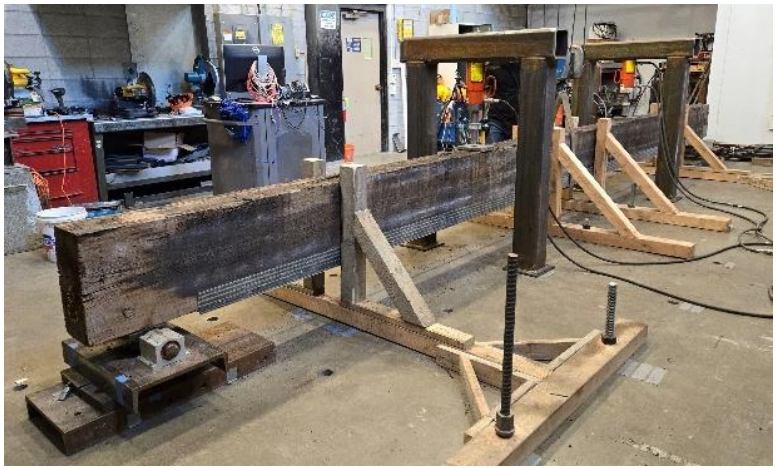

(c) Strengthened - 8-Fl-St(S)

Figure 87: Control, crack-repair and strengthened 8”x18” beams with strip only

Figure 88-a compares the moment-deflection curves for the 6”x18” control beam (6-Fl(2)), the crack-repair beam with only FRP strips (6-Fl(2)-CR(S)), and the strengthened beam with only FRP strips (6-Fl-St(S)). The control beam exhibited a brittle failure, reaching an ultimate moment of 126.1 kip-ft before suddenly fracturing at a deflection of 1.96”. The crack-repair beam, which was the same beam repaired by screwing FRP strips to its sides and bottom, initially mirrored the control’s response and successfully restored the beam’s original strength. However, a sharp drop in its curve occurred when a split opened at about 136.5 kip-ft and 2.02″ deflection. The strengthened beam, reinforced with strips on an undamaged beam, achieved a higher ultimate moment of 165.1 kip-ft and avoided the sudden post-peak drop observed in the repaired beam. All three 6″ beams displayed very similar initial stiffness.

Figure 88-b shows the moment-deflection curves for the 8″×18″ beams: control (8-Fl(2)), crack-repair with strips (8-Fl(2)-CR(S)), and strengthened with strips (8-Fl-St(S)). The control beam suddenly failed due to cracking at the mid-span, achieving an ultimate moment of approximately 96.0 kip-ft at a deflection of 2.50”. The crack-repair beam, which had been heavily damaged in its initial test and then mended with FRP strips, demonstrated greatly improved performance: it reached roughly 188.0 kip-ft and sustained larger deflections than the control before failure. The strengthened beam, despite exhibiting some moderate pre-test checking along its length, carried the highest moment—nearly 232 kip-ft—and far outperformed the others. The strengthened beam’s ability to maintain moment capacity illustrates the effectiveness of the strip reinforcement, providing enhanced structural resilience and delaying catastrophic failure. The initial stiffness of the crack-repair beam closely matched that of the control beam, while the stiffness of the strengthened beam surpassed the other two beams.

The comparison of the moment-deflection curves for both sets of beams highlights the significant benefits of either crack repair or strengthening using the FRP strip reinforcement. The control beams in each set displayed typical brittle failure with sudden fracture. The crack repair restored and even improved the beams' original strength, but a sudden drop in the moment-deflection graph was still observed due to the splitting of the 6”x18” beam. In contrast, the strengthened beams demonstrated superior performance, carrying the highest moments and maintaining structural integrity even after initial signs of damage. This indicates that FRP strip reinforcement enhances moment capacity and improves the beams' overall stiffness and resilience, effectively delaying catastrophic failure.

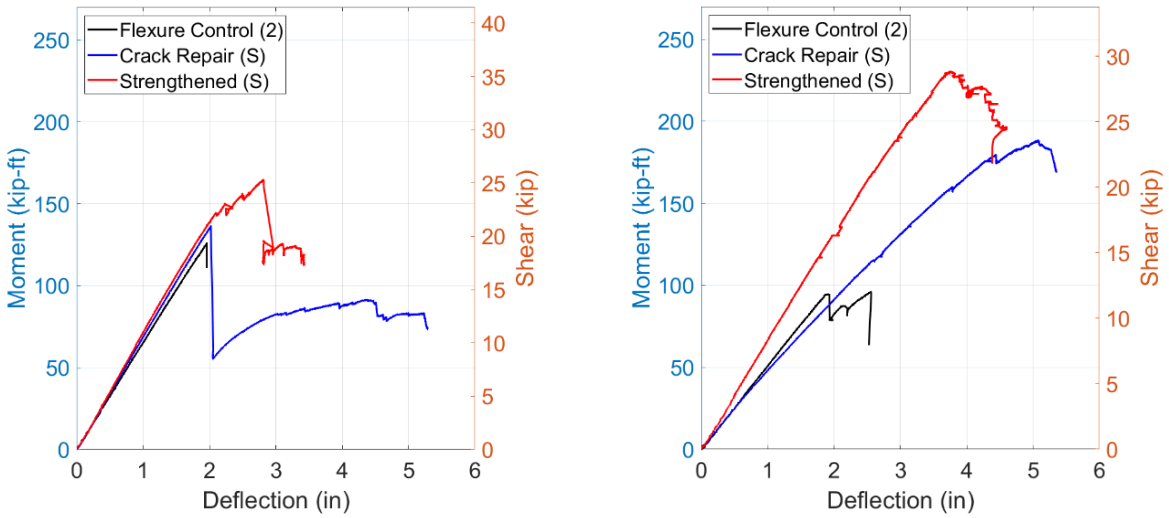

(a) 6”x18” beam data (b) 8”x18” beam data

Figure 88: Comparison of control vs crack repair and strengthened beams with strips

4.1.3 Control vs split-repair flexure beams

Several beams in the flexure test series have preexisting splits near their ends. This section demonstrates the effectiveness of several repair methods at repairing these splits. Figure 89 show the three split repair configurations for 6"×18", respectively: split repair with channel and strip combination, split repair with 6’ channels, and split repair with 3’ channels. The 8"×18" split repair beam with channel and strip combination is shown in Figure 90.

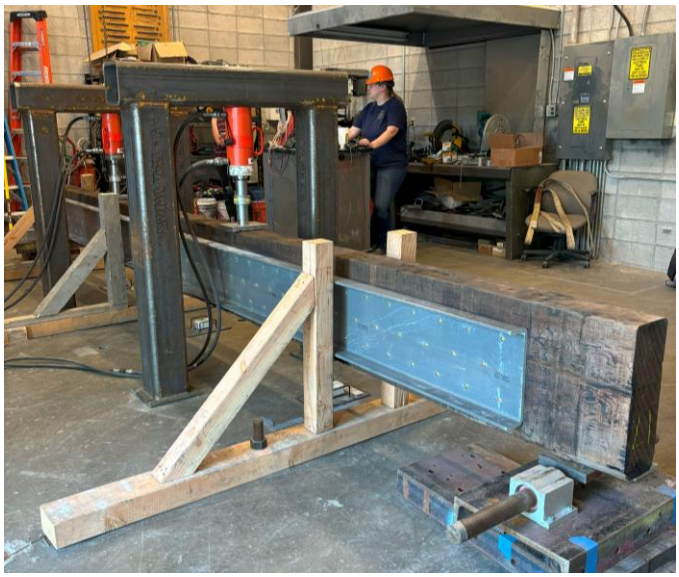

(a) Split repair – 6-Fl-SR(C-S)

(b) Split repair - 6-Fl-SR(C6)

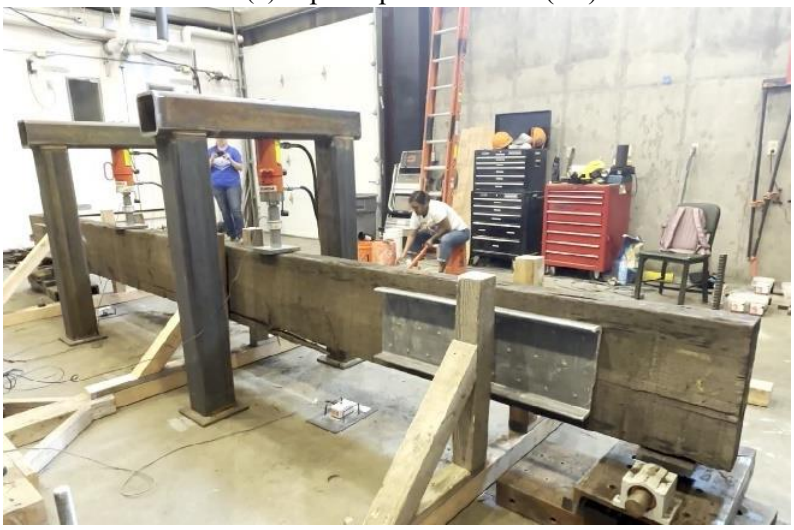

(c) Split repair - 6-Fl-SR(C3)

Figure 89: 6"x18" split repair beams tested in flexure setup

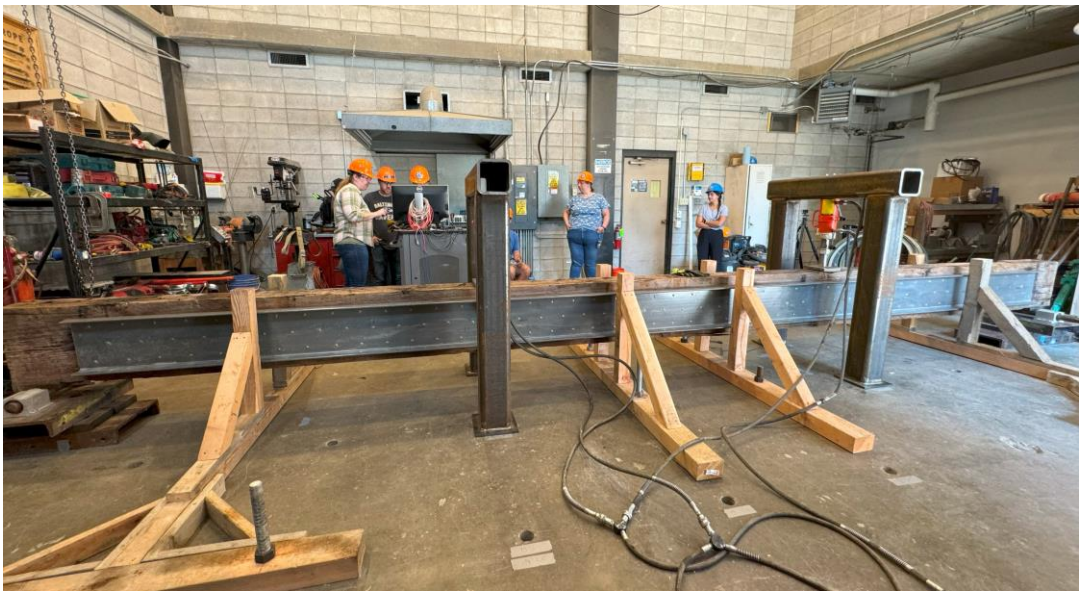

Figure 90: 8"x18" split repair beam with C-S tested in flexure setup - 8-Fl-SR(C-S)

Figure 91-a presents moment-deflection curves comparing two control beams and three different split-repair strategies for 6”×18” beams. Among the repaired beams, the one retrofitted with full-length side channels plus a bottom strip (6-Fl-SR(C-S)) was the most effective, reaching an ultimate moment of 200.9 kip-ft at a deflection of 4.27”. This is a significant improvement compared to the control beams, where the first control beam (6-Fl(1)) reached 145.6 kip-ft and the second control beam (6-Fl(2)) reached 126.1 kip-ft. Additionally, the fully repaired beam demonstrates similar stiffness as the control beams, while maintaining its stiffness and continuing to carry higher moments surpassing the control ultimate capacities. The beam repaired with 6’ channels on each end (blue line) achieved an ultimate moment of 141.1 kip-ft at a deflection of 2.77”, which is closer to the performance of the control beams but significantly lower than the robust repair with full-length channels and strip. The repair method with 3’ channels on the ends (green line) was least effective, with this beam reaching a moment of only 64.4 kip-ft at a deflection of 2.16”. This method offered minimal improvement compared to the second control beam and fell short compared to the other repair methods, suggesting that 3’ of the channel sections is insufficient to fully repair an existing split and restore shear capacity. The analysis shows that the split repair method using side channels combined with a strip is the most effective, providing the highest moment capacity, but a minimum of 6’ channels for a split repair can result in capacities comparable to undamaged beams.

The performance of the 8″×18″ beams with split repairs is shown in Figure 91-b. The beam repaired with side channels and a strip (8-Fl-SR(C-S)) attained an ultimate moment of 198.4 kip-ft, substantially higher than the two control beams (8-Fl(1) at 176.0 kip-ft, and 8-Fl(2) at 96.0 kip-ft). It is noteworthy that the two 8″ control beams had a large disparity in strength, likely due to pre-existing defects (such as severe checks and wane in the weaker beam) and the inherent variability in timber, such as knots, cracks, and variations in growth patterns in the timber. The repaired beam not only recovered the capacity lost due to the split but actually exceeded the stronger control’s capacity, and it also exhibited higher stiffness than both controls (unlike the 6″ case, where the repaired beam’s stiffness was on par with the controls). The load-deflection response of the repaired beam featured multiple smaller peaks, indicating a progressive failure with stages

of damage rather than one sudden break. Overall, the split-repair technique with full-length channels and a strip significantly improved the structural performance of the 8″ beam, making it much more resilient under load than either control beam.

Overall, the split repair method using side channels combined with a strip significantly enhanced the structural performance of both the 6"x18" and 8"x18" beams, making it the most effective repair technique among those tested. This method increased the ultimate moment capacity and maintained or improved the stiffness compared to the control beams. In the short channels repair method, the 6' channel successfully repaired the split, achieving a moment capacity comparable to the control beam, whereas the 3' channel proved insufficient for effective repair. Overall, this comprehensive repair approach significantly improves the moment capacity, demonstrating the importance of robust reinforcement strategies in structural repair. Figure 89 and Figure 90 show the 6"x18" and 8”x18” split repair beams tested in flexure setup, respectively.

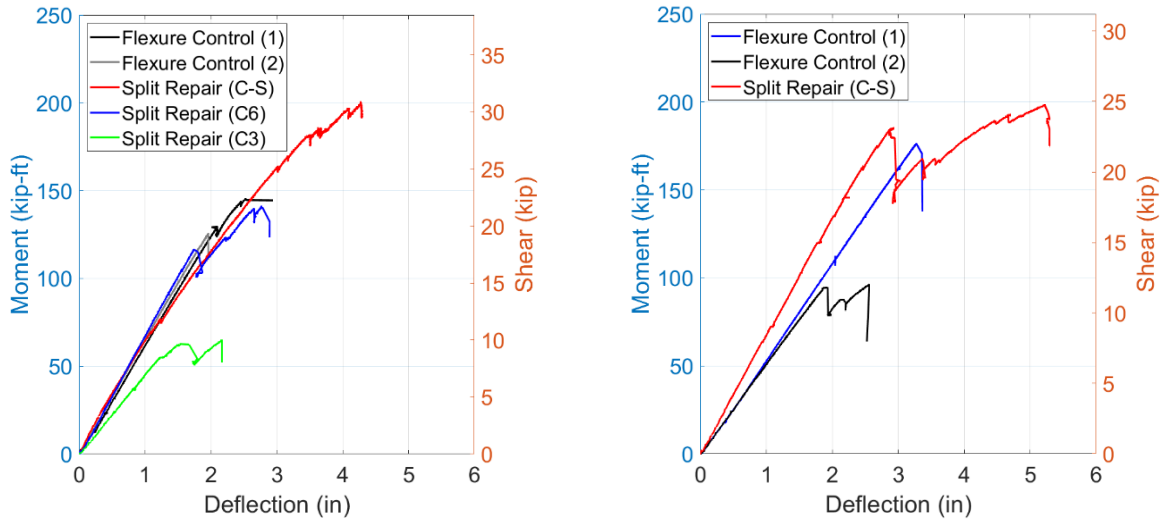

(a) 6”x18” beam data (b) 8”x18” beam data

Figure 91: Comparison of control vs split repair beams

4.2 Shear test-setup beam results

This section discusses the performance of beams tested in the shear setup, including control beams and those that were split-repaired or strengthened with side channels along the entire length of the beam, for both 6”×18” and 8”×18” members. Figure 92 and Figure 93 show the three tested configurations of 6”×18” and 8”x18” timber beams, respectively: control, split repair with channels, and strengthened with channels. The control beam displays the damage from testing. The repair beam is the same beam retrofitted with channels, while the strengthened beam is an intact beam reinforced with channels.

(a) Control – 6-Sh(1)

(b) Split repair – 6-Sh(1)-SR(C)

(c) Strengthened - 6-Sh-St(C)

Figure 92: Control, split repair and strengthened 6”x18” beams with channels only

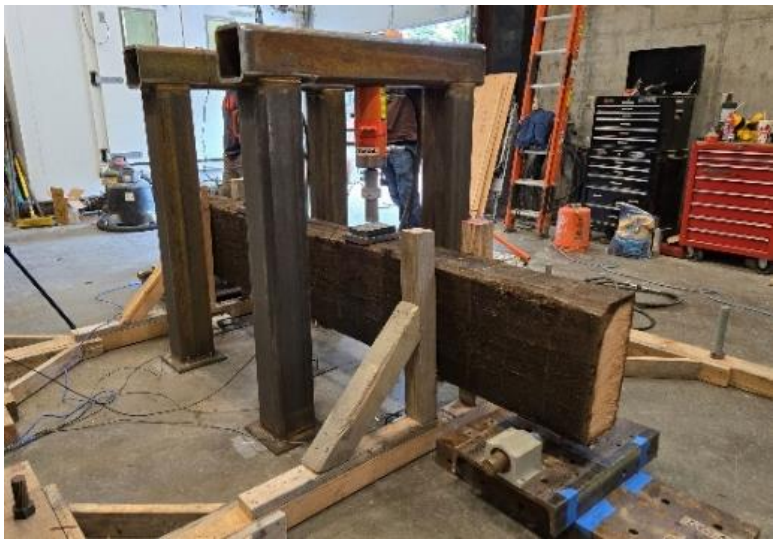

(a) Control – 8-Sh(1)

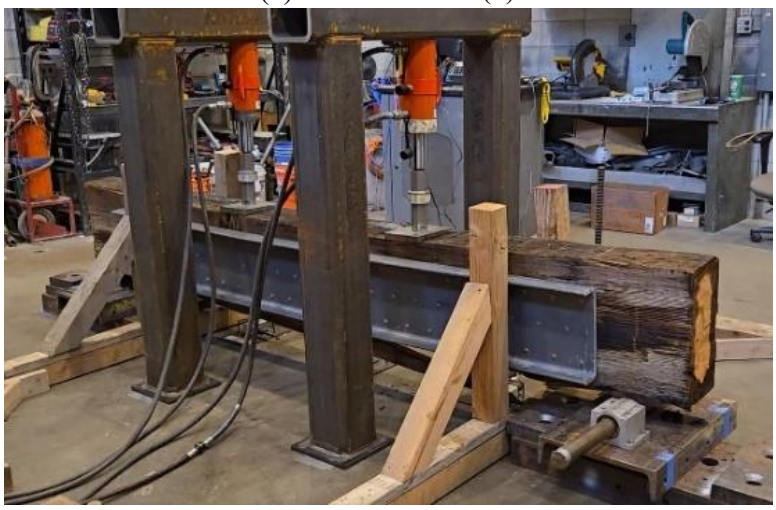

(b) Split repair – 8-Sh(1)-SR(C)

(c) Strengthened - 8-Sh-St(C)

Figure 93: Control, split repair and strengthened 6”x18” beams with channels only

Figure 94-a compares the shear-deflection curves of the three 6”x18” beams tested in this configuration: the control beam (6-Sh(1)), the split-repair (6-Sh(1)-SR(C)), and the strengthened beam (6-Sh-St(C)). The control beam reached an ultimate shear of 27.0 kips with a mid-span deflection of 0.89” before failing abruptly due to the formation of a horizontal split near the supports of the beam. In contrast, the split-repair beam, which had its end split repaired by attaching full-length FRP channels to the sides, demonstrated a more gradual load increase and ultimately bore a higher shear of 30.1 kips at a deflection of about 1.69”. The strengthened beam exhibits the best performance, achieving the highest ultimate shear of 33.2 kips at a mid-span deflection of 1.1”.

Figure 94-b shows the shear-deflection graphs of the three 8”x18” beams tested in this configuration: control beam (8-Sh(1)), split-repair beam (8-Sh(1)-SR(C)), and strengthened beam (8-Sh-St(C)). The control beam exhibited an ultimate shear of 37.9 kips at a mid-span deflection of 0.98” before failing due to a split at its end. In contrast, the split-repair beam (same original control beam repaired with channels on its sides) had an increased shear capacity, reaching 42.3 kips at a mid-span deflection of 1.58”. The most significant improvement is seen in the strengthened beam, which achieved a peak shear of 56.3 kips due to the strengthening channels and initially undamaged state of the beam.

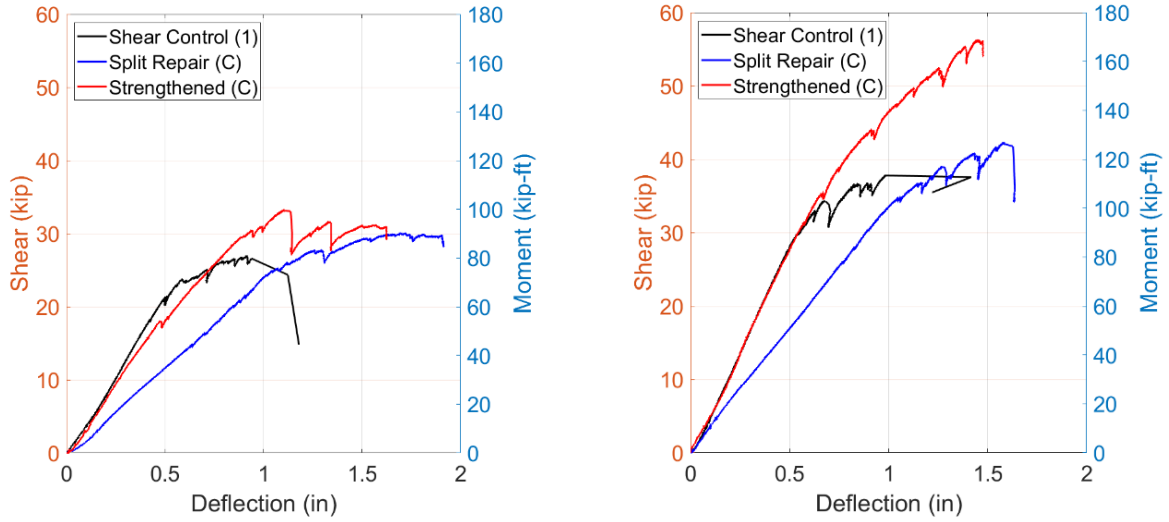

(a) 6”x18” beam data (b) 8”x18” beam data

Figure 94: Comparison of control vs split repair and strengthened beams with channels in shear setup

Another observation from Figure 94 is the distinct differences in initial stiffnesses between the control beams and their repaired counterparts. The split-repair beams exhibited lower stiffnesses than their control counterparts, primarily due to bearing failures that occurred during the original control beam testing. This damage caused significant softening of the wood at the load and support points. Although FRP channels were attached on the sides to repair the splits, the bearing damage itself was not addressed, resulting in greater deflections when the repaired beams were reloaded. In contrast, the initial stiffness of the strengthened beams closely matched that of the control beams, as these beams had not experienced prior bearing damage.

Overall, for both beam sizes, the side-channel repairs restored and modestly increased the shear capacity relative to the control beams, but the repaired beams showed reduced initial stiffness due to the unrepaired

bearing damage from the control-phase failures. The strengthened beams, on the other hand, achieved the highest ultimate shears and closely maintained the initial stiffness of the control beams. These results confirm the effectiveness of applying FRP channels on the sides of timber beams in both restoring and enhancing shear performance after shear-split damage.

4.3 Comparison of repair/strengthening techniques

This section compares the different repair/strengthening techniques for addressing cracks and splits in the 6"x18" and 8"x18" beams. The crack-repair beams are repaired either with the combination of FRP channels on the sides and an FRP strip on the bottom or FRP strips on the sides and bottom. For the 6"x18" beams, the crack-repair beam with channels on the sides and a strip on the bottom (Figure 95-a, red line) demonstrated superior performance compared to the beam repaired with only strips (Figure 95-a, blue line). The combination of channels and strip provided enhanced reinforcement and better moment capacity than the strips alone. Specifically, the channel-strip repair increased capacity by 29.9% over its corresponding control (145.6 to 189.2 kip-ft), while the strip-only repair showed 8.3% improvement (126.1 to 136.5 kip-ft). The added channels contributed additional support, particularly for beams with more severe damage.

Similarly, in the 8"x18" beam set, the repair using channels and a strip (Figure 95-b, red line) outperformed the repair with strips alone (Figure 95-b, blue line). The channel-strip repair led to a 50.5% increase in capacity compared to its control (176.0 to 264.8 kip-ft), whereas the strip-only repair doubled the capacity, showing a 96.7% increase over its respective control (96.0 to 188.8 kip-ft). The 8"x18" beams, with four FRP strips on the sides and one on the bottom, showed that while strips provided substantial improvement compared to the control, particularly because the corresponding control beam underperformed. Overall, the combination of channels and strips offered more significant enhancement, reinforcing the beam more effectively and improving overall structural performance. Control beam capacities are shown as dashed lines in Figure 95 for direct comparison.

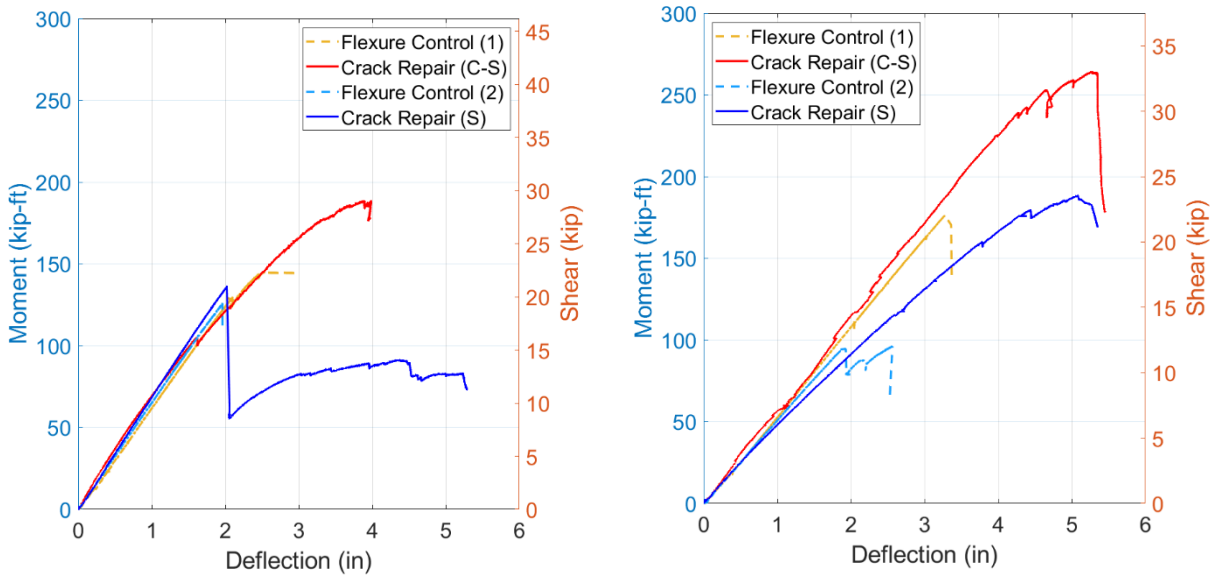

(a) 6"x18" beam data (b) 8"x18" beam data

Figure 95: Comparison of different techniques of crack repair

The comparison between beams strengthened with a channel-strip combination and those strengthened with only strips shows that both techniques performed well, with the channel-strip configuration demonstrating a slight improvement in structural performance for both the 6”x18” and 8”x18” beams. For the 6”x18” beam, the configuration with two channels on the sides and a strip at the bottom (Figure 96-a, red line) achieved an ultimate moment capacity of 182.0 kip-ft, representing a 25% increase over its corresponding control (145.6 kip-ft). The beam strengthened with strips only (Figure 96-a, blue line) reached 165.1 kip-ft, showing a 30.9% increase over its respective control (126.1 kip-ft).

Similarly, for the 8”x18” beam set, the channel-strip strengthened beam (Figure 96-b, red line) achieved an ultimate moment of 255.2 kip-ft, a 45.0% improvement compared to the control (176.0 kip-ft), while the strip-only beam (Figure 96-b, blue line) reached 230.4 kip-ft, marking a 140.0% increase over the control beam (96.0 kip-ft). This higher gain is partly attributed to the relatively lower performance of the corresponding control beam. While the channel-strip combination offers slightly higher moment capacity and improved structural integrity, the strips-only configuration also provided substantial reinforcement, indicating that both strategies are effective in enhancing beam performance. Control beam capacities are shown as dashed lines in Figure 96 for direct comparison.

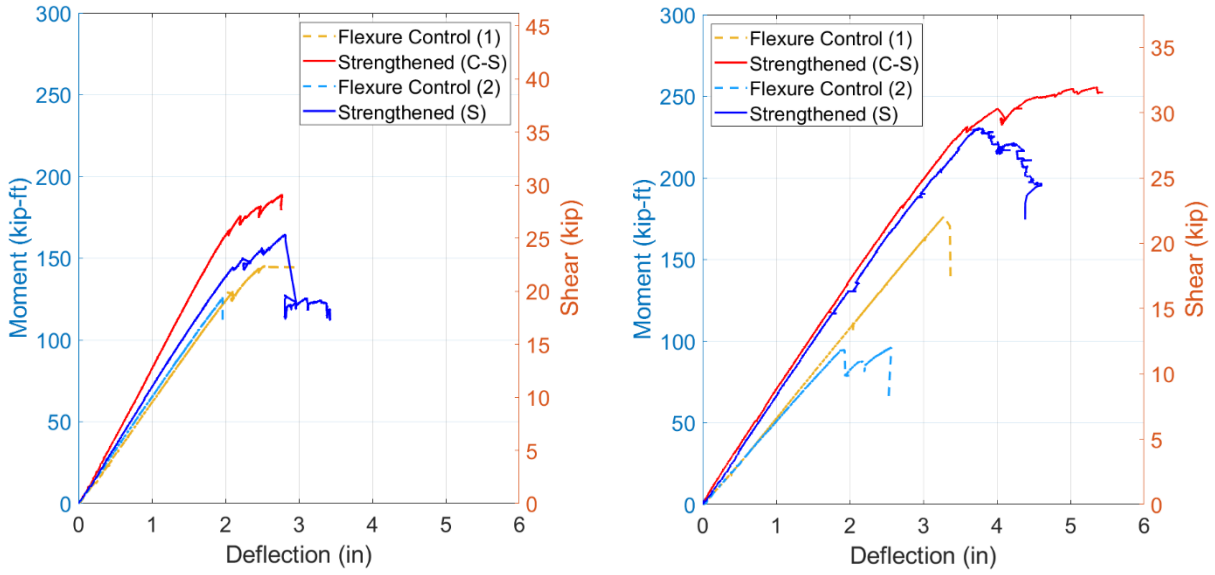

(a) 6”x18” beam data (b) 8”x18” beam data

Figure 96: Comparison of different techniques of strengthening

The comparison of the three split-repair 6”x18” beams, presented in Figure 97, reveals notable differences in performance based on the repair techniques used. The beam repaired with FRP channels on the sides and an FRP strip on the bottom (red line) exhibited the most robust performance, with the highest moment capacity. In contrast, the beam with 6’ channels on the ends of each side (blue line) demonstrated improved shear capacity but struggled with significant tension cracks and compression failures. The beam repaired with shorter 3’ channels on the ends (green line) showed no improvement and underperformed compared to the controls (showed in dashed line Figure 97), as the limited channel length did not adequately support the beam and arrest the split growth, leading to premature failure. Thus, the combination of channels and

strips proved to be the most effective repair method, offering superior reinforcement and performance compared to channel-only approaches.

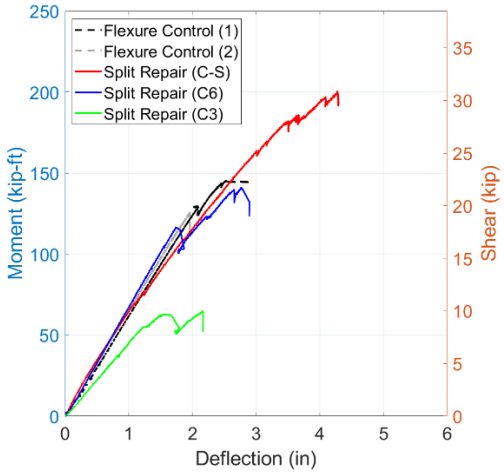

Figure 97: Comparison of different split repair techniques

Overall, the comparison of repair techniques for crack and split repair in both 6”x18” and 8”x18” beams shows that using a combination of FRP channels on the sides and an FRP strip on the bottom consistently outperformed the use of FRP strips alone. However, the strip only repair/strengthening beams still performed well and exceeded control capacities. The added channels significantly improved moment capacity, especially when repairing beams with more severe damage. In split-repair beams, the channels and strip combination proved to be the most effective, offering better structural performance and preventing premature failure, while shorter channel-only repairs were less successful.

4.4 Summary of repaired beams

This section does not present any new data but instead provides a detailed, side-by-side comparison of each beam that was tested, repaired, and retested (6 beams total). Because the same beam was used in both the initial control test and the repaired test, the comparisons directly reflect the effects of the repair methods.

As previously discussed, the 6”x18” and 8”x18” beam sets include three control beams each, one tested in the shear test setup and two in flexure test setups. After the control beams were tested for failure, they were subsequently repaired and retested. The shear setup beams (6–Sh(1) and 8–Sh(1)) failed due to splitting at the ends and were repaired with FRP channels attached to the sides (6–Sh(1)–SR(C) and 8–Sh(1)–SR(C)). The flexure setup beams (6–Fl(1), 8–Fl(1) and 6–Fl(2), 8–Fl(2)) failed due to tension cracking at the bottom mid-span. For the flexure beams, one set (6–Fl(1) and 8–Fl(1)) was repaired with FRP channels on the sides and an FRP strip on the bottom (6–Fl(1)–CR(C-S) and 8–Fl(1)–CR(C-S)). The other set (6–Fl(2) and 8–Fl(2)) was repaired with FRP strips attached on both the sides and bottom (6–Fl(2)–CR(S) and 8–Fl(2)–CR(S)).

For all 6”x18” beams, the repaired beams showed improvements in capacity compared to their respective control beams, highlighting the effectiveness of the repair techniques. The split-repair beam (Figure 98-a, blue line) which had channels attached on the sides, restored and enhanced the shear capacity by approximately 11% compared to the control beam (Figure 98-a, black line), demonstrating that the side

channels effectively mitigated the damage and provided additional shear resistance. In the flexure setup, the crack-repair beam (Figure 98-b, blue line), reinforced with channels on the sides and a strip on the bottom, exhibited a substantial 30% increase in ultimate moment capacity compared to the control beam (Figure 98-b, black line). The crack-repair beam, strengthened with strips on the sides and bottom (Figure 98-c, blue line), showed a 9% increase in moment capacity compared to the control beam (Figure 98-c, black line). Although this was slightly less optimal than the performance of the beam reinforced with both channels and strips, it still demonstrates an effective repair.

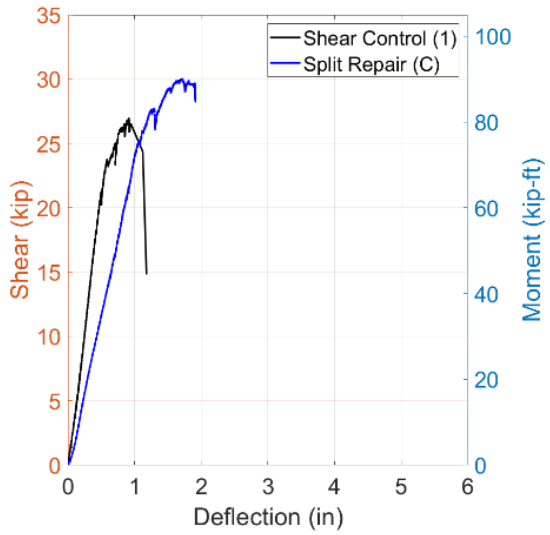

(a) Shear control vs split repaired with channels

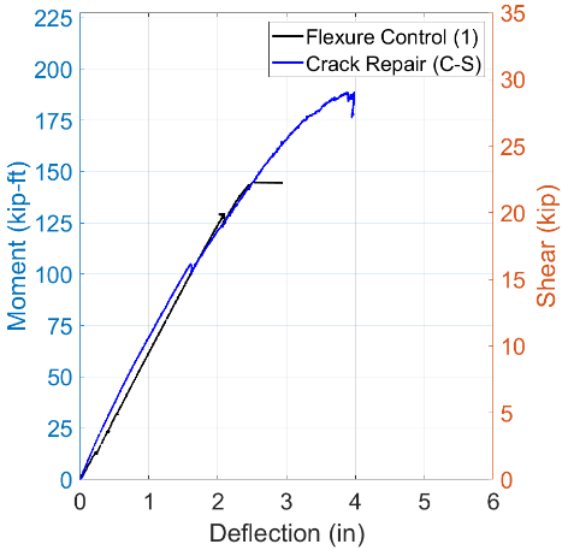

(b) Flexure control vs crack repaired with channels and strip

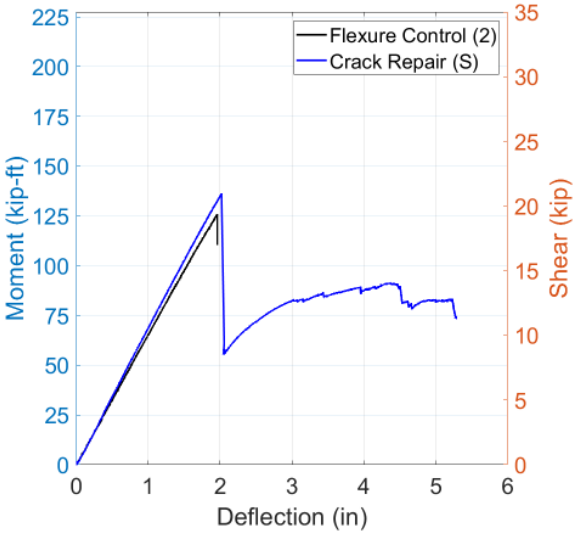

(c) Flexure control vs crack repaired with strip

Figure 98: 6”x18” control vs. repair beam results

The comparison of the control beams and their repaired versions in the 8"x18" beam set reveals significant improvements in capacity due to the repair techniques employed. In the shear setup, the control beam (Figure 99-a, black line) was repaired with channels on the sides (Figure 99-a, blue line), resulting in an

11.5% increase in shear capacity. This enhancement indicates that the side channels effectively repaired the split and strengthened the beam's shear resistance. For the flexure setup, the first control beam (Figure 99-b, black line) was repaired with channels on the sides and a strip on the bottom (Figure 99-b, blue line), which led to a substantial 50.1% increase in moment capacity. This approach significantly reinforced the beam against tension cracking and remarkably improved its performance. Similarly, the second flexure control beam (Figure 99-c, black line) was repaired with strips on the sides and bottom (Figure 99-c, blue line) resulting in an impressive 96.1% increase in moment capacity. The strips effectively confined cracking and greatly enhanced the flexural strength of the beam. However, it is important to note that the 96.1% increase may be artificially high as a result of the repaired capacity being compared with the lower capacity of the second control beam due to the pre-existing checking and wane defects.

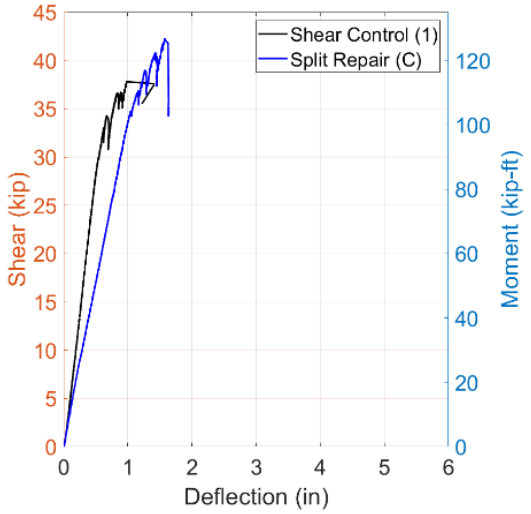

(a) Shear control vs split repaired with channels

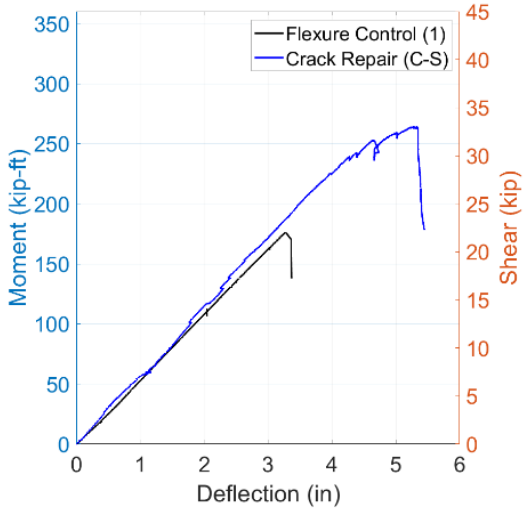

(b) Flexure control vs crack repaired with channels and strip

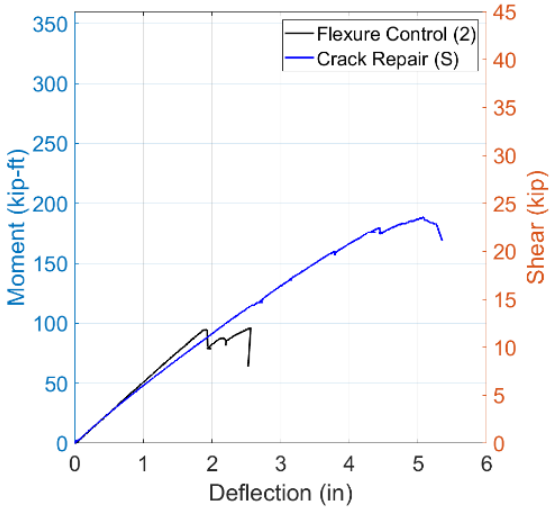

(c) Flexure control vs crack repaired with strip

Figure 99: 8”x18” control vs. repair beam results

Overall, the repair techniques applied to both the 6"x18" and 8"x18" beams restored the original capacities of the control beams, often increasing their capacities by significant amounts, and enhanced their performances. The combination of channels and strips was particularly effective in providing comprehensive reinforcement and resulting in the largest increases in capacity.

4.5 Consistency of Channel-Strip combination technique

The control beams (Figure 100), both 6” and 8”, exhibited variability in their capacities due to the inherent inconsistencies, including grain orientation, and initial internal/external defects, typical for timber members. For the 6” beams, the difference between control beams (145.6 kip-ft and 126.1 kip-ft, respectively) resulted in a variation of approximately 13.4%. The 8” control beams showed even greater variability, with a substantial 45.45% difference between the control beams (176.0 kip-ft and 96.0 kip-ft, respectively), again keeping in mind the lowered capacity of the second control beam likely due to existing initial defects.

In contrast, the beams repaired and strengthened with the FRP channel and strip combination demonstrated notably consistent performance. For the 6” beams (Figure 101-a), the C-S combination resulted in a maximum variation of only 6.19%. The split repair beam (200.9 kip-ft) showed minimal deviation from the crack repair and strengthened beams, both of which achieved an ultimate moment capacity of 189.2 kip-ft. Similarly, the 8” beams (Figure 101-b) exhibited almost identical performance, with the crack repair and strengthened beams reaching ultimate moment capacities of 264.8 kip-ft and 271.2 kip-ft, respectively, showing a minimal variation of 3.63%. While the split repair beam exhibited slightly more variability, with a lower moment of 198.4 kip-ft and a 25.15% difference from the crack repair beam. This consistent performance underscores the effectiveness of applying FRP to timber beams in reducing the inherent variability, providing more reliable structural performance.

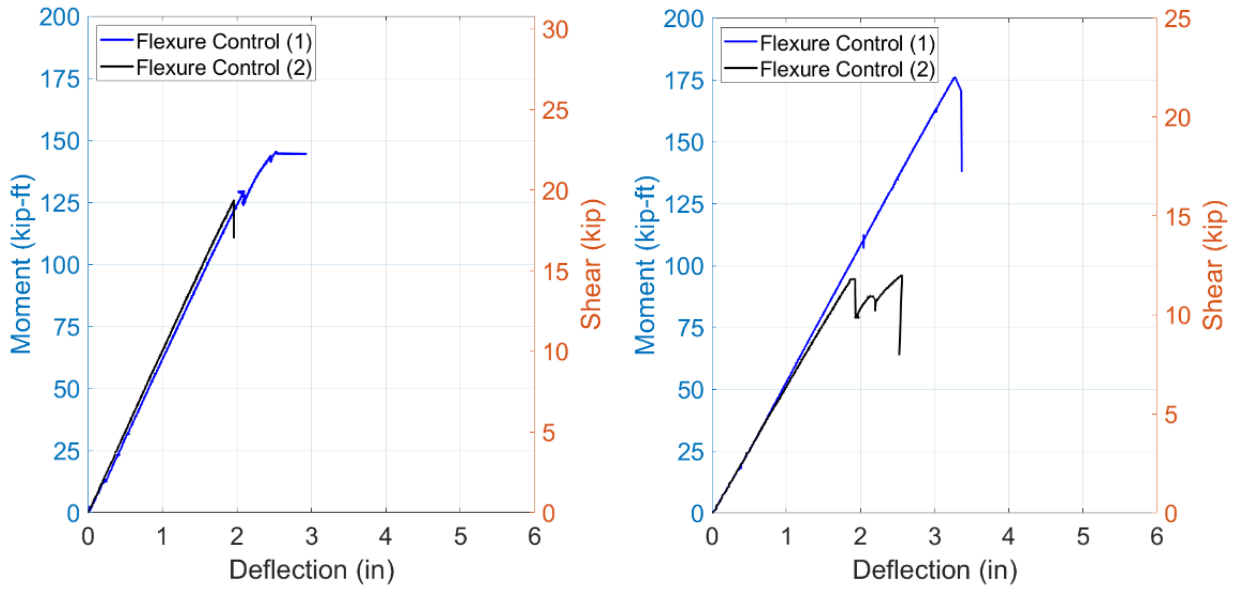

(a) 6”x18” beam data (b) 8”x18” beam data

Figure 100: Moment vs deflection graph of control beams, tested in flexure setup

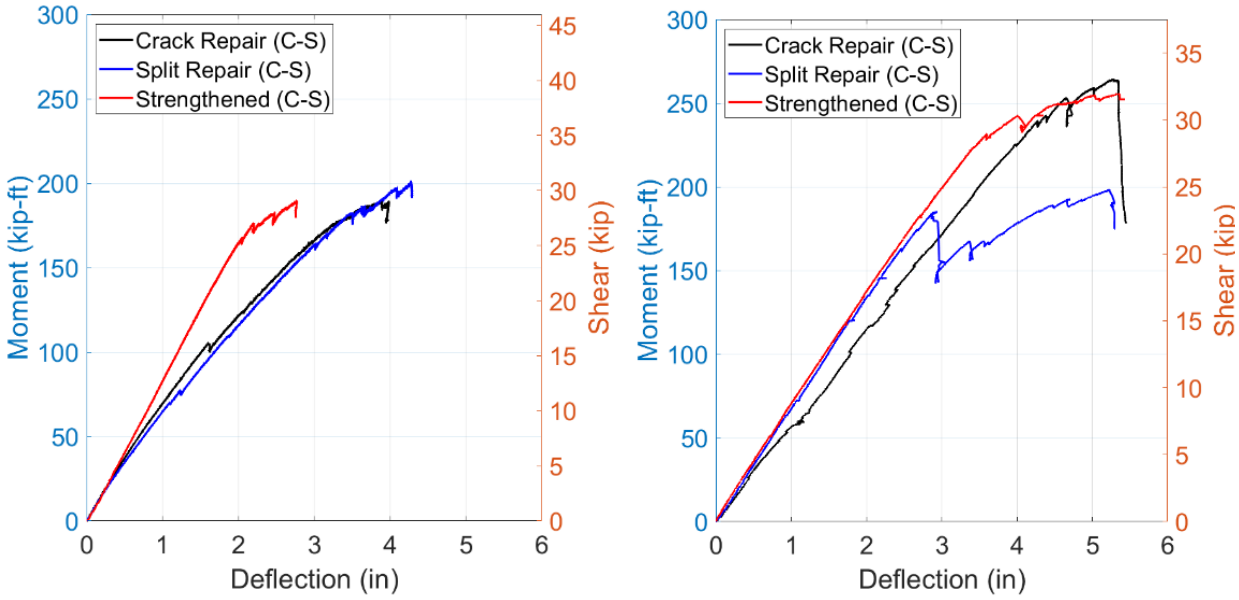

(a) 6”x18” beam data (b) 8”x18” beam data

Figure 101: Moment vs. deflection graph of beams with C-S combination, tested in flexure setup

4.6 Comparison between measured and AASHTO predicted capacities

A comparison between the measured ultimate moments obtained from the experimental test and the calculated moment capacities based on standard design equations is presented in Table 19. The calculations follow procedures outlined in AASHTO Standard Specifications for Highway Bridges (2002), Chapter 13 [51]. This method includes factors that account for load duration, moisture content, lateral support conditions, and other variables influencing timber behavior. For the control timber beams, the baseline allowable bending and shear stresses were adjusted considering the effects of wet service conditions, load duration, member size, volume of stressed wood, lateral stability, non-uniform stress distribution, and repetitive member use. These adjustments produced the design values for bending and shear capacity used in the comparison.

For the FRP-strengthened beams, a transformed-section method was applied to account for the composite action between the timber and FRP components. The transformed section assumed a perfect bond and linear-elastic behavior between materials. Separate modular ratios were calculated for the FRP channels and strips based on their elastic moduli and the adjusted modulus of elasticity of the timber. The composite section was analyzed by transforming FRP widths into equivalent timber, calculating the transformed centroid and moment of inertia, and determining capacity based on the material that governed failure. In both control and strengthened cases, failure was assumed to occur when the stress in timber reached its adjusted allowable limit. More specific details on the calculations can be found in Appendix E.

As shown in the table, the calculated moment capacities are consistently lower than the experimentally measured values, highlighting the conservative nature of standard code predictions. This conservatism is expected: design codes include safety factors and use cautious assumptions to account for uncertainties in material properties, construction quality, and loading conditions. Consequently, all of the tested beams exceeded their calculated capacities, in many cases by a substantial margin.

On average, the 6”x18” beams exhibited a measured-to-calculated moment ratio of 3.1, indicating that the tested beams performed more than three times better than what the design equations predicted. The 8”x18” beams had a slightly lower average ratio of 2.8, which was influenced by one underperforming specimen. Even with this variation, the measured capacities significantly exceeded the calculated ones.

The consistency of the experimental results is also reflected in the coefficient of variation (CoV) values. For the 6”x18” beam group, the CoV is 0.07, indicating highly repeatable performance. In the 8”x18” group, the CoV was 0.31, primarily due to a single underperforming beam. When that outlier is excluded, the CoV drops to 0.10. This supports the reliability of the testing procedure and the overall effectiveness of the strengthening technique.

Table 19: Comparison of Measured and Calculated Moment Capacities

Beam	Measured Capacity (kip-ft)	Calculated Capacity (kip-ft)	Measured/calculated
6-Fl(1)	145.6	46.0	3.2
6-Fl(2)	126.1	46.0	2.7
6-Fl-St(C-S)	189.2	59.4	3.2
6-Fl-St(S)	165.1	51.0	3.2
-	-	Average:	**3.1**
-	-	CoV:	**0.07**
8-Fl(1)	176.0	61.3	2.9
8-Fl(2)	96.0	61.3	1.6
8-Fl-St(C-S)	255.2	75.1	3.4
8-Fl-St(S)	230.4	66.5	3.5
-	-	Average:	**2.8**
-	-	CoV:	**0.31**

4.7 Summary of test results

This experimental test program successfully achieved its objectives by evaluating the feasibility and benefits of fiber-reinforced polymer (FRP) repair and strengthening techniques for timber bridges through full-scale testing of Douglas-fir/Larch beams. Although the sample size was relatively limited, the experimental program was extensive and conducted under realistic loading conditions, providing valuable insights into the structural performance improvements attainable through various FRP applications.

A key takeaway is that the FRP retrofitting strategies explored here restore the original capacity of damaged timber beams and can significantly enhance their strength and stiffness, especially when applied before severe deterioration occurs. This underscores the importance of proactive rehabilitation, as reinforcing intact or lightly damaged members enables more effective composite action and greater performance gains. While the FRP-strengthened and repaired beams exhibit behavior similar to control beams in the linear elastic range, the FRP materials are essential for repairing damage and recovering lost capacity. However, the additional strength provided may not be fully utilized in service, as actual bridge loads are typically shared among multiple members and are unlikely to reach the ultimate capacities observed in laboratory testing.

From an implementation perspective, these findings provide MDT engineers and bridge maintenance professionals (as well as other state DOTs) with clear, actionable guidance for applying FRP repair techniques in the field. The FRP channel and strip combination proved especially effective for both crack and split repairs, offering consistent improvements in load capacity, stiffness, and overall structural reliability. Full-length FRP channels are recommended for end-split repairs to ensure robust shear capacity restoration, while the use of both channels and strips provides optimal results in flexural strengthening and crack repair.

Additionally, the comparison between measured and design-predicted capacities revealed that even control beams outperformed standard code estimates, and FRP-strengthened beams exceeded them by an even greater margin. This confirms the conservative nature of current design codes and indicates that retrofitted members are likely to provide significant reserve capacity, contributing to increased safety and durability.

In summary, this chapter delivered comprehensive results and validated the effectiveness of several FRP-based repair and strengthening methods. The findings equip engineers and practitioners with practical knowledge to select appropriate repair strategies, improve the performance of aging timber infrastructure, and confidently implement FRP solutions in real-world applications.

5. FIELD IMPLEMENTATION

This chapter presents the field implementation of fiber reinforced polymer (FRP) repair techniques on two in-service timber bridges in Montana. As an extension of the laboratory testing phase, this task aimed to evaluate the feasibility, constructability, and efficiency of selected FRP-based repair strategies under real-world conditions. Two timber bridges, located near Toston, Montana, were chosen based on their accessibility, structural condition, and suitability for repair. This chapter documents the decision and implementation processes, including descriptions of each bridge, damage pre-assessment, and step-by-step installation of FRP materials based on the lab-validated procedures. This is followed by details on a post-implementation inspection to evaluate the condition and effectiveness of the repair. The implementation occurred on February 27th, 2025 for both bridges and the post-implementation inspection took place on October 7th, 2025. This practical application verified the methods developed during lab testing and demonstrated their potential for improving the performance and longevity of aging timber bridges.

5.1 Decision Matrix

Based on the experimental program test results discussed in Chapter 4 and the comparative performance of channel–strip (C-S) combination and strip-only (S-only) repairs, a decision matrix was developed to guide the FRP repair techniques selected for the field implementation of this current project, as well as future field implementations. The selection between the C-S combination and the S-only repair method is primarily governed by damage severity and crack characteristics. Girders exhibiting severe flexural cracking or complete fracture benefit from the C-S configuration due to its combined flexural reinforcement and confinement, which improves load distribution and limits crack widening. In contrast, girders with minor, localized cracking can be effectively addressed using the S-only technique, which restores tensile capacity, limits crack propagation, minimizes material use, and allows for faster installation. Table 20 summarizes these considerations and provides a practical framework for selecting an appropriate FRP repair strategy for timber bridge girders based on observed damage conditions and constructability needs.

Table 20: Decision Matrix for FRP Repair Technique Selection

Decision Criterion	Channel–Strip Combination	Strip-Only
Observed Damage Severity	Severe cracking or fully fractured girder	Minor or early-stage cracking
Crack Characteristics	Deep tension-side crack propagating along grain; flexural failure pattern	Localized tension-side crack, often associated with knots or defects
Load Rating Condition	Girder capacity significantly compromised or failed	Crack controls rating but girder otherwise intact
Primary Structural Function	Flexural strengthening **and** confinement	Flexural strengthening
Crack Control and Confinement	Excellent crack mitigation and confinement	Limits crack growth but provides less confinement
Installation Complexity	Low	Low
Constructability	Good	Excellent
Recommended Use Case	Broken girders or advanced flexural damage	Minor cracking
MDT Application	Bridge #06581 (broken girder G9)	Bridge #06583 (minor crack in girder G3)

5.2 Bridge overview and pre-assessment

Two timber bridges, #06581 and #06583, were chosen to implement the FRP repairs for Task 3 of this project. The bridge selections were based on their close proximity to each other, easy accessibility under the bridges, and their structural characteristics. Both bridges are located on State Route S285 over different branches of Crow Creek, a few miles west of Toston, Montana. The specific locations of these bridges are shown in Figure 102.

Figure 102: Bridge locations

Bridge #06581 is a 15’ single-span timber bridge constructed in 1948 and is located two miles west of Toston, Montana [48]. The bridge consists of 13 larch/fir timber girders. The cross section of the girders is 6”x15.5”, which are supported by pile bents. This bridge is an essential crossing over Crow Creek along State Route S285. The superstructure includes a 5.61” timber deck with a bituminous wearing surface. There is no additional membrane or deck protection. Figure 103 shows an image of the bridge, highlighting its structural configuration and surroundings.

An inspection prior to implementation revealed a completely broken timber girder (G9), and preliminary load rating calculations indicated that it would require a load posting if not repaired. A picture of the broken G9 girder is shown in Figure 104.

Figure 103: Bridge #06581

Figure 104: The broken girder G9 (red arrow) on Bridge #06581

Bridge #06583 is a 25’ single-span timber bridge constructed in 1948 and is located six miles west of Toston, Montana [48]. The bridge consists of 13 larch/fir timber girders. The cross-section of the girders consists of a 17.5” height and the widths vary from 7.5” to 7.75”. The bridge has a 24’ roadway width and a 1.5” thick timber deck with a 7” thick asphalt overlay. Figure 105 provides an image of Bridge #06583, showing its structural configuration and surroundings.

Prior to implementation, the bridge had a reduced load rating and was posted for SHV 4-7 axle. The reduced load capacity was based on a minor to moderate crack in one of the girders (G3). Figure 106 shows the pre-repair condition of girder G3.

Figure 105: Bridge #06583

Figure 106: Cracked girder G3 (red arrow) on Bridge #06583

5.3 FRP Materials

As previously discussed, the two FRP materials explored as part of this project include glass fiber-reinforced channels (Figure 107-a) and carbon-glass hybrid FRP strengthening strips (Figure 107-b). Both are manufactured by Strongwell [52]. The materials will be briefly reintroduced here, and more details can be found in Section 3.3 and Appendix D. The glass FRP channels are EXTREN Series 525 and are made with a general-purpose polyester resin that provides excellent corrosion resistance, making them suitable for various structural applications, especially in harsh environmental conditions. The FRP strengthening strip (SAFSTRIP®) is a pultruded composite carbon/glass hybrid and is comprised of carbon tows sandwiched between layers of fiberglass mats and rovings, bonded together by a highly corrosion-resistant vinyl ester resin. The inclusion of carbon fibers increases the stiffness of the strip, while the glass mat provides the necessary bearing strength.

(a) Glass FRP channel

(b) Carbon-glass hybrid FRP strip

Figure 107: FRP materials

5.4 Selected Repair Techniques

The FRP channel and strip (C-S) combination, shown in Figure 108, was selected as the repair method for the broken girder G9 of Bridge #06581. This decision was based on the nature of the crack observed in the girder, which closely resembles the severity of the tension cracks studied in laboratory testing. As shown in Figure 104, the crack in girder G9 originates on the tension face of the beam and propagates at an angle along the wood grain, a pattern commonly associated with flexural failure in timber structures. The C-S combination was chosen due to its proven effectiveness in laboratory testing for addressing this type of failure. The FRP bottom strip enhances flexural strength through reinforcement of the tension zone, whereas the side channels provide supplemental flexural resistance and overall confinement, mitigating crack widening and increasing structural stiffness. This integrated approach ensures better load distribution, mitigates stress concentrations, and enhances the girder's durability.

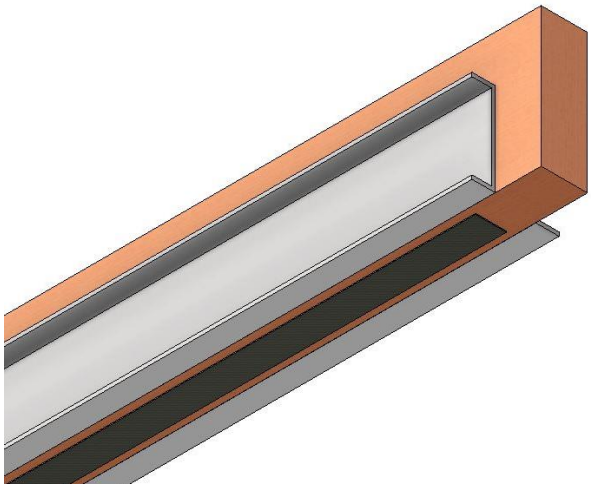

Figure 108: FRP channel-strip combination repair technique

The FRP strip (S-only) technique, shown in Figure 109, was selected as the repair method for girder G3 on Bridge #06583 due to the minor crack currently controlling the load rating. The crack, located on the tension face, indicates early-stage flexural distress, and most likely initiated due to the knot in the timber. Laboratory testing showed that for undamaged or slightly damaged beams, the S-only technique is an effective repair solution. Unlike severely damaged girders, which require additional confinement by the FRP channels, applying the FRP strips significantly improves tensile capacity while minimizing material use and installation complexity. To restore strength and prevent further crack propagation, FRP strips were applied to both the bottom and sides of the girder, reinforcing the tension zone while maintaining the girder's structural integrity.

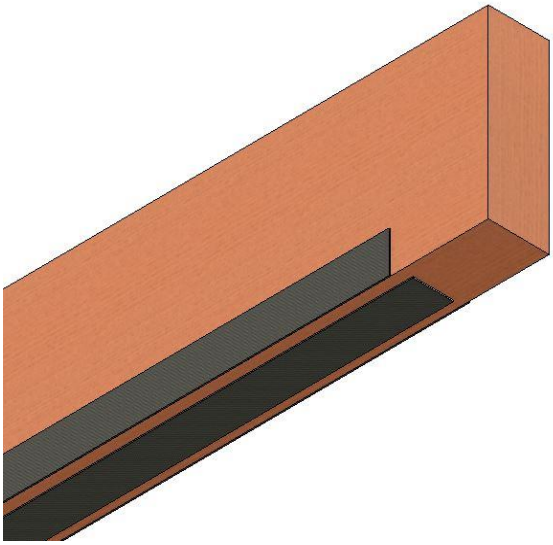

Figure 109: FRP strip-only repair technique

5.5 Safety Consideration

To ensure a safe working environment during the repair process, a lane closure (Figure 110) was implemented on each bridge for the duration of the work. This closure provided a designated staging area for materials, tools, and equipment while accommodating vehicles on-site. Proper Personal Protective Equipment (PPE) was mandatory for all workers, including high-visibility vests and hard hats, to mitigate risks associated with active construction zones. As recommended by the manufacturer, proper masks and gloves should be worn when FRP cuts are being made to avoid inhaling dust and skin irritation. These measures helped maintain a controlled and secure workspace, minimizing disruptions and ensuring the safety of both the repair crew and passing traffic.

Figure 110: Lane closure

5.6 Equipment

The successful implementation of the FRP repairs on the bridges required a carefully selected set of materials, tools, and site-specific equipment to ensure efficient installation. A detailed breakdown of the key items is as follows:

- FRP materials (Figure 111)
    - Girder G9 (Bridge #06581)
        - Two 14’ long GFRP channels
        - One 13.5’ long FRP strip
    - Girder G3 (Bridge #06583)
        - Three 23.5’ long FRP strips
- SPAX Powerlag Screws (Figure 112)
    - 5/16” × 3-1/8” for attaching channels
    - ¼” × 3-1/2” for attaching strips
- Standard saws (Figure 113)
- Impact drivers

More detailed descriptions of each item and installation procedures are provided in the following sections.

(a) Channel

(b) Strip

Figure 111: FRP materials used in the implementation

Figure 112: SPAX Powerlag screws [56]

(a) Circular saw

(b) Reciprocating saw

Figure 113: Standard saws

Due to the locations of the bridges over Crow Creek, an access platform (Figure 114) was installed to facilitate work over the water for Bridge #06581. In contrast, Bridge #06583, located over a shallow creek branch that was dry during implementation, did not require an access platform.

Figure 114: Access platform for Bridge #06581

5.7 Installation Procedure

This section summarizes the step-by-step installation procedures for both bridges that occurred on February 27th, 2025.

5.7.1 Installation procedure for bridge #06581

The predrilled FRP channels and bottom strip were cut to fit the 15’ span timber beam. Because the beam was slightly skewed, the side channels were cut to two different lengths: 175” and 174”, using a reciprocating saw with wood blade (Figure 115-a). The bottom strip was cut to 168” using a circular saw (Figure 115-b).

(a) Channel (b) Strip

Figure 115: Cutting the FRP materials

The FRP channels were notched at both ends using a circular saw to avoid interference with the pile caps located at both ends and to facilitate placement on the timber girders (Figure 116). One channel was notched 3”x3.5” at both ends, while the other was notched 3”x3” at both ends. These notch sizes were determined in the field based on the specific dimensions at each end of the girder, with the goal of spanning as much of the girder as possible on both sides.

(a) Notching FRP channel end

(b) Installed FRP channel on girder

Figure 116: Example notched end

The beam surface was cleaned, and the dirt, debris, and loose material were removed. Cross bracing, nests, and other obstructions were also removed to ensure a clear working area for the FRP installation. Following this, the crack in the broken beam was closed using long GRK connectors. Figure 117 shows the surface preparation of the beam and installation of screws to close the gap and secure the crack.

(a) Before

(b) After

Figure 117: Surface preparation of girder G9 on Bridge #06581

The strip was held in place, along the bottom of the girder, while initial connectors were secured at midspan. Once positioned, the remaining connectors were installed, working from the center toward both ends to maintain a tight fit and keep the strip straight. The entire process took approximately five minutes using three impact drivers.

Subsequently, the channels were installed on both sides of the girder. Each channel was manually positioned and stabilized as initial connectors were fastened to maintain proper alignment. The remaining connectors were then installed along the full length of each channel. Installation of each channel required approximately 15 minutes, using three impact drivers. The attachment of the strip and channel are shown in Figure 118 and Figure 119, respectively. The complete repair of girder G9 on Bridge #06581 is shown in Figure 120.

Figure 118: Attaching bottom strip on girder G9, Bridge #06581

Figure 119: Attaching side channel on girder G9, Bridge #06581

(a) Girder side (b) Girder bottom

Figure 120: Repaired girder G9 on Bridge #06581

5.7.2 Installation procedure for bridge #06583

No cutting was required for the predrilled FRP strips installed on Bridge #06583. All three strips were 23.5’ (282”) in length, consistent with the dimensions used in laboratory testing.

The beam surfaces were thoroughly cleaned to ensure proper bonding and installation of the FRP strips. Cross bracings, nests, debris, and loose material were removed from the area. Existing nails were extracted using a claw hammer. The surface preparation also included closing the gap in the broken beam using long GRK connectors. Figure 121 shows the surface preparation of girder G3 on Bridge #06581.

(a) Removing bracings (b) Existing nails (c) Closing the crack

Figure 121: Surface preparation of girder G3 on Bridge #06581

The FRP strips were installed along the bottom and sides of the timber girder. The bottom strip was centered and held in place while initial connectors were secured at midspan (Figure 122). Once aligned, the remaining connectors were installed outward from the center to each end, ensuring the strip remained taught.

Figure 122: Attaching the bottom strip

The side strips were installed with an approximate 1” offset on each side to avoid screw overlap. Figure 123 shows the end of the bottom and side strips. The strips were installed to be flush with the bottom of the girder; however, a slight offset of approximately 0.25” was observed at midspan due to the pre-existing dead load deflection of the timber beam (Figure 124) and the strip being initially straight. This process took approximately five minutes per strip using three impact drivers. The complete repair of girder G3 on Bridge #06583 is shown in Figure 125.

Figure 123: End of the bottom and side strips

Figure 124: Approximately 0.25" FRP offset at midspan

Figure 125: Repaired girder G3 on bridge #06583

5.8 Implementation Timeline

The field implementation for both bridges was completed on the same day. For Bridge #06581, the process began with surface preparation, followed by cutting and preparing the strip and channels. The bottom strip was installed first, then the two channels were individually prepared and attached to the sides of the girder using three impact drivers. A detailed breakdown of the task schedule is provided in Table 21.

Table 21: Timeline of field implementation for Bridge #06581 (~1.5 hours)

Task description	9:20 AM	9:25 AM	9:30 AM	9:35 AM	9:40 AM	9:45 AM	9:50 AM	9:55 AM	10:00 AM	10:05 AM	10:10 AM	10:15 AM	10:20 AM	10:25 AM
Surface preparation														
Cutting/preparing strip														
Attaching strip (three drivers)														
Cutting/preparing 1st channel														
Attaching 1st channel (three drivers)														
Cutting/preparing 2nd channel														
Attaching 2nd channel (three drivers)														

For Bridge #06583, the process also began with surface preparation, followed by the installation of three strips: one along the bottom and one on each side of the girder. Each strip was secured using three impact drivers, starting at midspan and working toward the ends to ensure proper alignment. A detailed breakdown of the task schedule is provided in Table 22.

Table 22: Timeline of field implementation for Bridge #06583 (~30 minutes)

Task description	11:20 AM	11:25 AM	11:30 AM	11:35 AM	11:40 AM	11:45 AM	11:50 AM
Surface preparation							
Attaching bottom strip (three drivers)							
Attaching 1st side strip (three drivers)							
Attaching 2nd side strip (three drivers)							

All FRP strips and channels used in the field were predrilled during lab testing. If layout and drilling were done on-site, it would add approximately 1 hour per bridge. Also, the access platform was installed the day before for efficient working conditions during the repair.

5.9 Inspection

The FRP-repaired bridges west of Toston, MT were inspected on October 7th, 2025, approximately seven months after installation. Each bridge had one cracked or broken girder that was repaired using pultruded FRP sections, and both were evaluated for overall condition and signs of deterioration. As seen in the following photographs (Figure 126 and Figure 127), no major issues were observed, and the FRP materials appeared mostly unchanged from the day they were installed, with no evidence of cracking, delamination, or fastener location deterioration. Additionally, in a few select locations, fasteners were removed to inspect the fastener holes and confirm there were no signs of cracking or deterioration around the fastener locations or to the fasteners themselves. These checks verified that the FRP and fasteners remained intact and undamaged (Figure 128, Figure 129, and Figure 130), with no evidence of moisture intrusion or material degradation at the connection points. All fasteners were replaced after the photographs were taken. The only noted condition during the inspection was the accumulation of bird droppings on the flanges of both channels on Bridge #06581 (Figure 131), where birds have been roosting. Otherwise, the FRP systems and surrounding timber remained in excellent condition, indicating good performance of the repair under field conditions. However, it should be noted that this inspection took place only seven months after installation, prior to the materials experiencing a full winter season.

Future inspections of the FRP-repairs should focus on locations most susceptible to environmental exposure and localized damage, particularly fastener locations and cut ends of the FRP members. For the pultruded channels, inspections should include checks for exposed fibers due to any new severe surface abrasion. For the strengthening strips, inspectors should look for signs of splitting, delamination, or surface damage. The fastener holes and termination locations represent potential pathways for moisture ingress and therefore should receive particular attention during routine bridge inspections. If minor surface damage or fiber exposure is observed, sealing the affected area with a thin polyurethane coating or comparable protective sealant is recommended by the manufacturer to prevent moisture penetration and limit further deterioration. For future applications including external girders exposed to frequent wetting and drying cycles, additional protection may be provided by sealing fastener holes and cut ends after pre-drilling, but before installation. Incorporating these inspection and maintenance practices into routine bridge inspection protocols will support the long-term durability of the FRP repair systems.

(a) Day of initial installation

(b) Day of post-implementation inspection

Figure 126: Before and after photographs of repaired girder G9 on Bridge #06581

(a) Day of initial installation

(b) Day of post-implementation inspection

(c) Day of post-implementation inspection

Figure 127: Before and after photographs of repaired girder G3 on Bridge #06583

(a) Removed fastener location on channel

(b) Close-up view of fastener hole

(c) Fastener

Figure 128: Removed channel fastener on Bridge #06581

(a) Removed fastener location on strip

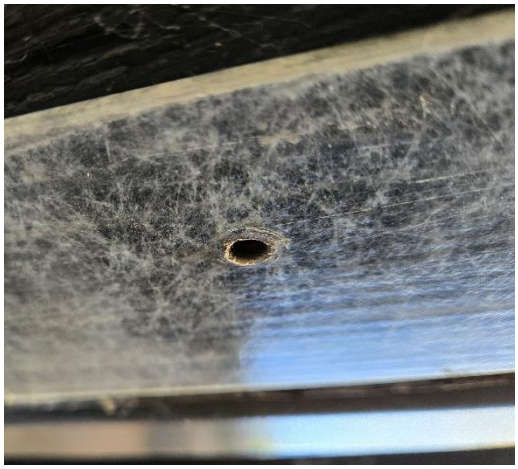

(b) Close-up view of fastener hole

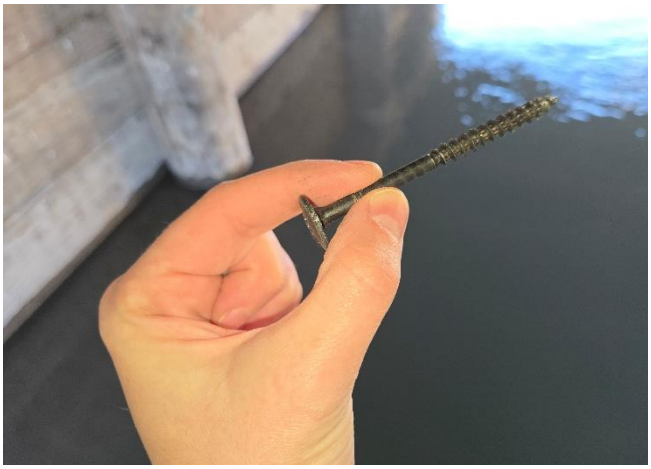

(c) Fastener

Figure 129: Removed strip fastener on Bridge #06581

(a) Close-up view of fastener hole

(b) Fastener

Figure 130: Removed strip fastener on Bridge #06583

Figure 131: Bird droppings accumulated on FRP channel on Bridge #06581

5.10 Summary

This chapter presented the field implementation of FRP repair techniques on two damaged timber bridges in Montana. The objective of this part of the project was to apply and evaluate lab-validated repair methods in real-world conditions to improve the structural performance of the bridges and guide future applications.

Two single-span timber bridges, #06581 and #06583, located along State Route S285 over Crow Creek, near Toston, Montana, were selected based on their close proximity, easy accessibility, and the damaged conditions of the bridges. Pre-assessment revealed a fully broken girder on Bridge #06581 and a minor crack in a girder on Bridge #06583, both located on the tension face of the girders.

Based on damage severity, two repair techniques were used: a channel-strip (C-S) combination for Bridge #06581 and a strip-only (S-only) approach for Bridge #06583. All FRP materials were predrilled during lab testing. Standard tools such as circular saws, reciprocating saws, and impact drivers were used, along with SPAX connectors for connection.

The installation process included surface preparation and preparing and securing the FRP components. The bottom strip and side channels were installed sequentially on Bridge #06581, while three strips were attached to the bottom and sides of the girder at Bridge #06583. Both installations were completed efficiently using three impact drivers.

Safety was maintained through lane closures, use of PPE, and designated work zones. The full implementation for both bridges was completed on the same day. Bridge #06581 required approximately

1.5 hours for surface preparation and FRP installation, while Bridge #06583 was completed in about 30 minutes.

Notably, the FRP repairs restored sufficient strength to both bridges to avoid further load postings, preventing weight restrictions that could have disrupted local traffic movement. This outcome highlights the effectiveness of the repair approach in preserving bridge functionality and extending service life with minimal intervention.

A post-implementation inspection was conducted approximately seven months after installation, to assess the in-service performance of the FRP repairs. Both bridges showed no visible signs of deterioration or distress in the repaired girders. The FRP materials appeared unchanged from the time of installation, with no evidence of cracking or fastener location deterioration. A few fasteners were removed (and then replaced) and no cracking or degradation was observed around the fastener holes. The only condition noted was the accumulation of bird droppings along the FRP channels where birds have been roosting. Overall, the repairs remain in excellent condition, indicating good durability and performance under initial field exposure. Consistent with the manufacturer's recommendations, future inspections should pay particular attention to fastener locations, cut ends, and any exposed fibers, and minor surface damage may be addressed by sealing the affected areas with a thin polyurethane or comparable protective coating to prevent moisture intrusion and long-term deterioration.

This successful field application demonstrates the feasibility and efficiency of FRP repairs for deteriorated timber girders and provides a guideline for similar future rehabilitation projects.

6. SUMMARY AND CONCLUSIONS

This research project investigated the use of pultruded fiber-reinforced polymer (FRP) composites to repair and strengthen deteriorated timber bridge girders. The primary goal was to develop effective, lightweight, and field-applicable retrofit solutions to extend the service life of aging timber bridge infrastructure in Montana. The research combined a comprehensive literature review, full-scale laboratory testing, and field implementation to evaluate the performance and applicability of FRP systems.

The literature review highlighted the potential of retrofitting deteriorated timber beams using pultruded FRP sections with mechanical fasteners and its efficient installation process, especially compared to traditional wet lay-up systems. These insights guided the next phases of this investigation. This chapter summarizes the major findings from the experimental test results and field implementation.

6.1 Experimental test results

This section details the conclusions of the experimental test results. This study evaluated the use of FRP repairs on timber bridge girders through full-scale testing of salvaged Douglas-fir/Larch beams. Two groups of beams, sized 6”x18” and 8”x18”, were tested in both flexure and shear. These groups included undamaged control beams, pre-existing/induced (cracks or splits) damage repair beams, and undamaged beams strengthened with FRP. Material tests were also conducted on the FRP components to confirm their mechanical properties. The capacity comparisons demonstrated that the FRP repair and strengthening techniques provided notable improvements in material performance, flexural and shear capacity, consistency in structural response, and design reliability. The key findings are summarized below:

- FRP material performance

Tensile tests on FRP coupons confirmed excellent strength and stiffness retention after undergoing full scale testing on the beams. Virgin GFRP channel coupons exceeded manufacturer values, achieving 177% of the reference tensile strength and 164% of the reference modulus. Channel coupons extracted from mid-span and end-regions of tested beams still retained over 150% of expected strength and over 120% of stiffness. Hybrid FRP strips also remained within ±10% of the tabulated values, confirming their durability and consistent mechanical performance.

- Flexural capacity gains

The application of FRP channels and strips significantly improved the flexural performance of timber beams. For 6”x18” beams, crack-repair using the channel-strip (C-S) combination method resulted in a 29.7% increase in moment capacity, while strengthening of undamaged beams with the same configuration yielded a 29.9% improvement. In the 8”x18” group, crack-repair beams showed a 45% gain, and strengthened beams achieved a 50% increase over the controls.

FRP strips used alone (S-only) also proved effective, though to a lesser extent in the smaller beams. For 6”x18” beams, crack-repair with strips produced an 8.4 % improvement, and S-only strengthening achieved a 30.9 % increase. For 8”x18” beams, crack-repair using strips resulted in a 96.1 % increase, while S-only strengthened beams exhibited a 139.9% gain. These results confirm that FRP significantly enhances flexural strength, particularly when applied to intact or lightly damaged beams.

- Addressing shear splits

FRP channels provided effective restoration and improvement in the shear capacity for beams with end splits. In 6”x18” beams tested in shear setup, split repair using full-length channels improved capacity by 11.3%, while channel strengthening of undamaged beams achieved a 23.1% increase. For 8”x18” beams tested in shear setup, split-repair beams gained 11.5 %, and strengthened beams demonstrated a 48.5% improvement in shear capacity compared to controls.

Additional testing on beams with existing splits reinforced the value of combining channels and strips. For 6”x18” beams tested in flexure setup, this approach resulted in moment capacity increases of 37.9% and 59.4%. For 8”x18” beams tested in flexure, gains of 12.5% and 106.2% were observed. In contrast, split repair with 6’ channels restored capacity to 97.1% and 112.2% of the controls, while 3’ channel repairs underperformed. These findings emphasize the importance of using full-length channels when feasible for reliable split repair and shear strengthening, and 6’ minimum end channels when full length is not feasible.

- Channel-strip combination provided more effectiveness than strip-only

For crack repair, the C-S configuration significantly outperformed the S-only method, improving moment capacity by 29.9% (6”x18”) and 50.5% (8”x18”), compared to 8.3% and 96.7% gains from S-only repairs. For strengthening, both techniques enhanced capacity, with the C-S method achieving 25.0% (6”x18”) and 45.0% (8”x18”) improvements, while S-only strengthening showed 30.9% and 140.0% gains, respectively. The higher gain in the 8”x18” S-only case was influenced by an underperformed control, reaffirming the consistent advantage of the C-S method across conditions.

Despite the superior capacity and more consistent performance of the C-S configuration, the S-only technique still offers notable advantages. Its lighter weight and ease of installation make it a practical and cost-effective option, particularly in scenarios where access, equipment limitations, or installation time are critical factors. As such, the S-only method may still be the preferred choice in certain applications.

- FRP repaired pre-tested beams effectively

The capacities of the pretested 6”x18” and 8”x18” beams repaired with FRP were restored to their original capacities and often achieved significant improvements. For 6”x18” beams, C-S crack repair increased capacity by 29.7%, while S-only repair showed an 8.4% improvement, and channel split repairs achieved an 11.3 % increase. In 8”x18” beams, C-S crack repair achieved a 50.0% increase, S-only repair improved by 96.1%, and channel split repair showed an 11.5% enhancement.

- FRP enhanced consistency in structural performance

Although the number of test specimens was limited, the beams repaired or strengthened with C-S combination demonstrated reduced variability and more consistent performance compared to the control beams. For the 6”x18” beams, the controls exhibited a 13.4% variation, while the C-S repairs significantly improved consistency. Both the C-S crack repair and strengthened beams reached the same capacities. For the 8”x18” beams, the control group showed a much higher variation of 45.45%. In contrast, the C-S beams had improved consistency, with only a 3.63% difference between the crack repair and strengthened beams. The channel placement for the split repair beams differed slightly (at mid-height). Despite this difference, the results remained comparable, showing 6.19% and 25.15% difference between the split repair and crack repair cases for the 6”x18” and the 8”x18” beam, respectively.

- Measured vs. calculated capacities

The comparison between measured and calculated moment capacities clearly demonstrated that the tested beams outperformed code-based predictions by a wide margin, with 6”x18” beams showing an average measured-to-calculated ratio of 3.1, and 8”x18” beams exhibiting a ratio of 2.8. This highlights the inherent conservatism of standard design codes, which intentionally include safety factors to ensure structural reliability.

6.2 Field implementation

This section documents conclusions from the successful field implementation of FRP repair techniques on two damaged timber bridges in Montana. The objective was to translate lab-validated methods into practical repairs that could restore girder capacity, maintain serviceability, and provide guidance for future bridge rehabilitation.

- Bridge #06581, which had a fully broken girder, was repaired using a channel-strip combination configuration, while bridge #06583, with only a minor crack, was repaired using a strip-only approach. This demonstrated that FRP repair strategies can be tailored to different levels of deterioration/damage.
- Both installations were completed on the same day using standard tools and SPAX connectors. Bridge #06581 required about 1.5 hours for surface preparation and installation, while bridge #06583 was completed in just 30 minutes, showing that FRP systems can be deployed quickly with minimal disruption.
- The repairs restored sufficient strength to both bridges to prevent load posting. By avoiding weight restrictions, the project ensured continued traffic flow on State Route S285, benefiting the local community and preventing potential disruptions.
- A post-implementation inspection conducted approximately seven months after installation revealed that neither bridge showed any visible signs of deterioration or distress in the repaired girders.

Overall, this field application confirmed the feasibility and efficiency of FRP repairs for deteriorated timber girders. The combination of quick installation, minimal resource demand, and restored serviceability highlights FRP as a sustainable and cost-effective solution for bridge preservation.

6.3 Summary

Overall, this study demonstrated the feasibility and effectiveness of using pultruded FRP to retrofit deteriorated timber bridge girders. Building on the promising results from the experimental phase, the field implementation successfully applied the developed repair techniques to two in-service bridges in Montana. The post-implementation inspection revealed that the repairs remain in excellent condition, indicating good durability and performance under initial field exposure.

7. REFERENCES

[1] F. C. McCormick, "Why not Plastic Bridges," *J. of Structural Division,* vol. 98, pp. 1757-1767, 1972.

[2] L. C. Bank, "Application of FRP Composites to Bridges in the USA.," *Proceedings of the International Colloquium on Application of FRP to Bridges,* vol. 1, pp. 9-16, 2006.

[3] H. H. Mhanna, R. A. Hawileh, and J. A. Abdalla, "Shear strengthening of reinforced concrete beams using CFRP wraps.," *Procedia Structural Integrity,* vol. 17, pp. 214-221, 2019.

[4] R. Nandhini, M. M. Saravanan, and A. Karunya Grace, "Retrofitting of concrete structures using fiber-reinforced polymer (FRP): A review," *International Journal of Scientific and Technology Research,* vol. 9, no. 2, pp. 1694–1700, 2020.

[5] W. Frankhauser, K. Jamal Elkaissi, S., , S. McMillan *et al.*, "Advances in fiber-reinforced polymer composites in transportation infrastructure.," 2015.

[6] M. Chajes, T. Rollins, H. Dai *et al.*, *Report on Techniques for Bridge Strengthening: Main Report*, 2019.

[7] R. Sen, "Advances in the application of FRP for repairing corrosion damage," *Progress in Structural Engineering and Materials,* vol. 5, no. 2, pp. 99-113, 2003.

[8] J. F. Davalos, K. E. Barth, I. Ray *et al.*, *DISTRICT 3-0 Investigation of fiber-wrap technology for bridge repair and rehabilitation (Phase-I)*, 2006.

[9] B. M. Ehsani, M. Farahani, and E. Raatz, "Repair of columns with FRP laminates," *Structure Magazine*, pp. 35-37, 2012.

[10] A. Ghaffary, and M. A. Moustafa, "Synthesis of Repair Materials and Methods for Reinforced Concrete and Prestressed Bridge Girders," *Materials,* vol. 13, no. 18, Sep, 2020.

[11] ACI, "440.2R-17, Guide for the Design and Construction of Externally Bonded FRP Systems for Strengthening Concrete Structures," American Concrete Institute, 2017.

[12] A. Aiswarya, and P. Prabhakaran, "A Review on Strengthening of RC Beams Using Near Surface Mounted (NSM)," *International Journal of Innovative Research in Science, Engineering and Technology,* vol. 6, no. 4, pp. 60-64, 2017.

[13] S. Chołostiakow, and R. Kotynia, "Flexural strengthening of RC beams by using a near surface mounted T-section profiles," *Budownictwo i Architektura,* vol. 13, no. 3, pp. 071-078, 2014.

[14] M. A. Hosen, M. Z. Jumaat, U. J. Alengaram *et al.*, "Near Surface Mounted Composites for Flexural Strengthening of Reinforced Concrete Beams," *Polymers (Basel),* vol. 8, no. 3, Mar 3, 2016.

[15] A. M. Khalifa, "Flexural performance of RC beams strengthened with near surface mounted CFRP strips," *Alexandria Engineering Journal,* vol. 55, no. 2, pp. 1497-1505, Jun, 2016.

[16] M. Sarafraz, and F. Danesh, "Use Near Surface Mounted FRP Rods for Flexural Retrofitting of RC Columns," *Advances in Frp Composites in Civil Engineering*, pp. 833-836, 2010.

[17] A. Prota, A. Nanni, G. Manfredi *et al.*, "Seismic Upgrade of Beam-Column Joints with FRP Reinforcement," *Industria Italiana del Cemento*, pp. 1-17, 2000.

[18] A. Hosny, H. Shaheen, A. Abdelrahman *et al.*, "Performance of reinforced concrete beams strengthened by hybrid FRP laminates," *Cement & Concrete Composites,* vol. 28, no. 10, pp. 906-913, Nov, 2006.

[19] A. Morsy, and E. Mahmoud, "Bonding techniques for flexural strengthening of R.C. beams using CFRP laminates," *Ain Shams Engineering Journal,* vol. 4, no. 3, pp. 369-374, Sep, 2013.

[20] W. Wenwei, and L. Guo, "Experimental Study of RC Beams Strengthened with CFRP Sheets Under Sustaining Loads. ," *Journal of Wuhan University of Technology,* vol. 21, no. 3, pp. 28-31, 2006.

[21] R. Sadone, M. Quiertant, E. Ferrier *et al.*, "Anchoring FRP laminates for the seismic strengthening of RC columns," *International Conference on Concrete Repair, Rehabilitation and Retrofitting - ICCRRR 2012*, 2013.

[22] Anthony J. Lamanna, Lawrence C. Bank, David T. Borowicz *et al.*, "STRENGTHENING OF CONCRETE BEAMS WITH MECHANICALLY FASTENED FRP STRIPS," 2002.

[23] G. W. C. III, *ASSESSMENT OF MECHANICALLY FASTENED FIBER REINFORCED POLYMER (MF-FRP) STRIPS FOR EXTENDING BRIDGE SERVICE LIFE*, Vermont Agency of Transportation Research & Development Section, 2015.

[24] Alyssa E. Schorer, Lawrence C. Bank, Michael G. Oliva *et al.*, *FEASIBILITY OF REHABILITATING TIMBER BRIDGES WITH MECHANICALLY FASTENED FRP STRIPS*, Midwest Regional University Transportation Center, University of Wisconsin-Madison, 2008.

[25] R. Kalfat, R. Al-Mahaidi, and S. T. Smith, "Anchorage Devices Used to Improve the Performance of

Reinforced Concrete Beams Retrofitted with FRP

Composites: State-of-the-Art Review," *Journal of Composites for Construction,* vol. 17, 2013.

[26] T. M. Pham, and H. Hao, "RC beams strengthened with longitudinal and U-wrap FRP," *Proceedings of the 8th International Conference on Fibre-Reinforced Polymer (FRP) Composites in Civil Engineering, CICE 2016*, pp. 1356–1361, 2016.

[27] J. Lee, and M. Lopez, "Application of Frictional Bond-Slip Model to Large-Scale FRP-Strengthened T-Beams with U-wraps," *International Journal of Concrete Structures and Materials*, 2020.

[28] Dionysios A. Bournas, Alberto Pavese, and W. Tizani, "Tensile capacity of FRP anchors in connecting FRP and TRM sheets to concrete," *Engineering Structures,* vol. 82, pp. 72-81, 2015.

[29] H. Y. Lee, W. T. Jung, and W. Chung, "Flexural strengthening of reinforced concrete beams with pre-stressed

near surface mounted CFRP systems," *Composite Structures,* vol. 163, pp. 1-12, 2017.

[30] R. El-Hacha, R. G. Wight, and M. F. Green, "Prestressed carbon fiber reinforced polymer sheets for strengthening concrete beams at room and low temperatures," *Journal of Composites for Construction,* vol. 8, no. 1, pp. 3-13, Jan-Feb, 2004.

[31] R. Al-Mahaidi, and R. Kalfat, "Investigation into CFRP plate end anchorage utilising uni-directional fabric wrap," *Composite Structures,* vol. 93, no. 2, pp. 821-830, 2011.

[32] H.N. Garden, and L. C. Hollaway, "An experimental study of the influence of plate end anchorage carbon fibre composite plates used to strengthen reinforced concrete beams," *Composite Structures,* vol. 42, pp. 175-188, 1998.

[33] Y. J. Kim, *Rehabilitation and Load Rating of Deteriorated Timber Bridges in Colorado: Parametric Investigations and Implementation*, 2023.

[34] F. Fanous, J. May, and T. Wipf, "Development of Live-Load Distribution Factors for Glued-Laminated Timber Girder Bridges," vol. 16, no. 2, pp. 179-187, 2011.

[35] U. Meier, "Composite Materials in Bridge Repair," *Applied Composite Materials,* vol. 7, pp. 75-94, 2000.

[36] B. Kasal, and L. Yan, "Fiber-Reinforced Polymers as Reinforcement for Timber Structural Elements," *Reinforcement of Timber Elements in Existing Structures: State-of-the-Art Report of the RILEM TC 245-RTE*, J. Branco, P. Dietsch and T. Tannert, eds., pp. 51-78, Cham: Springer International Publishing, 2021.

[37] A. W. Smith, "Rehabilitation of timber railroad bridges using glass fiber reinforced polymer composite wraps," Department of Civil and Environmental Engineering, West Virginia University, 2004.

[38] T. Hosteng, B. Phares, T. J. Wipf *et al.*, "Evaluation of a Timber Bridge for the Secondary Road System Using FRP Reinforced Glued-Laminated Girders."

[39] FATMIR MENKULASI, HADI BAGHI, DAVID HALL *et al.*, *Rehabilitation of Deteriorated Timber Piles Using FRP Composites*, Southern Plains Transportation Center, 2017.

[40] Roberto Lopez-Anido, Antonis P. Michael, and Thomas C. Sandford, "Experimental characterization of FRP composite-wood pile structural response by bending tests," *Marine Structures,* vol. 16, no. 4, pp. 257-274, 2003.

[41] Ching Chiaw Choo, Tong Zhao, and I. E. Harik., *Retrofit Of The Louisa-Fort Gay Bridge Using CFRP Laminates.*, Kentucky Transportation Center, 2007.

[42] Benjamin M. Carmichael, and R. W. Barnes, *REPAIR OF THE UPHAPEE CREEK BRIDGE WITH FRP LAMINATES*, 2005.

[43] OSMAN HAG-ELSAFI, JONATHAN KUNIN, SREENIVAS ALAMPALLI *et al.*, *Strengthening of Route 378 Bridge Over Wynantskill Creek In New York Using FRP Laminates*, TRANSPORTATION RESEARCH AND DEVELOPMENT BUREAU, NEW YORK STATE DEPARTMENT OF TRANSPORTATION, 2001.

[44] Ronald S. Harichandran, and M. I. Baiyasi, *Repair of Corrosion-Damaged Columns using FRP Wraps*, Michigan State University, 2000.

[45] Rajan Sen, and G. Mullins, "Application of FRP composites for underwater piles repair," *Composites Part B: Engineering,* vol. 38, no. 5-6, pp. 751-758, 2007.

[46] P. N. Balaguru, and K. W. Lee, *Construction of Fiber Reinforced Polymer (FRP) Jackets for the Protection of Pier Caps*, Rutgers University, 2005.

[47] Vijaya Gopu, and P. N. Balaguru, *Repair of Morganza Spillway Bridge Bent Pile Cap Using Carbon Fiber Reinforcement (CFR)*, Louisiana State University, 2016.

[48] "OKTA," Montana Department of Transportaion, 2023.

[49] Mohammad Shekarchi, Asghar Vatani Oskouei, and Gary M. Raftery, "Flexural behavior of timber beams strengthened with pultruded glass fiber reinforced polymer profiles," *Composite Structures,* vol. 241, 2020.

[50] A. B. Marco Corradi, Luca Righetti, Emanuela Speranzini "Uncertainty analysis of FRP reinforced timber beams," *Composites*, 2017.

[51] AASHTO, "Standard specifications for highway bridges (17th ed.)," American Association of State Highway and Transportation Officials, 2002.

[52] "Strongwell Corporation," https://www.strongwell.com/.

[53] "GRK screws," https://www.grkfasteners.com/.

[54] "Milwaukee titanium twist metal drill bits," https://www.milwaukeetool.com/.

[55] ASTM, "D198 − 22a: Standard Test Methods of Static Tests of Lumber in Structural Sizes," American Society for Testing and Materials, 2023.

[56] "SPAX® T-STAR Washer Head PowerLags," https://spax.us/.

[57] ASTM, "D638 − 14: Standard Test Method for Tensile Properties of Plastics," American Society for Testing and Materials, 2015.

APPENDIX A: FRP-REPAIRED TIMBER BRIDGES IN MONTANA

Table 23: Basic information on FRP-repaired timber bridges in Montana

MDT Bridge Number	Construction Year	Location	Repairing Year	Repaired Area	Last Inspection Year
#02526	1934	4M W SIMMS, Cascade, Great Falls	2021	Bent 2: Pile 4.	2022
#02568	1928	19M NE Miles City, Custer, Glendive	2020	Bent 2: Piles 4 and 5.	2022
#02569	1929	20M NE Miles City, Custer, Glendive	2020	Bent 2: Pile 4.	2022
#03201	1931	4M W Whitehall, Jefferson, Butte	2020	Bent 2: Pile 6. Bent 3: Pile 1.	2022
#03202	1931	7M W Whitehall, Jefferson, Butte	2021	Bent 2: Pile 2, 3.	2022
#03344	1933	1M NE Wolf Creek, Lewis and Clark, Great Falls	2021	Abutment 1: Pile 5. Abutment 2: Pile 2.	2022
#03345	1933	2M NE Wolf Creek, Lewis and Clark, Great Falls	2021	Abutment 1: Pile 5. Abutment 2: Pile 1.	2022
#03347	1933	5M NE Wolf Creek, Lewis and Clark, Great Falls	2021	Abutment 2: Pile 1, 3.	2022
#03728	1947	3M W Huson, Missoula	2017	Bent 6: Pile 1. Bent 8: Pile 3. Bent 12: Pile 4.	2022
#04649	1933	10M E Hysham, Tressure, Billings	2018	Bent 2: Pile 3. Bent 3: Piles 1-4.	2021
#04862	1947	2M W Huntley, Yellowstone, Billings	2020	Bent 3: Piles 1, 2, and 8. Bent 4: Pile 8.	2022
#05070	1942	Chinook, Blaine, Great Falls	2021	Abutment 1: Piles 1, 2. Bent 2: Pile 7.	2021
#05072	1942	1M E Chinook, Blaine, Great Falls	2021	Bent 2: Pile 5. Bent 3: Pile 5.	2021
#05081	1940	Zurich, Blaine, Great Falls	2021	Abutment 4: Pile 3. Bent 2: Pile 5.	2021
#05170	1940	2M NE Sun River, Cascade, Great Falls	2021	Bent 3: P2.	2022
#05246	1933	5M S Ronan, Lake, Missoula	2021	Bent 1: pile 4 and 5. Bent 2: pile 1 and 2. Bent 4: pile 4.	2023
#05445	1935	1M E Lavina, Golden Valley, Billings	2020	Bent 2: Pile 4. Bent 3: Pile 3.	2022
#05493	1947	3M W Sumatra, Rosebud, Billings	2022	Abutment 3: Pile 4.	2022
#05496	1947	Ingomar, Rosebud, Billings	2020	Abutment 1: Pile 5. Abutment 2: Pile 4.	2022
#05498	1941	32M NW Forsyth, Rosebud, Glendive	2022	Abutment 3: Pile 5.	2022
#05690	1941	11M NE Ekalaka, Carter, Glendive	2022	Abutment 1: Pile 5. Bent 2: Pile 1.	2022
#05726	1931	7M E Pipestone Pass, Jefferson, Butte	2021	Bent 3: Pile 6. Bent 5: Pile 5.	2022
#05735	1939	15M S Opheim, Valley, Glendive	2022	Abutment 1: Piles 1 and 2.	2022
#05807	1936	13M NW Avon, Powell, Butte	2019	Bent 2: Piles 4, 5, and 7. Bent 3: Piles 4 and 5.	2021
#05811	1965	4M SE Helmsville, Powell, Great Falls	2021	Abutment 1: Pile 3, 5. Abutment 2: Pile 7.	2021
#05812	1965	2M SE Helmsville, Powell, Great Falls	2021	Abutment 1: Pile 6.	2021
#05850	1942	14M S Harlowton, Wheatland, Billings	2020	Abutment 1: Piles 1 and 2.	2022
#05942	1953	9M SW Whitehall, Jefferson, Butte	2022	Abutment 1: Piles 2-6. Bent 2: Pile 5.	2022

				Abutment 3: Pile 4.	
#05995	1939	7M NW Grass Range, Fergus, Billings	2021	Bent 2: Pile 4.	2022
#05998	1939	4M NW Grass Range, Fergus, Billings	2020	Bent 3: Piles 4 and 5.	2022
#06005	1930	8M NE Grass Range, Fergus, Billings	2020	Bent 3: Piles 2 and 4. Bent 4: Pile 1.	2022
#06078	1955	2M NE White Sulphur Spring, Meagher, Butte	2019	Abutment 1: Piles 1, 6.	2022
#06131	1940	11M SW Malta, Phillips, Glendive	2021	Bent 4: Pile 1.	2021
#06198	1949	2M SE Geraldine, Chouteau, Great Falls	2019	Bent 2: Piles 3 and 4. Bent 3: Pile 3.	2021
#06204	1949	17M S Geraldine, Fergus, Billings	2021	Abutment 11: Pile 6.	2022
#06205	1934	6M NE Stanford, Judith Basin, Billings	2022	Bent 2: Pile 3. Bent 3: Pile 2.	2022
#06216	1934	6M W Brooks, Fergus, Billings	2020	Abutment 1: Pile 4.	2022
#06233	1952	9M NE Norris, Madison, Butte	2022	Abutment 1: Pile 3.	2022
#06264	1951	1M S Lolo Hot Springs, Missoula	2018	Abutment 2: Pile 3.	2022
#06265	1957	Lolo Hot Springs, Missoula	2018	Bent 3: Pile 5. Abutment 4: Piles 1, 2, 4, 5.	2022
#06266	1957	Lolo Hot Springs, Missoula	2018	Abutment 1: Piles 4, 6. Bent 2: Pile 5. Bent 3: Pile 4.	2022
#06415	1941	13M E Great Falls, Cascade, Great Falls	2021	Pier 2: Pile 1 and 6. Pier 3: Pile 2.	2021
#06460	1936	1M N Saco, Phillips, Glendive	2020	Abutment 1: Pile 1. Bent 2: Pile 2, 3. Abutment 3: Pile 5.	2021
#06469	1939	Flatwillow, Petroleum, Billings	2020	Abutment 1: Pile 2.	2022
#06471	1948	5M S Winnett, Petroleum, Billings	2022	Abutment 5: Pile 4.	2022
#06512	1940	18M NW Terry, Prairie, Glendive	2022	Bent 3: Pile 5.	2022
#06548	1947	1M NE Helmville, Powell, Great Falls	2019	Abutment 1: Piles 1-5. Abutment 2: Piles 3 and 4.	2022
#06567	1954	2M SE Canyon Creek, Lewis and Clark, Great Falls	2021	Abutment 1: Piles 2 and 5. Abutment 2: Pile 1.	2022
#06571	1949	5M N Canyon Creek, Lewis and Clark, Great Falls	2021	Abutment 1: Piles 1 and 5. Abutment 2: Pile 4.	2023
#06574	1949	6M NW Canyon Creek, Lewis and Clark, Great Falls	2019	Bent 2: Pile 1.	2021
#06579	1958	3M E Canyon Ferry, Lewis and Clark, Great Falls	2021	Abutment 1: Pile 1. Abutment 2: Pile 1.	2022
#06606	1959	1M N Shawmut, Wheatland, Billings	2022	Abutment 4: Piles 1 and 3.	2022
#06682	1964	1M S Glendive, Dawson, Glendive	2022	Bent 2: Pile 6.	2022
#06720	1958	Jefferson Island, Madison, Butte	2022	Abutment 1: Pile 4.	2022
#06738	1955	2M S Outlook, Sheridan, Glendive	2019	Abutment 1: Pile 3.	2021
#06895	1960	6M W Billings, Yellowstone, Billings	2021	Abutment 1: Piles 1, 3, 5, 6. Abutment 2: Pile 4.	2022
#06982	1936	Havre- 7th Ave N	2021	Bent 4: Pile 6. Bent 5: Pile 5. Bent 8: Pile 6. Bent 11: Pile 6. Bent 12: Pile 6. Bent 23: Pile 7. Bent 24: Pile 9. Bent 25: Piles 6, 8, 9, 12. Bent 27: Pile 5. Bent 28: Piles 5 and 9. Bent 29: Pile 8.	2022

Table 24: Notes on FRP-repaired timber bridges in Montana

MDT Bridge Number	Notes
#02526	Bent 2 Pile 4 was jacketed with FRP wrap from ground line to 2 ft (0.61 m) up.
#02568	No crushing or distortion was noted in 2022 inspection
#02569	No decay was found in 2022 inspection.
#03201	Bent 2 Pile 6 and Bent 3 Pile 1 were wrapped with FRP for the full pile height.
#03202	Bent 2 piles 2 and 3 were FRP wrapped.
#03344	FRP wrap repair required due to decay.
#03345	FRP wrap was applied over the full exposed heights of the piles due to decay.
#03347	A2P1 and A2P3 were wrapped with FRP from the ground line to 3 ft (0.91 m) and 1.8 ft (0.55 m) above ground, respectively.
#03728	From bent cap down 10 ft (3 m), 6 ft (1.83 m) and 8 ft (2.44 m) FRP wrap was applied to Bent 6, 8, and 12, respectively.
#04649	The repair was in good condition as of 2021 inspection
#04862	The piles were FRP jacketed.
#05070	The piles were RFP wrapped at full height. No defects were found in 2021 inspection.
#05072	The piles were RFP wrapped.
#05081	The piles were RFP wrapped.
#05170	Bent 3 Pile 2 was jacketed with an FRP wrap from ground line up to 4.9 ft (1.5 m) due to decay at the ground line.
#05246	The piles were FRP wrapped. No visible sign of deterioration.
#05445	Nothing to note.
#05493	Abutment 3 Pile 4 was FRP Jacketed.
#05496	The piles were RFP wrapped.
#05498	The pile was RFP wrapped.
#05690	Abutment 1, Pile 5 and Bent 2, Pile 1 were treated with FRP wrap and epoxy injection. No significant defects noted in 2022 inspection.
#05726	The pile was RFP wrapped.
#05735	Abutment 1 Piles 1 and 2 were treated with FRP pile wraps. Piles were functioning as intended and no defects were noted in 2022 inspection.
#05807	The piles were repaired with fiber reinforced polymer. The repair appears to be functioning as intended in 2021 inspection.
#05811	The piles were RFP jacketed.
#05812	The pile was RFP jacketed 3 ft (0.91 m) above groundline.
#05850	The piles were FRP jacketed.
#05942	The piles were FRP wrapped.
#05995	The pile was jacketed with FRP.
#05998	The piles were jacketed with FRP.
#06005	The piles were jacketed with FRP.
#06078	Abutment 1 Piles 1 and 6 were wrapped with FRP. The FRP jackets were in good condition in 2022 inspection.
#06131	Bottom 4ft of Bent 4 Pile 1 was FRP repaired.
#06198	The piles had an RFP jacket retrofit around decayed sections.
#06204	Abutment 11, Pile 6 was wrapped in FRP.
#06205	The piles were wrapped with FRP.
#06216	The FRP wrap appears to be functioning as intended in 2022 inspection.
#06233	Abutment 1 Pile 3 was wrapped with FRP over the full exposed height.
#06264	Abutment 2, Pile 3 was wrapped with FRP.
#06265	The piles were wrapped with FRP 2018.
#06266	The piles were wrapped with FRP.
#06415	Three piles were RFP retrofitted.
#06460	All the jacketed piles were functioning as intended in 2021 inspection.
#06469	Abutment 1, Pile 2 was wrapped in FRP.
#06471	The pile was jacketed with FRP.
#06512	The pile was jacketed with FRP.
#06548	The piles were wrapped with FRP.
#06567	The piles were wrapped with FRP due to decay.
#06571	The piles were wrapped with FRP.

#06574	The pile was wrapped with FRP.
#06579	The piles were wrapped with FRP for the full pile height.
#06606	The piles were wrapped with FRP.
#06682	The pile was covered with a FRP wrap retrofit prior to 2022 inspection.
#06720	Abutment 1 Pile 4 was wrapped with FRP 4.5 ft (1.37 m) above the groundline.
#06738	Abutment 1, Pile 3 previously showed center rot and crushing, was retrofitted with FRP jacket. No decay was found in 2021 inspection.
#06895	The piles were FRP jacketed.

APPENDIX B: TIMBER BEAM INVENTORY

Table 25: Timber beam inventory

Acronym	Actual cross-section	Actual length	Pre-existing crack/split	Misc. Notes
6-Sh(1)	5.5" x 17"	10.08'	Minor checks and wane-type defects from handling.	Beam cut in half for shear setup.
6-Fl(1)	5.75" x 17"	19.50'	Clean.	Exterior beam. Some holes and bolts on both ends. Shorter beam, supports need to be moved 3" closer.
6-Fl(2)	5.75" x 17"	20.06'	Minor checking.	-
6-Fl(1)-CR(C-S)	5.75" x 17"	19.50'	Crack from control beam test.	Shorter beam, supports need to be moved 3" closer.
6-Fl(2)-CR(S)	5.75" x 17"	20.06'	Crack from control beam test.	-
6-Sh(1)-SR(C)	5.75" x 17"	10.08'	Split from control beam test. Indentation at the bearing plates. Split on the left end of the beam through a knot.	Beam cut in half for shear setup.
6-Fl-SR(C-S)	5.75" x 17"	20.17'	Small splits on one end.	Missing screw on the east channel.
6-Fl-SR(C3)	5.75" x 17"	20.21'	18" long split on end.	-
6-Fl-SR(C6)	5.75" x 17.25"	20.17'	12" long split on one end.	Notched end.
6-Sh-St(C)	5.75" x 17"	10.04'	The top surface was uneven. Tested upside down.	Beam cut in half for shear setup.
6-Fl-St(C-S)	5.75" x 17"	19.83' + 3"	Clean.	Inclined cut in one end.
6-Fl-St(S)	5.75" x 17"	19.06' + 3	Pre-existing damage on top. Uneven bottom.	Inclined cut in one end.
8-Sh(1)	7.75" x 17.25"	10.08'	Clean.	Cut in 10.08' for the shear setup.
8-Fl(1)	7.5" x 17"	25.75'	Clean.	-
8-Fl(2)	7.75" x 17"	26.00'	Minor checking. Wane-type defect.	-
8-Fl(1)-CR(C-S)	7.75" x 17.25"	25.75'	Crack from control beam test.	-
8-Fl(2)-CR(S)	7.5" x 17"	26.00'	Crack from control beam test.	5-strips were attached.
8-Sh(1)-SR(C)	7.75" x 17"	10.08'	Split from control beam test. Existing split on the end.	Beam cut in half for shear setup.
8-Fl-SR(C-S)	7.5" x 17"	26.06'	Moderate checking along the length.	Tapered ends. Through bolt removal from the end.
8-Sh-St(C)	7.5" x 17.5"	10.00'	Heavy checking on the other half.	Beam cut in half for shear setup.
8-Fl-St(C-S)	7.5" x 17"	26.13'	Clean.	-
8-Fl-St(S)	7.75" x 17.5"	26.56'	Moderate checking.	Large notch on one end, causing the strips to hang over.

APPENDIX C: FRP COUPON TESTING

Specimen preparation

Tensile test coupons were prepared from the two types of FRP materials used in this study: glass FRP channels and carbon-glass hybrid FRP strengthening strips. For clarity, these are referred to throughout the study as channel coupons and strip coupons, respectively. Each material set consisted of the following three types of specimens:

- Control: untested and undamaged raw materials
- Tested coupon (mid): material cut from the middle region of a full-scale FRP material that was tested on a timber beam
- Tested coupon (end): material cut from the end region of a full-scale FRP material that was tested on a timber beam

A total of three channel coupons and four strip coupons were tested. All coupons were cut to a standard tensile specimen shape using a water jet cutter to maintain dimensional accuracy and avoid specimen damage. Testing followed the procedures outlined in ASTM D638-14 standard [57], where channel coupons were dimensioned as Type III specimens due to their thickness, and strip coupons were Type I. Figure 132 and Figure 133 show schematic diagrams of the channel and strip coupon geometries, respectively.

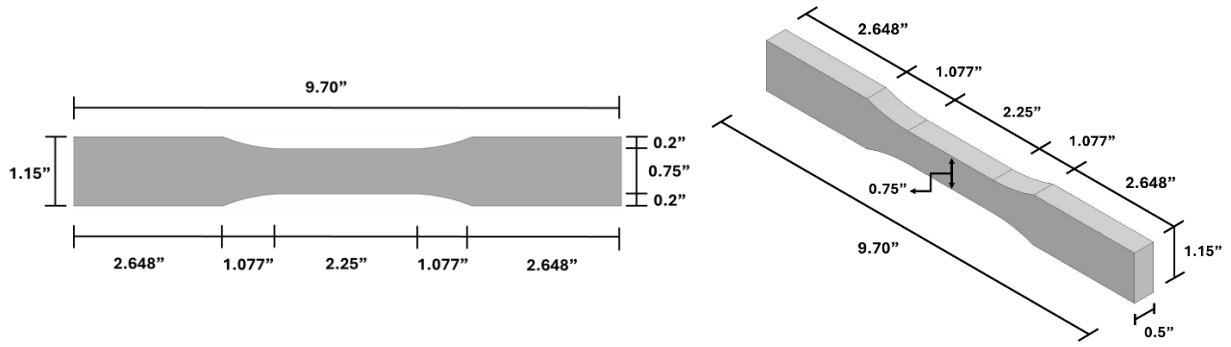

Figure 132: Schematic of the GFRP channel coupon geometry

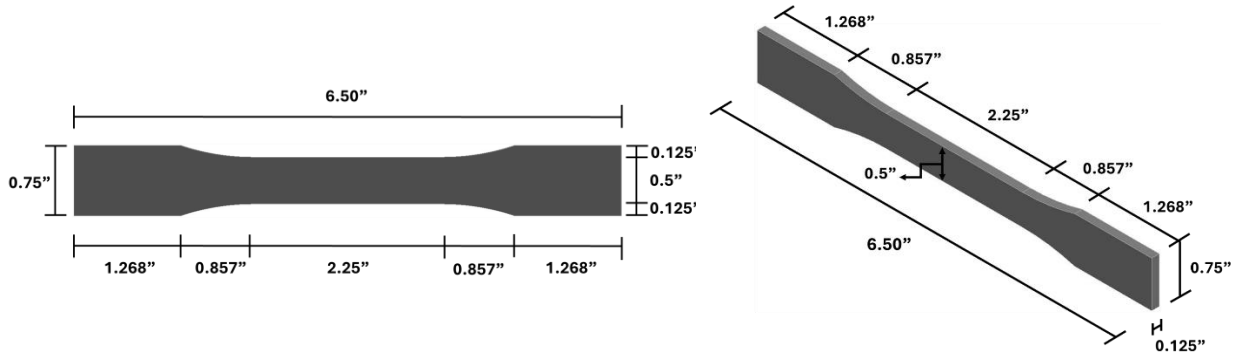

Figure 133: Schematic of the carbon-glass hybrid FRP strengthening strip coupon geometry

Coupon dimensions were measured prior to testing using slide calipers. The measured values were used to calculate the cross-sectional area for stress calculations. Dimensional data for the channel coupons are shown in Table 26, while Table 27 summarizes the data for the strip coupons.

Table 26: GFRP channel coupon dimensions

Coupon	Width (in)	Thickness (in)	Area (in^2)
Control	0.752	0.500	0.376
Tested (mid)	0.755	0.497	0.375
Tested (end)	0.754	0.498	0.375

Table 27: Hybrid FRP strip coupon dimensions

Coupon	Width (in)	Thickness (in)	Area (in^2)
Control 1	0.504	0.127	0.064
Control 2	0.504	0.125	0.063
Tested (mid)	0.505	0.126	0.063
Tested (end)	0.505	0.126	0.063

Test setup and instrumentation

All tensile tests were conducted at the Materials Testing Lab, Montana State University, using an MTS Testing Machine. The tests followed the guidelines of ASTM D638-14 [57], and the loading rate was maintained at 0.0033 in/sec for all specimens. Proper alignment of the coupons in the grips was ensured to avoid eccentric loading. Specimens were instrumented with an MTS extensometer to capture accurate strain responses and stress was calculated using the measured loads and cross-sectional areas. Photographs of the test setup and mounted coupons are provided in Figure 134.

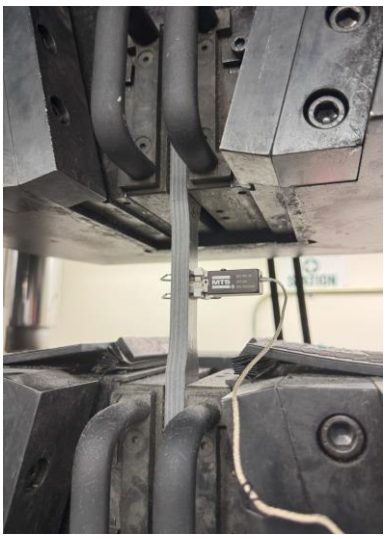

(a) Glass FRP channel coupon

(b) Hybrid FRP strip coupon

Figure 134: Tensile test setup for FRP coupons

Results

The primary goals of the coupon testing were to determine the tensile properties of the GFRP channels and carbon-glass hybrid FRP strips and to assess what level of damage (if any) occurred on the FRP during the timber beam testing. The experimental values measure here were used in the theoretical capacity calculations presented previously.

The measured tensile strength and modulus of elasticity values for each coupon are summarized in Table 28 and Table 29, along with their corresponding tabulated reference values. Ratios of measured to tabulated values are included to quantify performance retention.

Table 28: Tensile strength of FRP coupons

FRP Coupon	Tabulated Tensile Strength (ksi)	Measured Tensile Strength (ksi)	Measured/tabulated (%)
Channel Control	30	53.2	177
Channel Tested (mid)	30	47.1	157
Channel Tested (end)	30	45.7	152
Strip Control 1	123	131.8	107
Strip Control 2	123	133.7	109
Strip Tested (mid)	123	125.1	102
Strip Tested (end)	123	121.8	99

Table 29: Modulus of elasticity of FRP coupons

FRP Coupon	Tabulated Modulus (ksi)	Measured Modulus (ksi)	Measured/tabulated (%)
Channel Control	2500	4090	164
Channel Tested (mid)	2500	3351	134
Channel Tested (end)	2500	3076	123
Strip Control 1	9020	9822	109
Strip Control 2	9020	9413	104
Strip Tested (mid)	9020	8817	98
Strip Tested (end)	9020	9619	107

In the case of the GFRP channels, the control specimen exhibited a tensile strength 77% above the tabulated value and an elastic modulus 64% higher than tabulated. Although there was a reduction in strength and modulus from the raw material to the tested channel coupons, the tested specimens still demonstrated substantial mechanical performance, retaining over 150% of the expected tensile capacity and more than 120% of the expected modulus. The FRP strip coupons showed consistent behavior. All control and tested specimens had tensile strengths near or above the design values, and modulus values stayed within ±10% of the reference across all specimens.

Figure 135-a shows the stress–strain response of the strip coupons, while Figure 135-b presents the data for the channel coupons. To prevent damage while still capturing a substantial portion of the linear elastic zone,

the extensometer was removed before the specimens reached ultimate failure. For the strip coupons, it was removed at approximately 55 ksi, and for channel coupons, at approximately 25 ksi. Enough of the linear elastic region was captured to calculate slope and the data was used to determine the modulus of elasticity for each coupon.

In both materials, the tested coupons (mid and end) exhibited slightly lower stiffness compared to the corresponding control coupons, indicating minor degradation after full-scale experimental testing. However, the stiffness of all tested specimens remained higher than the tabulated design values (with the exception of the strip coupon tested (mid) at 98%), confirming the retention of structural integrity and supporting the reuse potential of these FRP materials.

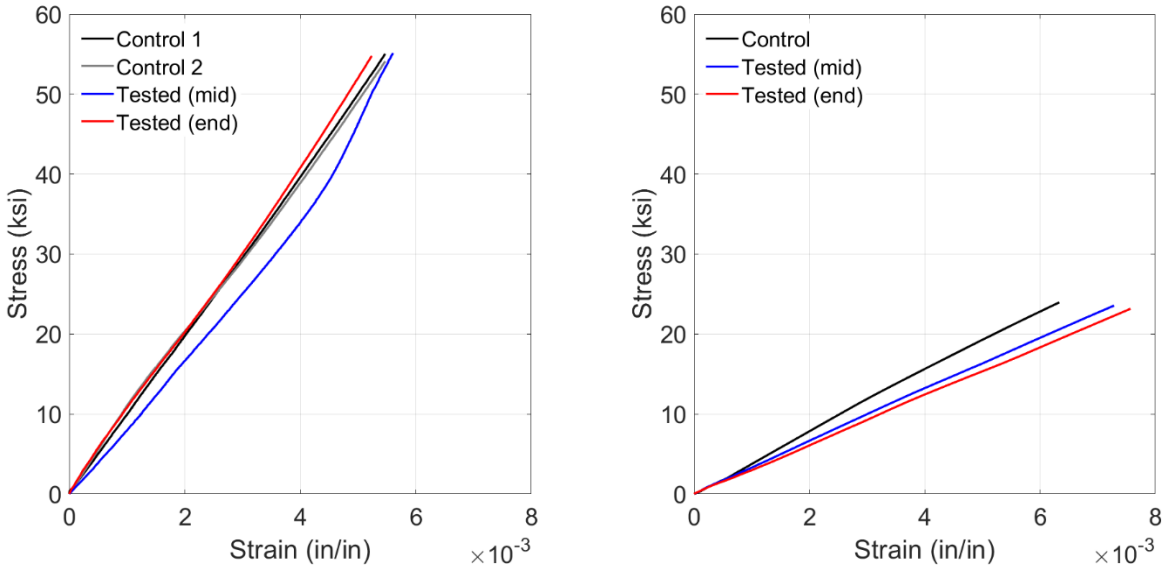

(a) Strip coupon (b) Channel coupon

Figure 135: Stress–strain curves of FRP coupons

APPENDIX D: MANUFACTURER INFORMATION

This section presents manufacturer brochures for the FRP strip, FRP channel, and GRK screws.

FRP strip

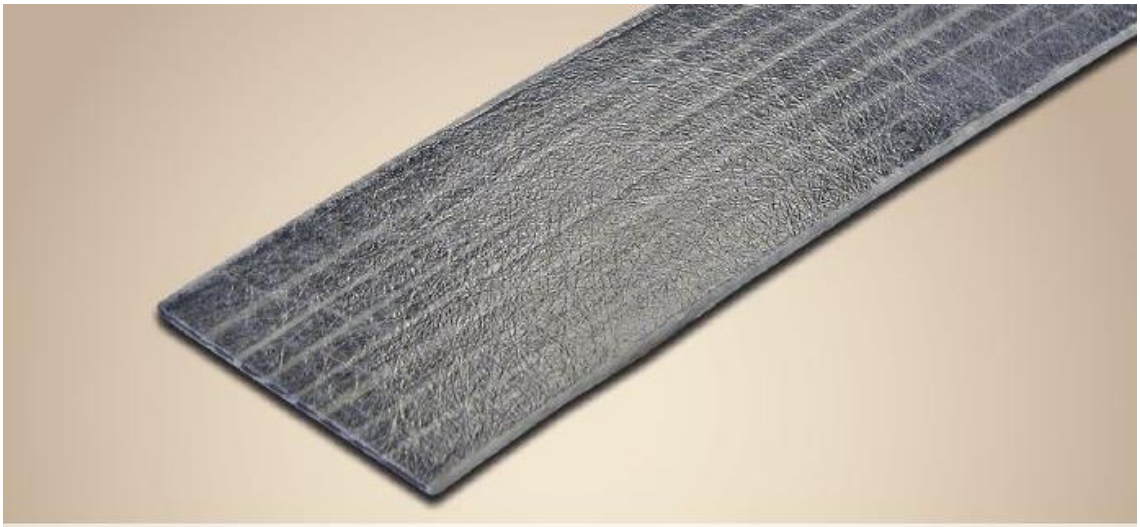

STRONGWELL.

EXCLUSIVELY MADE IN THE USA

SAFSTRIP®

FIBER REINFORCED STRENGTHENING STRIP

SAFSTRIP® is a pultruded composite strip that improves the strength of an existing structural member when mechanically fastened to the structure. SAFSTRIP® has high bearing and longitudinal properties and is designed to strengthen the flexural capacity on the tension face of concrete girders, slabs, and decks. Installation on bridges can occur without any interruption of service.

SAFSTRIP® is supplied in rolls and may be pre-drilled with holes at the required fastener spacing to receive fasteners. SAFSTRIP® measures 4" wide x 1/8" thick and is shipped in rolls up to 100 ft. long. SAFSTRIP® is designed to be easily field cut by the customer into shorter lengths using standard carpenter tools.

SAFSTRIP® provides these features:

- Easy to install, no skilled labor necessary
- Minimal surface preparation is needed for installation
- Structure is usable immediately after installation
- Cost effective system for increasing load capacity of bridges
- Will not split or delaminate when drilled

FIBER REINFORCED STRENGTHENING STRIP

Workers installed SAFSTRIP® on this bridge in Edgerton, Wisconsin, using the MF-FRP system. The load rating for the bridge increased from HS-17 to HS-25 as a result.

The posted load for this bridge that spans the Meramec River in Missouri was increased from 10 tons to 18 tons by installing SAFSTRIP® using the MF-FRP system.

The abutment and deck of this bridge in Phelps County, Missouri, was strengthened using SAFSTRIP®. As a result, the existing 12-ton load posting was removed.

Materials of Construction

SAFSTRIP® is composed of carbon tows sandwiched between layers of fiberglass mats and rovings. The materials are bonded together by a highly corrosion resistant vinyl ester resin. Carbon fibers increase the stiffness of the strip while glass mat provides the proper bearing strength. These combined properties allow SAFSTRIP® to be mechanically attached to a structural member. A synthetic surfacing veil is also incorporated into the composite to improve resistance to corrosion and UV degradation.

What is MF-FRP?

SAFSTRIP® is designed to be installed using an attachment method known as mechanically-fastened fiber reinforced polymer (MF-FRP). Using this method, SAFSTRIP® is attached to an existing concrete girder, slab, or deck using closely spaced powder actuated fastening pins or steel expansion anchors. The pins are applied by using a powder actuated fastener gun or other portable fastener gun. Expansion anchors are installed with a pneumatic powered torque wrench. If desired, rubber or neoprene washers may be used between the fasteners and the strip prior to inserting the fastener through the strip.

MF-FRP is an alternative to externally bonded fiber reinforced polymer (EB-FRP). As opposed to the MF-FRP system, in which the load is transferred to the composite strip through a fastener, the EB-FRP system uses an adhesive.

Research and Development

Research and development for SAFSTRIP® was funded by the U.S. Army Engineer Research and Development Center (ERDC). Laboratory research was conducted at the University of Wisconsin Structures and Materials Testing Laboratory and at ERDC's test laboratories. Bridge demonstration projects were conducted in Wisconsin and Missouri.

Engineering Design

The repair of concrete structures using SAFSTRIP® is dependent upon the concrete's condition. The local engineer must determine the strength of the existing concrete. It must then be determined how much SAFSTRIP® is required and the spacing of fasteners.

Design of MF-FRP systems follows the methodology of *ACI PRC-440.2: Design and Construction of Externally Bonded Fiber-Reinforced Polymer (FRP) Systems for Strengthening Concrete Structures*. Design assistance can be obtained by contacting Strongwell – Chatfield Location.

MECHANICAL PROPERTIES

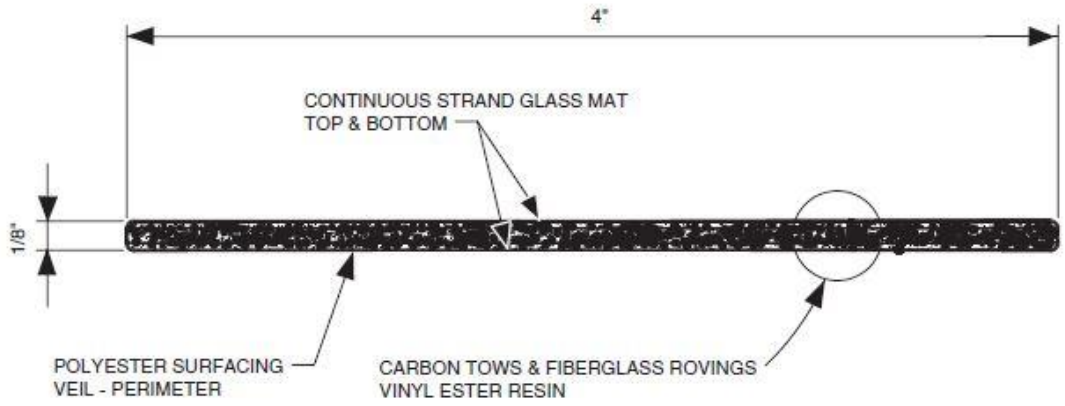

Property	ASTM Test Method	Average Value[1] psi (MPa)	Design Value[2] psi (MPa)
Tensile Strength*	D-638	123,613 (852)	92,902 (640)
Tensile Modulus*[3]	D-638	9.02 x 10⁶ (62,190)	9.02 x 10⁶ (62,190)
Clamped Bearing Strength*	D-5961	50,955 (351)	40,540 (279)
Unclamped Bearing Strength**	D-5961	31,044 (214)	26,046 (180)
Open Hole Strength*	D-5766	94,641 (652)	78,846 (543)

* 20 Sample coupons per test series
** 17 Sample coupons per test series
[1] Average value of test series
[2] Average value minus three standard deviations
[3] Modulus design values are not reduced in accordance with ACI 440.2R-17

This underground parking garage for an apartment complex in Ontario, Canada, recently underwent a concrete support renovation. To provide the necessary improvements, SAFSTRIP® was installed with a small team and minimal onsite equipment.

This bridge, located in St. James, Missouri, was load posted at the time of strengthening. After mechanically attaching SAFSTRIP® with concrete wedge bolts and anchors, the bridge load limit was raised to 20 tons.

Severe deterioration prevented the application of a bonded strengthening system to this bridge in Pulaski County, Missouri, but MF-FRP applied SAFSTRIP® was able to repair the bridge.

	MF-FRP INSTALLATION	VS.	EB-FRP INSTALLATION
FASTENING SYSTEM	Mechanical - concrete wedge bolts and anchors or powder actuated fasteners.		Adhesive - usually epoxy.
SURFACE PREPARATION	Minimal		Requires the time consuming process of sandblasting, cleaning, and application of epoxy putty that must be ground down for a smooth surface.
WEATHER CONDITIONS FOR APPLICATION	No restrictions. Can be installed even during inclement weather.		Application surface must be moisture-free. Cannot be properly installed in extreme temperatures.
INSTALLATION TIME	Minimal - generally a few hours		Extensive due to the surface preparation, mixing of adhesives, and care required to properly apply the adhesive.
LABOR COSTS	Unskilled labor using standard carpenter tools for cutting and installing strips reduces labor costs.		Skilled labor required to properly prepare the surface and mix the adhesives, which results in higher labor costs.
BOND STRENGTH	Not highly affected by poor condition of the existing outer/superficial concrete substrate.		Dependent on the quality of the concrete substrate.
AVAILABILITY OF STRUCTURE	Available for immediate use upon application.		May require up to seven days to achieve full adhesive strength.
DURABILITY	Tests show excellent retention strength for anchor bolts. Very good fatigue strength.		Research suggests high strain gradient is found in adhesive layer where strips terminate or in proximity of substrate discontinuity (such as cracks). Debonding can be problematic.

STRONGWELL

ISO 9001 Quality Certified Manufacturing Plants

CHATFIELD LOCATION*
1610 Highway 52 South
Chatfield, MN 55923 USA
(507) 867-3479
www.strongwell.com

FRP channel

EXTREN® FIBERGLASS STRUCTURAL SHAPES AND PLATE

This entire rooftop structure was built using EXTREN®, to take advantage of its transparency to RF and cellular signals.

EXTREN® structural shapes have become an ideal alternative for traditional wood in cooling tower construction.

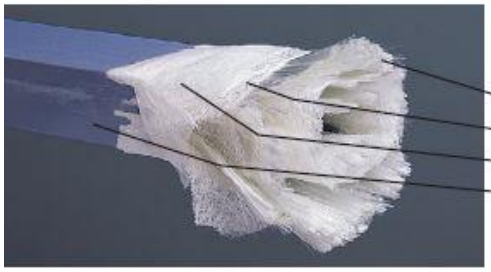

What is EXTREN®?

EXTREN® replaces steel, aluminum, and wood in a wide variety of structural applications. EXTREN® is a durable, lightweight, cost saving structural material. This brochure provides basic information about the EXTREN® product line and shows many examples of how EXTREN® provides solutions for end users in a variety of markets and applications.

EXTREN® is:

- Corrosion Resistant
- Structurally Strong
- Impact Resistant
- Lightweight
- Easy to Field Fabricate
- Low in Thermal and Electrical Conductivity

EXTREN® is manufactured by the pultrusion process. In its simplest terms, pultrusion is the process of pulling fiberglass (or other) reinforcements through a "bath" of thermosetting resin and into a heated forming-and-curing die to produce composite structural shapes. Reinforcement placement, resin formulation, catalyst levels, die temperature and pull speed are critical process parameters. Strongwell is world leader of the pultrusion process with more than 60 pultrusion machines in four plant locations across North America.

Why Use EXTREN®?

EXTREN® is the result of decades of experience in manufacture, design, and fabrication. EXTREN® offers the following advantages:

- **Corrosion Resistance** - Superior resistance to a broad range of chemicals. Unaffected by moisture or immersion in water when sealed. Will not rust like metal and will not rot like wood.
- **High Strength-to-Weight** - Pound-for-pound, EXTREN® pultruded fiberglass structural shapes are stronger than steel in lengthwise direction. Strongwell FRP weighs up to 75% less than steel and 30% less than aluminum - ideal when maximum performance is required but every pound counts.
- **Easy Installation** - Can be field fabricated using simple carpenter tools and is easily lifted into place during installation with less equipment or specialized labor vs. steel.
- **Cost Effective** - Because installation of Strongwell FRP is much simpler and quicker than steel, structures built using Strongwell's pultruded products can cost as much as 15% less than carbon steel, 30% less than galvanized steel, and as much as 50% less than stainless steel.
- **Virtually Maintenance Free** - Will not permanently deform under impact. Corrosion resistance eliminates need for constant painting and upkeep. Provides long-term, cost effective solutions with lower life cycle costs.
- **Durability & Weatherability** - Resists impact, non-denting and hard to break. Pigmented resin, surfacing veil, and UV-Inhibitors prevent moisture absorption, warping, fiber bloom, and delays fading.

Materials of Construction

EXTREN® is an engineered composite consisting of:

- Fiberglass rovings for increased strength
- Continuous strand mat for crosswise strength and imact resistance
- Synthetic surfacing veil for corrosion and UV protection
- Resin (specified by Series)

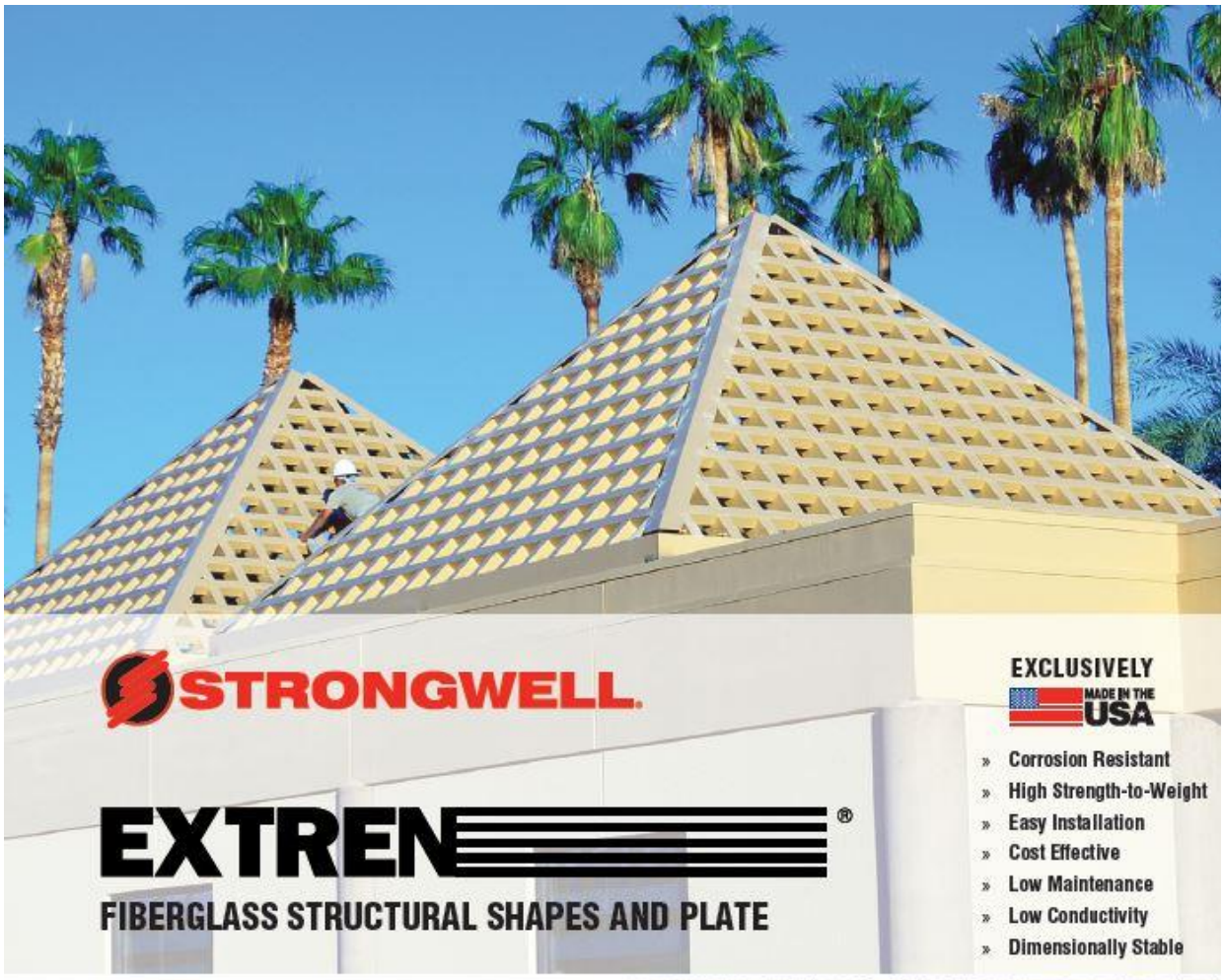
STRONGWELL
EXCLUSIVELY
MADE IN THE USA
EXTREN®
FIBERGLASS STRUCTURAL SHAPES AND PLATE
» Corrosion Resistant
» High Strength-to-Weight
» Easy Installation
» Cost Effective
» Low Maintenance
» Low Conductivity
» Dimensionally Stable

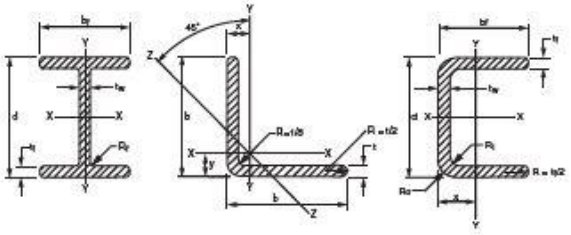

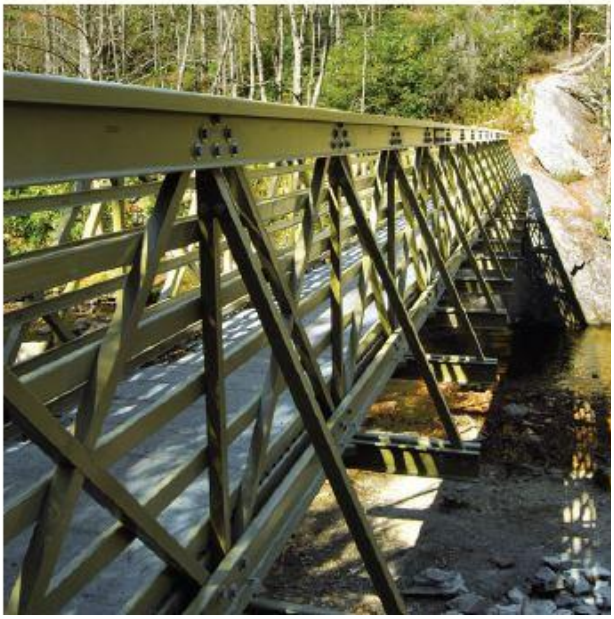

THE EXTREN® SERIES

EXTREN® is pultruded structural composite profiles and plate produced exclusively by Strongwell with the EXTREN® logo embedded in the surfacing veil. It meets or exceeds the minimum published mechanical, physical, electrical, flammability, and corrosive properties of the respective Series published in the *Strongwell Design Manual*.

EXTREN® Series 500

Premium Polyester Resin, UV inhibitor added
Standard Color: olive green
A general purpose resin with excellent corrosion properties

EXTREN® Series 525

Premium Polyester Resin, UV inhibitor added, Flame retardant additives
Standard Color: slate gray
A general purpose resin with excellent corrosion properties and improved fire performance

EXTREN® Series 600

Premium Vinyl Ester Resin, UV inhibitor added
Standard Color: light gray
For harsher corrosive environments and higher temperature applications

EXTREN® Series 625

Premium Vinyl Ester Resin, UV inhibitor added, Flame retardant additives
Standard Color: beige
For harsher corrosive environments, higher temperature applications, with improved fire performance

EXTREN® Series 900

In addition to the above EXTREN® products, Strongwell manufactures custom pultrusions. These pultrusions vary from EXTREN® in either shape, resin type, or reinforcement (type, amount, location and/or orientation). Designers may choose to vary one or all of these parameters to improve strength, temperature resistance, corrosion resistance, machinability, or some other characteristic. Consult Strongwell with specific needs or questions.

E23

All standard EXTREN® products meet and/or exceed the structural requirements of E17 European standards. EXTREN® can be manufactured upon request to meet the mechanical and physical properties of BS EN 13706 (E23) European standards.

NSF International

Most Strongwell products can be manufactured to meet NSF-61 certification upon request. Contact Strongwell for details.

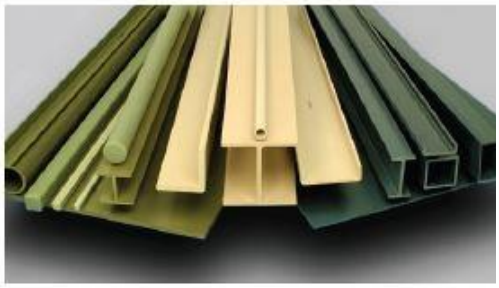

EXTREN® Series: (left to right) 500, 625, and 525.

EXTREN® structural shapes were used in a SXEW copper refinery because of the highly corrosive environment.

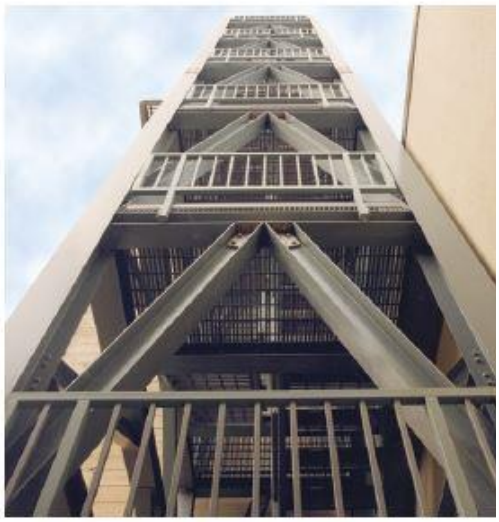

A 63' (19.2m) high freestanding fiberglass stair tower at Ft. Story Army Base, Virginia Beach, Virginia.

PROPERTIES

	ASTM TEST METHOD	UNITS/ VALUE	SERIES 500/525 SHAPES	SERIES 600/625 SHAPES	SERIES 500/525 PLATE ④ 1/8" 3.175mm	3/16" - 3/8" 4.76-9.5mm	1/2" - 1" 9.5-25.4mm	SERIES 600/625 PLATE ④ 1/8" 3.175mm	3/16" - 1/4" 4.76-6.35mm	3/8" - 1" 9.5-25.4mm
MECHANICAL										
Tensile Stress, LW	D638	psi	30,000	30,000	20,000	20,000	20,000	20,000	20,000	20,000
		N/mm²	207	207	138	138	138	138	138	138
Tensile Stress, CW	D638	psi	7,000	7,000	7,500	10,000	10,000	7,500	10,000	10,000
		N/mm²	48.3	48.3	51.7	68.9	68.9	51.7	68.9	68.9
Tensile Modulus, LW	D638	10^6 psi	2.5	2.6	1.8	1.8	1.8	1.8	1.8	1.8
		10^3N/mm²	17.2	17.9	12.4	12.4	12.4	12.4	12.4	12.4
Tensile Modulus, CW	D638	10^6 psi	0.8	0.8	0.7	0.9	1.0	1.0	1.0	1.0
		10^3N/mm²	5.52	5.52	4.83	6.21	6.89	6.89	6.89	6.89
Compressive Stress, LW	D695	psi	30,000	30,000	24,000	24,000	24,000	24,000	24,000	24,000
		N/mm²	207	207	165	165	165	165	165	165
Compressive Stress, CW	D695	psi	15,000	16,000	15,500	16,500	20,000	16,500	17,500	17,500
		N/mm²	103	110	107	114	138	114	121	121
Compressive Modulus, LW	D695	10^6 psi	2.5	2.6	1.8	1.8	1.8	1.8	1.8	1.8
		10^3N/mm²	17.2	17.9	12.4	12.4	12.4	12.4	12.4	12.4
Compressive Modulus, CW	D695	10^6 psi	0.8	0.8	0.7	0.9	1.0	1.0	1.0	1.0
		N/mm²	5.52	5.52	4.83	6.21	6.89	6.89	6.89	6.89
Flexural Stress, LW	D790	psi	30,000	30,000	24,000	24,000	24,000	24,000	24,000	24,000
		N/mm²	207	207	165	165	165	165	165	165
Flexural Stress, CW	D790	psi	10,000	10,000	10,000	13,000	17,000	10,000	13,000	17,000
		N/mm²	68.9	68.9	68.9	89.6	117	68.9	89.6	117
Flexural Modulus, LW	D790	10^6 psi	1.6	1.6	1.1	1.1	1.4	1.1	1.1	1.4
		10^3N/mm²	11.0	11.0	7.58	7.58	9.65	7.58	7.58	9.65
Flexural Modulus, CW	D790	10^6 psi	0.8	0.8	0.8	0.8	1.3	0.8	0.9	1.3
		10^3N/mm²	5.52	5.52	5.51	5.51	8.96	5.51	6.21	8.96
Modulus of Elasticity ①	full section	10^6 psi	2.6	2.8	LW: 2.0 CW: 0.8	2.0 0.8	2.0 1.3	2.0 0.8	2.0 0.9	2.0 1.3
		10^3N/mm²	17.9	19.3	LW: 13.7 CW: 5.51	13.7 5.51	13.7 8.96	13.7 5.51	13.7 6.21	13.7 8.95
Modulus of Elasticity: W & I shapes > 4"	full section	10^6 psi	2.5	2.5	-	-	-	-	-	-
W & I shapes > 102mm		10^3N/mm²	17.2	17.2	-	-	-	-	-	-
Shear Modulus, LW ②④	D5379	10^6 psi	0.425	0.425	-	-	-	-	-	-
		10^3N/mm²	2.93	2.93	-	-	-	-	-	-
Short Beam Shear, LW ②④	D2344	psi	4,500	4,500	-	-	-	-	-	-
		N/mm²	31.0	31.0	-	-	-	-	-	-
Ultimate Bearing Stress, LW	D953	psi	30,000	30,000	32,000	32,000	32,000	32,000	32,000	32,000
		N/mm²	207	207	221	221	221	221	221	221
Poisson's Ratio, LW ③	D3039	in/in	0.33	0.33	0.31	0.31	0.31	0.32	0.32	0.32
		mm/mm	0.33	0.33	0.31	0.31	0.31	0.32	0.32	0.32
Poisson's Ratio, CW ③	D3039	in/in	-	-	0.29	0.29	0.29	0.24	0.24	0.24
		mm/mm	-	-	0.29	0.29	0.29	0.24	0.24	0.24
Notched Izod Impact, LW	D256	ft-lbs/in	25	25	15	10	10	15	10	10
		J/mm	1.33	1.33	0.801	0.533	0.533	0.801	0.533	0.533
Notched Izod Impact, CW	D256	ft-lbs/in	4	4	5	5	5	5	5	5
		J/mm	0.214	0.214	0.267	0.267	0.267	0.267	0.267	0.267

	ASTM TEST METHOD	UNITS/ VALUE	SERIES 500/525 SHAPES	SERIES 600/625 SHAPES	SERIES 500/525 PLATE ④ 1/8" 3.175mm	3/16" - 3/8" 4.76-9.5mm	1/2" - 1" 9.5-25.4mm	SERIES 600/625 PLATE ④ 1/8" 3.175mm	3/16" - 1/4" 4.76-6.35mm	3/8" - 1" 9.5-25.4mm
PHYSICAL*										
Barcol Hardness	D2583	-	45	45	40	40	40	40	40	40
24 hr Water Absorption ⑥	D570	% Max	0.60	0.60	0.60	0.60	0.60	0.60	0.60	0.60
Density	D792	lbs/in³	0.062-0.070	0.062-0.070	0.060-0.068	0.060-0.068	0.060-0.068	0.060-0.068	0.060-0.068	0.060-0.068
		10^{-3} g/mm³	1.72-1.94	1.72-1.94	1.66-1.88	1.66-1.88	1.66-1.88	1.66-1.88	1.66-1.88	1.66-1.88
Coefficient of Thermal Expansion, LW ⑧	D696	10^{-6} In/In/°F	7	7	8	8	8	8	8	8
		10^{-5} mm/mm/°C	12	12	14.5	14.5	14.5	14.5	14.5	14.5
Coefficient of Thermal Expansion, CW ⑧	D696	10^{-6} In/In/°F	16	16	-	-	-	-	-	-
		10^{-5} mm/mm/°C	28.8	28.8	-	-	-	-	-	-
Thermal Conductivity ⑨	C177	BTU-in/ft²/hr/°F	4	4	-	-	-	-	-	-
		W/(m * °K)	0.58	0.58	-	-	-	-	-	-
*All values are minimum ultimate properties from coupon tests except as noted.										
ELECTRICAL										
Arc Resistance, LW ⑧	D495	seconds	120	120	-	-	-	-	-	-
Dielectric Strength, LW ⑤	D149	KV/in	35	35	35	35	35	35	35	35
		KV/mm	1.38	1.38	1.38	1.38	1.38	1.38	1.38	1.38
Dielectric Strength, PF ⑤	D149	volts/mil	200	200	200	-	-	250	-	-
FLAMMABILITY ⑤										
Flammability Classification	UL 94	V-0								
Tunnel Test	E84	25 Max								
NBS Smoke Chamber	E662	650-700 (Typical)								
Flammability	D635	Self Extinguishing								
UL Thermal Index	Generic	266°F								
		130°C								
British Fire Test	BS 476-7	Class 1								

④ This value is determined from full section simple beam bending of EXTREN® structural shapes.
⑦ The Shear Modulus value has been determined from tests with full sections of EXTREN® structural shapes. (See Strongwell's *Design Manual* for further information.)
③ Value would be 50 if the surfacing veil were not there.
④ Plate compressive stress/modulus measured edgewise and flexural stress/modulus measured flatwise.
⑤ Values apply to Series 525 and 625 (≥ 1/8" thickness).
⑥ Measured as a percentage maximum by weight.
⑦ Span to depth ratio of 3:1; EXTREN® angles will have a minimum value of 4000 psi and the I/W shapes are tested in the web.
⑧ Typical values.

LW - Lengthwise
CW - Crosswise
PF - Perpendicular to laminate face

Fastener spacing recommendation by Strongwell

STRONGWELL

Section 19
Fabrication

THREADED FASTENERS

BEARING

ALLOWABLE LOADS IN POUNDS

FIBERGLASS THICKNESS	BOLT DIAMETER 1/4"	3/8"	1/2"	5/8"	3/4"	1"
1/8"	234	352	469	586	703	938
1/4"	469	703	938	1172	1406	1875
3/8"	703	1055	1406	1758	2109	2812
1/2"	938	1406	1875	2344	2812	3750
3/4"	1406	2109	2812	3516	4219	5625

Allowable load = Allowable bearing stress x bearing area.

EXAMPLE

1/4" thickness with 1/2" dia. bolt

$$\text{Allowable load} = \frac{30{,}000 \text{ psi}}{4} \times .25" \times .50" = 938 \text{ lbs.}$$

NOTE: The above table assumes the bearing stress on fiberglass controls. The designer should verify that no other element of the connection controls.

SHEAR

ALLOWABLE LOADS IN POUNDS

BOLT TYPE	BOLT DIAMETER 1/4"	3/8"	1/2"	5/8"	3/4"	1"
S.S. Single Shear	1473	3312	5889	9204	13254	23562
S. S. Double Shear	2964	6624	11778	18408	26508	47124
FIBREBOLT®, Single Shear	—	400	650	950	1550	3750
FIBREBOLT®, Double Shear	—	750	1250	1875	3000	5000

NOTE: The above table assumes the shear capacity of the fastener controls. The designer should verify that no other element of the connection controls.

RECOMMENDED MINIMUM FASTENER EDGE DISTANCES AND PITCH RATIO OF DISTANCE TO FASTENER DIAMETER

	RANGE	COMMON
Edge Distance - end	2.0 to 4.5	3.0
Edge Distance - side	1.5 to 3.5	2.0
Pitch	4.0 to 5.0	5.0

GRK screw

GRK FASTENERS

ESR-2442

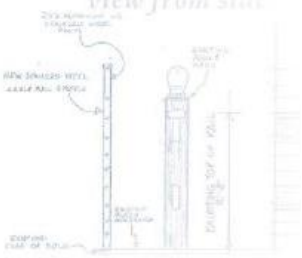

FASTENER TECHNICAL DATA

ICC ES

RSS™

TABLE 1—RSS™ FASTENER SPECIFICATIONS

FASTENER DESIGNATION		LENGTH[1] (inches)	THREAD LENGTH[2] (inches)	HEAD DIAMETER (inch)	DRIVE SIZE	HEAD HEIGHT (inch)	SHOULDER ø (inch)	MINOR THREAD DIAMETER (inch)	SHANK DIAMETER (inch)	OUTSIDE THREAD DIAMETER (inch)	SPECIFIED BENDING YIELD STRENGTH[3] F_{yb} (psi)	ALLOWABLE STEEL STRENGTH	
												TENSILE (lbf)	SHEAR (lbf)
RSS™	1/4 x 2 1/2"	2 1/2	1 1/2	0.533	T-25	0.110	0.244	0.152	0.169	0.236	153,400	1112	754
	1/4 x 2 3/4"	2 3/4	1 3/4										
	1/4 x 3 1/8"	3 1/8	2										
	1/4 x 3 1/2"	3 1/2	2 3/8										
	5/16 x 2 1/2"	2 1/2	1 1/2	0.620	T-30	0.157	0.301	0.167	0.195	0.276	171,800	1415	982
	5/16 x 2 3/4"	2 3/4	1 3/4										
	5/16 x 3 1/8"	3 1/8	2										
	5/16 x 3 1/2"	3 1/2	2 3/8										
	5/16 x 4"	3 7/8	2 1/2										
	5/16 x 5 1/8"	5	3 3/8										
	5/16 x 6"	5 7/8	3 7/8										
	3/8 x 3 1/8"	3 1/8	2	0.689	T-40	0.181	0.364	0.191	0.219	0.313	160,200	1941	1231
	3/8 x 4"	3 7/8	2 1/2										
	3/8 x 5 1/8"	5	3 3/8										
	3/8 x 6"	5 7/8	3 7/8										
	3/8 x 7 1/4"	7	4 3/8										
	3/8 x 8"	7 3/4	4 3/8										
	3/8 x 10"	9 3/4	5										
	3/8 x 12"	11 3/4	5 7/8										
	3/8 x 14 1/8"	14 1/8	5 7/8										
	3/8 x 16"	15 3/8	5 7/8										
RSS PHEinox™	1/4 x 2 1/2"	2 1/2	1 1/2	0.533	T-25	0.110	0.244	0.152	0.169	0.236	100,300	626	546
	1/4 x 3 1/8"	3 1/8	2										
	5/16 x 2 1/2"	2 1/2	1 1/2	0.620	T-30	0.157	0.301	.167	0.195	0.276	106,500	806	668
	5/16 x 3 1/8"	3 1/8	2										
	5/16 x 4"	3 7/8	2 1/2										
	5/16 x 5 1/8"	5	3 3/8										
	5/16 x 6"	5 7/8	3 7/8										
RSS JTS™				0.534	T-25	0.090	0.244	0.152	0.171	0.240	203,700	1104	769
	1/4 x 5"	5	1 3/8										
	1/4 x 6 3/4"	6 5/8	1 3/8										

For **SI**: 1 inch = 25.4 mm; 1 psi =6.9 kPa; 1 lbf = 4.4 N.

[1]The length of fasteners is measured from the underside of the head to bottom of the tip. See Figure 1.
[2]Length of thread includes tip. See Figure 1.
[3]Bending yield strength determined in accordance with ASTM F1575 using the minor thread diameter.
[4]See Figure 1 for additional dimensional information.

GRK FASTENERS

ESR-2442

ICC ES

RSS™ FASTENER TECHNICAL DATA

TABLE 4 - CONNECTION GEOMETRY

CONNECTION GEOMETRY/ CRITERIA	DIAMETERS[1]	REQUIRED DIMENSION (inches)		
		RSS, RSS PHEinox & RSS JTS 1/4" NOMINAL DIAMETER	RSS & RSS PHEinox 5/16" NOMINAL DIAMETER	RSS 3/8" NOMINAL DIAMETER
Minimum Edge Distance				
Loading Parallel to Grain	8	1 1/2	1 5/8	1 7/8
Loading Perpendicular to Grain, Loaded Edge	8	1 1/2	1 5/8	1 7/8
Loading Perpendicular to Grain, Unloaded Edge	8	1 1/2	1 5/8	1 7/8
Minimum End Distance				
Tension Load Parallel to Grain	15	2 5/8	3	3 3/8
Compression Load Parallel to Grain	10	1 3/4	2	2 1/4
Load Perpendicular to Grain	10	1 3/4	2	2 1/4
Spacing (Pitch) Between Fasteners in a Row.				
Parallel to Grain	15	2 5/8	3	3 3/8
Perpendicular to Grain	10	1 3/4	2	2 1/4
Spacing (Gage) Between Rows of Fasteners				
In-Line	5	7/8	1	1 1/8
Staggered	2 1/2	1/2	1/2	5/8
Minimum Penetration into Main Member for Single Shear Connections	6	1 1/8	1 1/4	1 3/8

For **SI:** 1 inch = 25.4 mm.

[1]Diameter is the shank diameter as specified in Table 1.

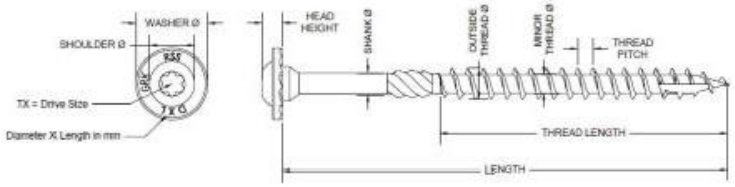

FIGURE 1—RSS™ AND RSS PHEINOX™ SCREWS

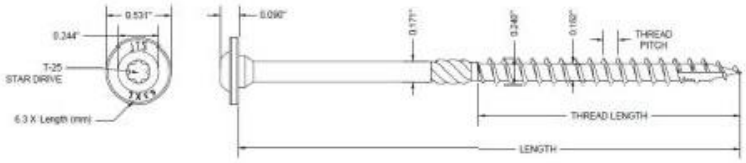

FIGURE 2—RSS JTS™ SCREWS

APPENDIX E: CALCULATIONS

This appendix provides a detailed discussion of the hand calculations for the capacities of both control and strengthened beams. It also includes the calculations for determining the required number of fasteners and the screw placement pattern for different lengths of FRP channels and strips.

Capacity calculations

The following calculations evaluate both the control timber beam and the FRP-strengthened timber beam to determine their flexural and shear strengths, incorporating adjustments for material properties and design specifications.

Control beam: For the control timber beam, section dimensions b_t (beam width) and h_t (beam height) and material properties F_b (allowable bending stress), F_v (allowable shear stress), and E_t (modulus of elasticity) establish the base parameters. Adjustment factors from the AASHTO Standard Specification for Highway Design - 2002 edition, chapter 13 [51], including C_M, C_D, C_F, C_V, C_L, C_f, C_{fu}, and C_r account for criteria such as loading conditions, moisture content, lateral support, and beam geometry. The assumptions for this calculation are as follows: the beam is subjected to vehicle live load (2 months) and is in a dry service environment with a moisture content below 19%. It also assumes adequate lateral support to prevent buckling, a standard depth-to-width ratio, and no incising or repetitive member use.

The adjusted bending capacity ($F_b{}'$) and shear capacity ($F_v{}'$) are calculated using eqn. 1 and 2, respectively.

$$F_b{}' = F_b\, C_M\, C_D\, C_F\, C_V\, C_L\, C_f\, C_{fu}\, C_r \quad \text{(Eqn. 1)}$$

$$F_v{}' = F_v\, C_M\, C_D \quad \text{(Eqn. 2)}$$

These adjustments yield conservative design values for bending and shear capacities. The centroid (y_c) and moment of inertia (I_b) for the timber beam are calculated. Using these properties, the moment capacity (M) and shear capacity (V) are then determined by eqn. 3 and 4, respectively.

$$M = \frac{F_b{}' \times I_b}{y_c} \quad \text{(Eqn. 3)}$$

$$V = \frac{F_v{}' \times a}{1.5} \quad \text{(Eqn. 4)}$$

Where, a is the support to load distance. The load required for failure, P, is calculated based on both moment capacity (eqn. 5) and shear capacity (eqn. 6), with the smaller load value controlling. This load represents the predicted maximum load the timber beam can support before failure under these design conditions.

$$P = \frac{M}{a} \quad \text{(Eqn. 5)}$$

$$P = V \quad \text{(Eqn. 6)}$$

Strengthened beams: The transformed section method is applied to analyze the FRP-strengthened composite beam consisting of a timber section reinforced with GFRP channels and hybrid FRP strip. This method simplifies the analysis by allowing the composite beam to be treated as a single homogeneous section, making it easier to calculate properties like centroid, moment of inertia, and load capacities under bending and shear. The following assumptions are made in calculating the strength:

The composite beam has a perfect bond between the timber and FRP materials, ensuring that the strain is consistent across the interface.

The composite section is assumed to remain within the elastic range, meaning that both timber and FRP exhibit linear elastic behavior under the applied loads.

The implementation of the transformed section method is started by calculating the modular ratio (n), defined as the ratio between the modulus of elasticity of the FRP (E_{fc} and E_{fs} for channel and strip, respectively) and timber ($E_t{}'$). The adjusted modulus of elasticity of timber ($E_t{}'$) is calculated by eqn. 7 considering adjustment factors.

$$E_t{}' = E_t\, C_M\, C_t\, C_i \quad \text{(Eqn. 7)}$$

Where, E_t is the tabulated modulus of elasticity for timber. Separate modular ratios are calculated for channels (n_c) and strip (n_s) using eqn. 8 and 9, respectively.

$$n_c = \frac{E_{fc}}{E_t{}'} \quad \text{(Eqn. 8)}$$

$$n_s = \frac{E_{fs}}{E_t{}'} \quad \text{(Eqn. 9)}$$

The widths of the FRP components are then transformed to equivalent timber widths using the modular ratios. The centroid (y_{tr}) and moment of inertia (I_{tr}) for the transformed section are calculated. The moment capacity (M, at either the top or bottom edge) and shear capacity (V, at the centroid) of the timber beam are then determined by eqn. 10 and 11, respectively.

$$M_c = \frac{F_c \times I_{tr}}{y_{tr}\,(bottom)}$$
$$M = min\,of\; M_s = \frac{F_s \times I_{tr}}{y_{tr}\,(bottom)} \quad \text{(Eqn. 10)}$$
$$M_t = \frac{F_b{}' \times I_{tr}}{y_{tr}\,(top)}$$

$$V = \frac{F_v{}' \times I_{tr} \times t}{Q} \quad \text{(Eqn. 11)}$$

Where, F_c and F_s are tensile strength of FRP channel and strip, respectively, and Q is the first moment of the area. The load required for failure, P, is calculated based on both moment capacity (eqn. 12) and shear capacity (eqn. 13), with the smaller load value controlled. This load represents the maximum allowable load the composite beam can support under these design conditions.

$$P = \frac{M}{a} \quad \text{(Eqn. 12)}$$

$$P = V \quad \text{(Eqn. 13)}$$

Screw pattern

The following calculations determine the number of fasteners required to securely attach FRP strips to the timber beam, ensuring that the strips can achieve their intended tensile capacity. 1/4"x3-1/2" RSS-GRK screws were selected for the strips. The calculation steps start by considering the properties of the FRP strip, including tensile strength (f_f), adjusted for exterior exposure conditions using the coefficient C_e, from ACI 440.2 [11]. The FRP geometric properties, such as the thickness (t_f) and width (b_f) are used to

calculate the strip's area (A_f). The area of the fastener hole (A_h) is also calculated from the hole diameter (d_h) and thickness of the FRP (t_f).

Fastener spacing in both horizontal (S_h) and vertical (S_v) directions are considered when calculating two configurations: fasteners in straight and staggered lines. The spacing requirements outlined in GRK specification (Appendix C) were satisfied. The area for each configuration is calculated with eqn. 14 and 15, where A_{st} and A_{diag} represent the areas along the straight line and diagonal line, respectively.

$$A_{st} = A_f - (N_{st} \times A_h) \quad \text{(Eqn. 14)}$$

$$A_{diag} = A_f - (N_s \times A_h) + (N_{stagg} \times \frac{t_f \times {S_h}^2}{4 \times S_v}) \quad \text{(Eqn. 15)}$$

Where, the N_{st}, N_s, and N_{stagg} are number of holes in a straight line, staggered line, and number of staggers, respectively. The smaller of these two areas is chosen as the effective area (A_e) to calculate the tensile capacity of the FRP (T_f) shown in eqn. 16.

$$T_f = A_e \times f_f \quad \text{(Eqn. 16)}$$

The tensile capacity (T_f) and shear capacity (V_b) of the selected fasteners are then used to calculate the total number of fasteners (n) using eqn. 17.

$$n = 2 \times \frac{T_f}{V_b} \quad \text{(Eqn. 17)}$$

Considering practical aspects such as potential load distribution along the length of the strip, the initially calculated total number of fasteners (n) is conservative. It is assumed that 50% of the fasteners, particularly those located near the strip ends, are effectively engaged in bearing. Accordingly, the final number of fasteners required (n_T) is determined using eqn. 18.

$$n_T = \frac{1}{2} \times n \quad \text{(Eqn. 18)}$$

The schematic diagrams of the fastener patterns of the 17.5’ strip for the 19’ span beam and 23.5’ strip for the 25’ span beam are shown in Figure 136 and Figure 137, respectively.

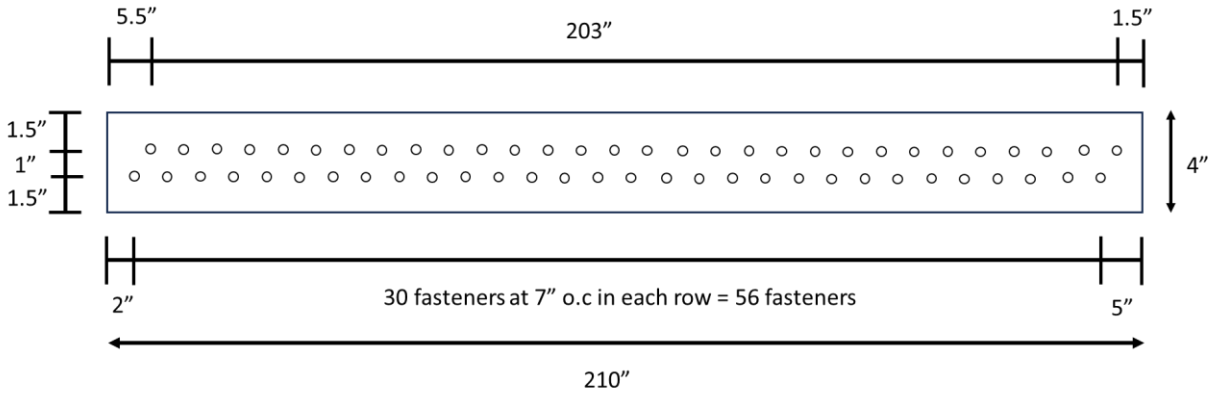

Figure 136: Fastener pattern of the 17.5’ strip

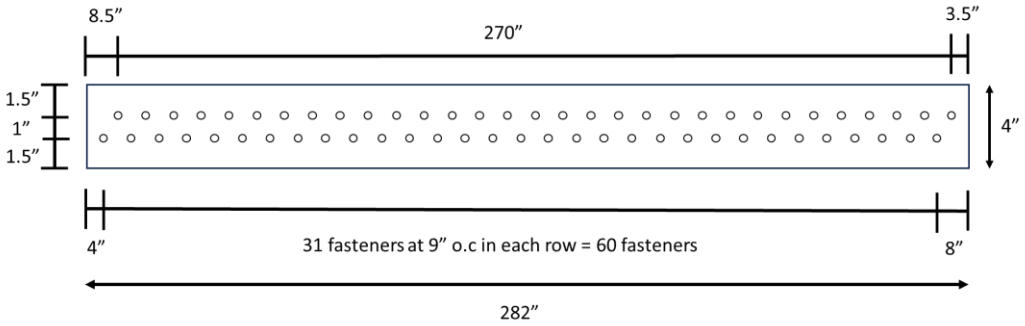

Figure 137: Fastener pattern of the 23.5’ strip

The calculations for determining the number of fasteners required to attach FRP strips to the timber beam securely are similar to the fastener calculation for the FRP strips. However, 5/16” x 3-1/8” RSS-GRK screws were selected for the channels. Two spacing requirements are outlined in the GRK specification (Appendix C) and the Strongwell Extern brochure (Appendix C), both of which were satisfied when determining the number of fasteners and their pattern for the channels. There are a total of five different channel lengths: 24’ channels for a 25’ span beam (Figure 138), 18’ channels for a 19’ span beam (Figure 139), 8’ channels for a 9’ span beam (Figure 140), and 6’ (Figure 141) and 3’ (Figure 142) channels for the existing split repair beams. However, the required number of fasteners for the 8’, 6’, and 3’ channels could not be provided due to the constraints of the minimum spacing requirement.

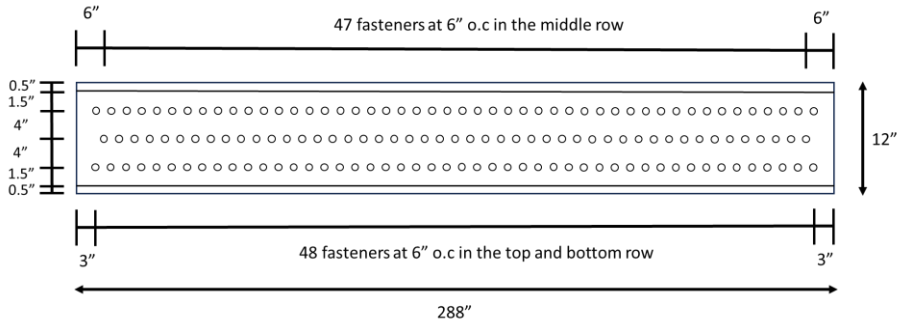

Figure 138: Fastener pattern of the 24’ channel

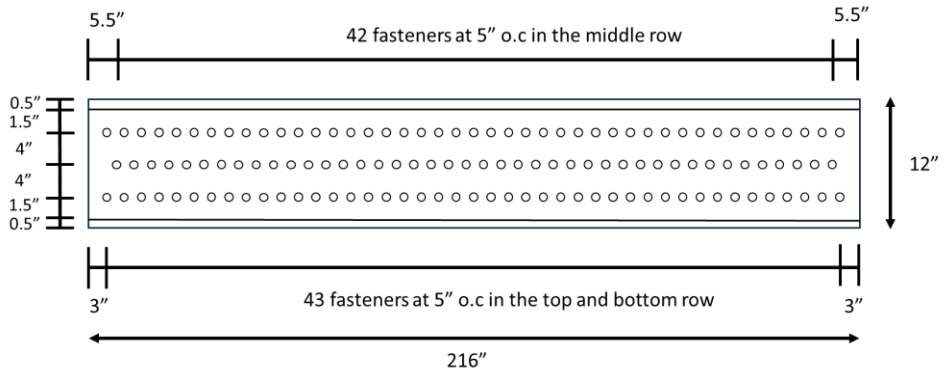

Figure 139: Fastener pattern of the 18’ channel

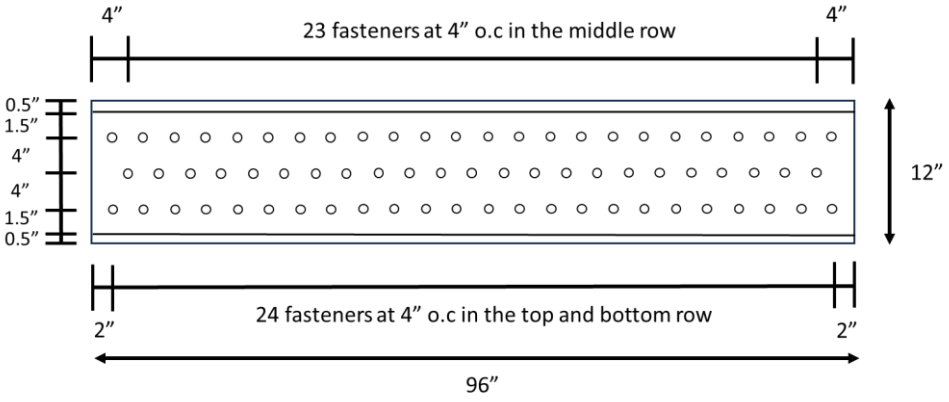

Figure 140: Fastener pattern of the 8’ channel

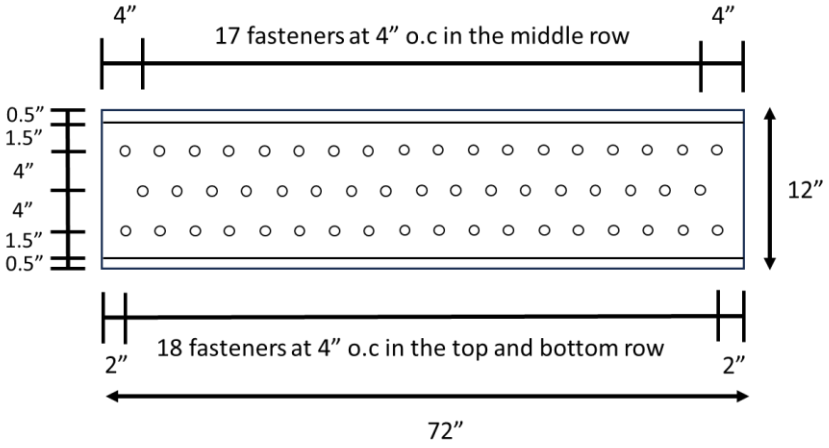

Figure 141: Fastener pattern of the 6’ channel

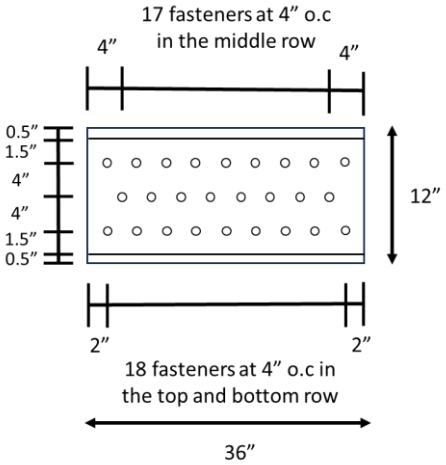

Figure 142: Fastener pattern of the 3’ channel

APPENDIX F: INDIVIDUAL BEAM RESULTS

6–Sh(1)

The beam had some minor checks and wane-type defects and some other minor handling impact damage on the top. Its actual dimensions were 5.75” x 17” and 10’ 1” long. The beam was cut in half for the shear test setup. The span length of the test beam was 9 ft, with a 6.48” overhang on each side. The shear vs. deflection graph is shown in Figure 143. The bearing failure at the load-bearing blocks started at around 22.0 kips. A split started forming at the end of the beam (which was originally the middle of the beam) as the load progressed. The beam failed by splitting on the end of the beam (Figure 144-b) through a knot. The ultimate shear carried by the beam was 27.0 kips when the midspan deflection was 0.89”.

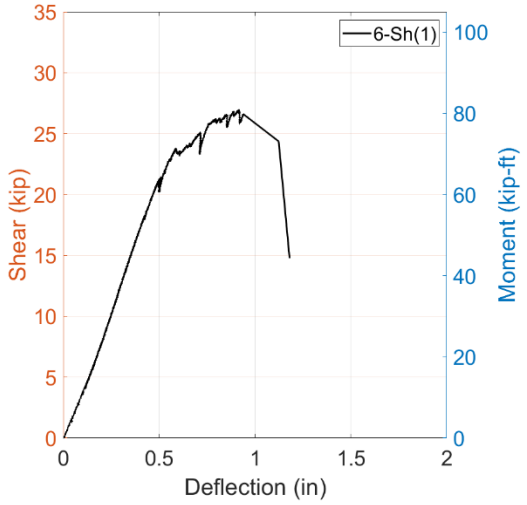

Figure 143: Shear vs deflection graph of 6-Sh(1)

(a) Bearing failure (b) Split at the end

Figure 144: Failure propagation of 6-Sh(1)

6-Fl(1)

The beam was shorter, with an 18.5’ span (19’ 6” beam), and the supports needed to be adjusted to be 3” closer. The actual cross-section of the beam was 5.75" x 17". There were holes and bolts on the ends. Some holes were found near D2 and D3. Upon inspection, it was confirmed that this was an exterior beam, and core drilling confirmed no rot. The moment vs. deflection graph is shown in Figure 145. Creaking started at around 110.5 kip-ft. A flexural crack (Figure 146) formed near D1 at around 130.0 kip-ft. The ultimate moment carried by the beam was 145.6 kip-ft when the deflection was 2.53”. The beam failed with a large pop as a flexural crack formed laterally with a diagonal run across the beam.

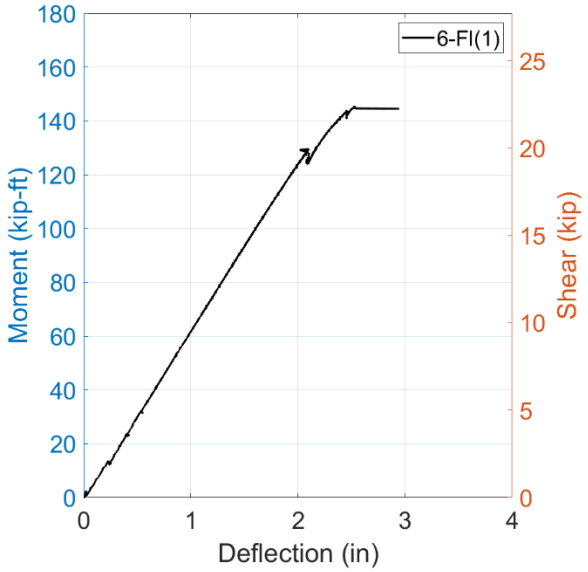

Figure 145: Moment vs deflection graph of 6-Fl(1)

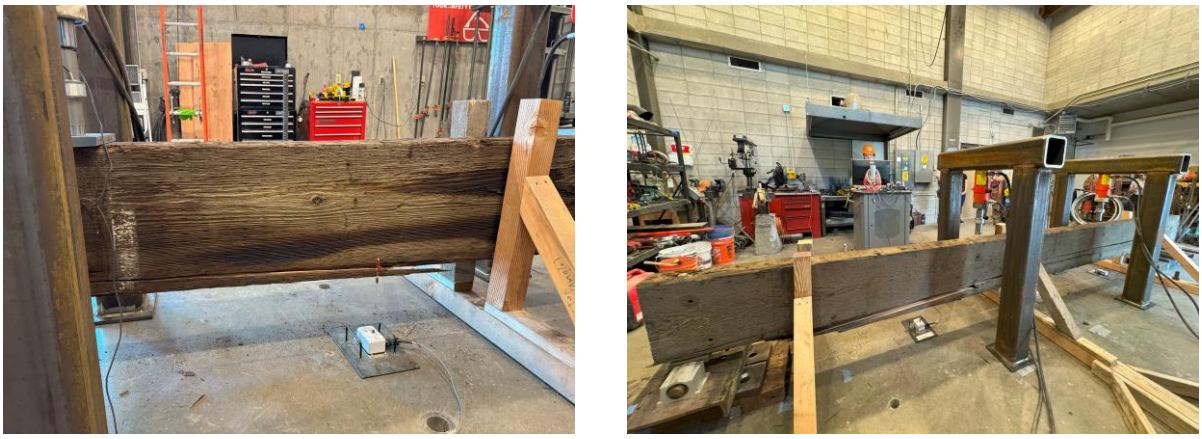

(a) Crack near D1 (b) Flexure crack across the beam

Figure 146: Failure propagation of 6-Fl(1)

6–Fl(2)

The beam's dimensions were 5.75" x 17" and 20’ 0.75” in length. The beam had some minor checking. Figure 147 presents the moment vs deflection graph of the beam. The first creaking started at around 107.3 kip-ft. The beam failed due to a sudden flexure crack (Figure 148). The ultimate moment carried by the beam was 126.1 kip-ft at a deflection of 1.96”.

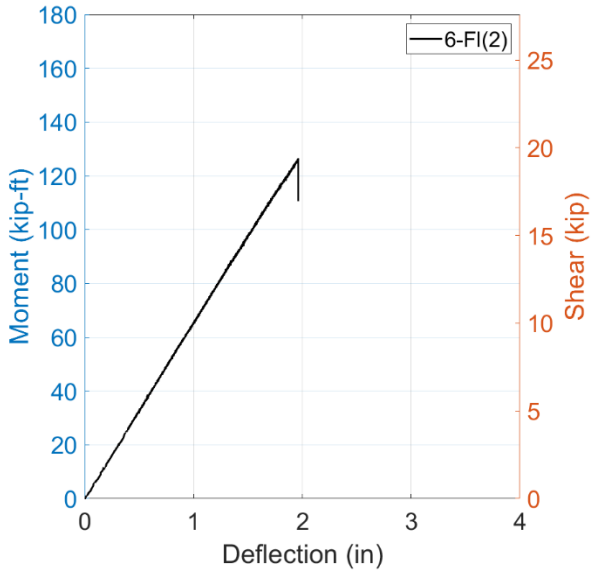

Figure 147: Moment vs deflection graph of 6-Fl(2)

Figure 148: Failure propagation of 6-Fl(2)

6–Fl(1)-CR(C-S)

This was the crack-repair beam of flexure control 1 (6-Fl(1)). The beam was repaired following the steps discussed in chapter three. The string potentiometers were attached to the bottom flange of the side channel. The moment vs deflection curve is presented in Figure 149. The first creaking started at 89.7 kip-ft. The first crack occurred at 105.3 kip-ft when the mid-span deflection was 1.6". Crushing occurred under load block (Figure 150-a) at around 185.3 kip-ft. The ultimate moment carried by the beam was 189.2 kip-ft when the deflection was 3.98". The test was stopped after noticing that the reaction blocks weren't centered.

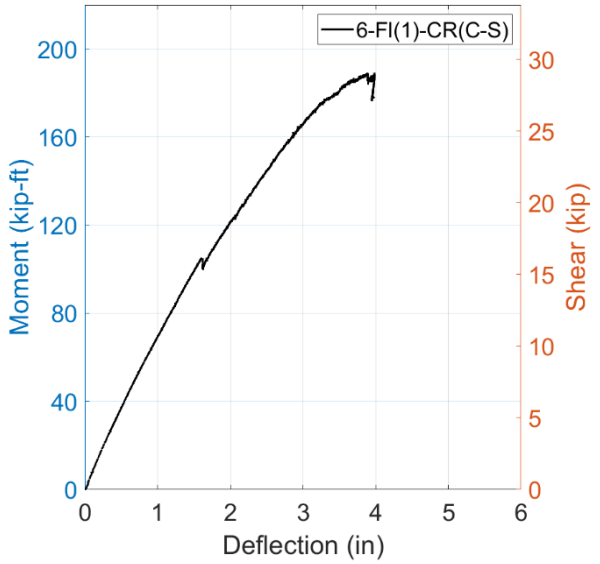

Figure 149: Moment vs deflection of 6-Fl(1)-CR(C-S)

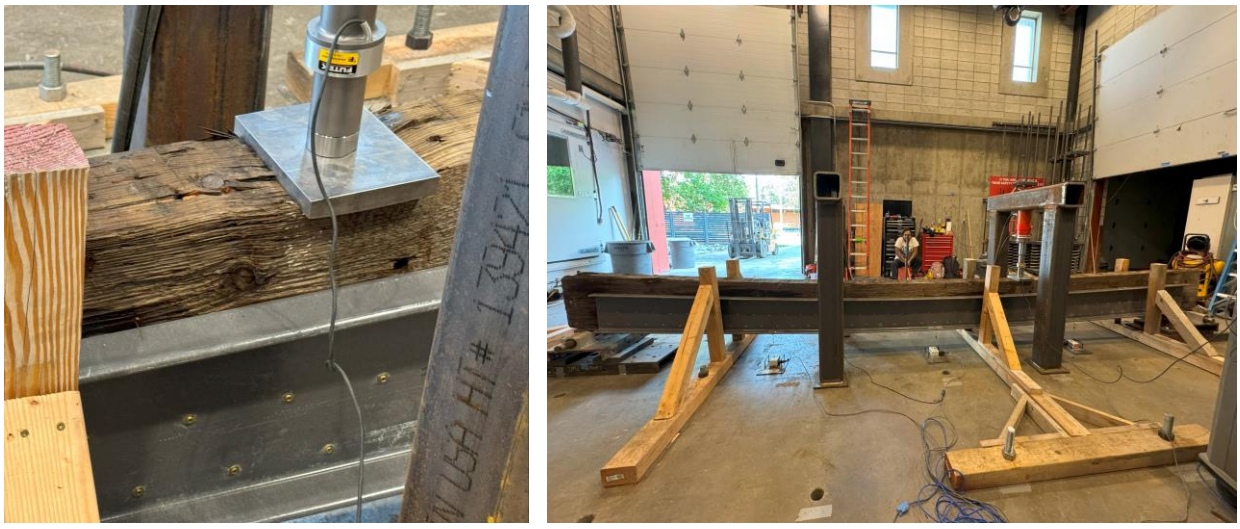

(a) Crushing under load block (b) Fully loaded beam before release

Figure 150: Failure propagation of 6-Fl(1)-CR(C-S)

6-Fl(2)-CR(S)

This was the crack-repair beam of flexure control 2 (6-Fl(2)), following the repair steps discussed in chapter three. The repair included attaching two strips on the sides and one at the bottom. The string potentiometers were anchored about 0.5” above the side strip. The moment vs deflection graph is depicted in Figure 151. The beam started making creaking sounds around the middle at around 97.5 kip-ft. When the moment reached 136.5 kip-ft at a 2.02” deflection, there was a loud pop, and the beam split (Figure 152) almost immediately at the end. The split rapidly propagated towards the center, causing the moment to drop sharply to 55.3 kip-ft, indicating that the beam had not been properly confined by the strip. When the moment was increased to 91.0 kip-ft, the split opened further. The test needs to be stopped because the stroke limit was reached, necessitating the removal of the load.

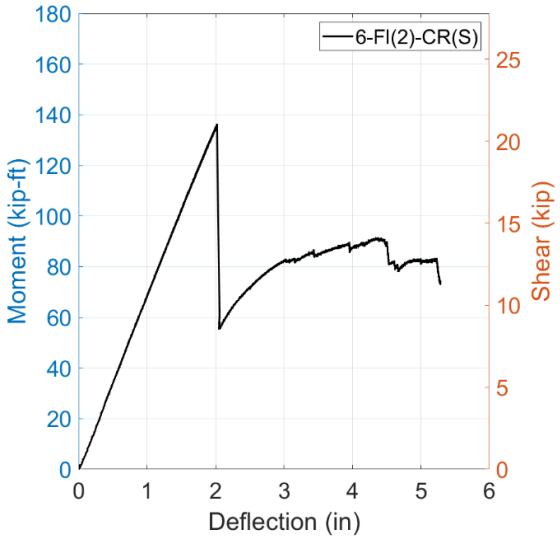

Figure 151: Moment vs deflection of 6-Fl(2)-CR(S)

(a) Split started on the end (b) Propagating to the middle

Figure 152: Failure propagation of 6-Fl(2)-CR(S)

6–Sh(1)-SR(C)

The beam was the split-repair beam shear control 1 (6-Sh(a)). The repair was carried out following the steps discussed in chapter three. There was an indentation at the bearing plates and a split on one end of the beam from the control beam testing. Figure 153 shows the shear vs deflection graph. The beam instantly settled into bearing dents at load points, and the split (Figure 154-a) instantly shifted with the load. There was a load pop at 21.0 kips. The beam started touching the garage side lateral bracing at around 26.0 kips. At around 29.0 kips, the beam started touching the lateral bracing. At around 30.0 kips, the beam leaned due to bearing failure (Figure 154-b), and the graph started to plateau, leading to the decision to end the test. The ultimate shear carried by the beam was 30.1 kips when the mid-span deflection was 1.69".

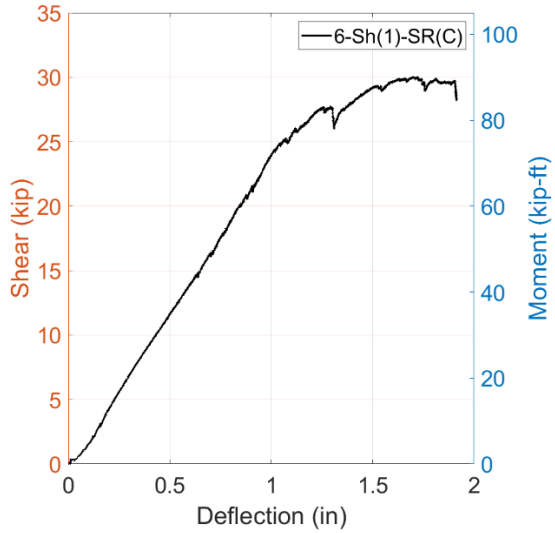

Figure 153: Shear vs deflection graph of 6-Sh(1)-SR(C)

(a) Split shifting on the end

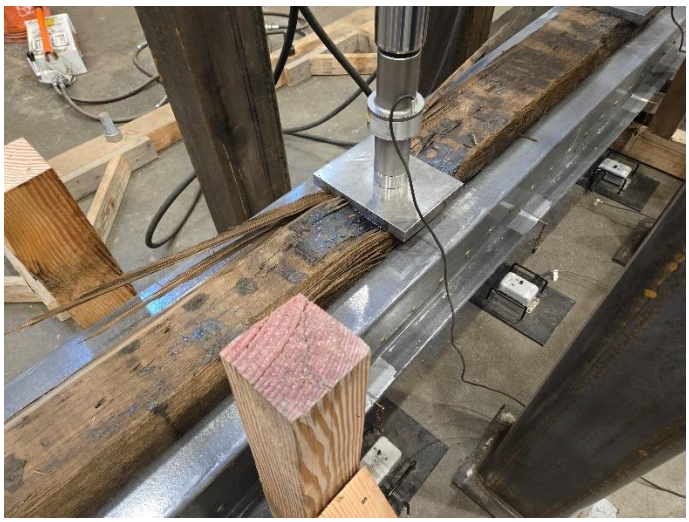

(b) Bearing failure under load block

Figure 154: Failure propagation of 6-Sh(1)-SR(C)

6-Fl-SR(C-S)

The actual dimensions of the beam were 5.75” x 17” with a length of 20’ 2”. There was a small split on one end. The beam was repaired following the steps previously discussed in chapter three. There was a missing screw on the east channel. The moment-deflection graph (Figure 155) showed a linear slope until 39 kip-ft, slightly stiffer than the two control beams (6-Fl(1) and 6-Fl(2)), with no lateral supports making contact. By 58.5 kip-ft, creaking noises were noted at the ends, and at 68.3 kip-ft, a 1” deflection occurred as the split on the end began to shift. A loud pop was heard at 74.8 kip-ft. At 107.3 kip-ft, slight noise emerged from the support. At 123.5 kip-ft, the beam started touching the middle top lateral support. When the moment reached 162.5 kip-ft, a screw sheared off from the channel, though no drop in load was observed. At 182.0 kip-ft and 3.51” deflection, there appeared to be some compression crack at the top, with creosote pushing out at the load cells, and loud popping was heard from mid-span as the moment held steady around 185.3 kip-ft. At 196.9 kip-ft and a 4.1” deflection, another pop was noted as the split shifted further, and a crack appeared on the east side string potentiometer (D3). With increased load, all east lateral supports were in contact with the beam, and slight eccentricity was observed on the load cells, leading to the decision to end the test. The failure propagation of the beam is shown in Figure 156. The ultimate moment carried by the beam was 200.9 kip-ft at a mid-span deflection of 4.27”.

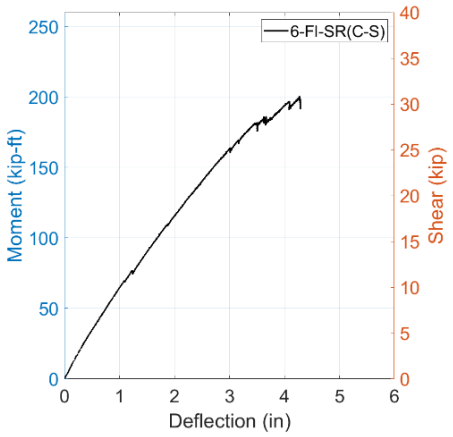

Figure 155: Moment vs deflection graph of 6-Fl-SR(C-S)

(a) Split shifting

(b) Creosote coming out

(c) Split shifting further

Figure 156: Failure propagation of 6-Fl-SR(C-S)

6-Fl-SR(C3)

The beam's actual dimensions were 5.75” x 17” with a length of 20’ 2”. It had an 18” long split at one end. The beam was split-repair with 3’ long channels on the ends of each side. The detail of the repair technique is outlined in chapter three. Figure 157 presents the moment vs deflection graph. Creaking started immediately when loading began. The first crack appeared in the mid-span at around 26.0 kip-ft. A distinct pop was heard as the moment increased to 32.5 kip-ft. The midspan crack noticeably widened at around 52.0 kip-ft, causing a 1.2” midspan deflection. At 55.3 kip-ft, the existing split shifted further and propagated beyond the channel. When the moment reached 62.4 kip-ft, the crack extended to the middle string potentiometer (D1) nail, leading to a sudden drop in the moment to 48.8 kip-ft. Shortly after, the D1 shot off the beam as the midspan crack expanded. Figure 158 shows the failure propagation of the beam. The ultimate moment carried by the beam was 64.35 kip-ft when the mid-span deflection was 2.16”.

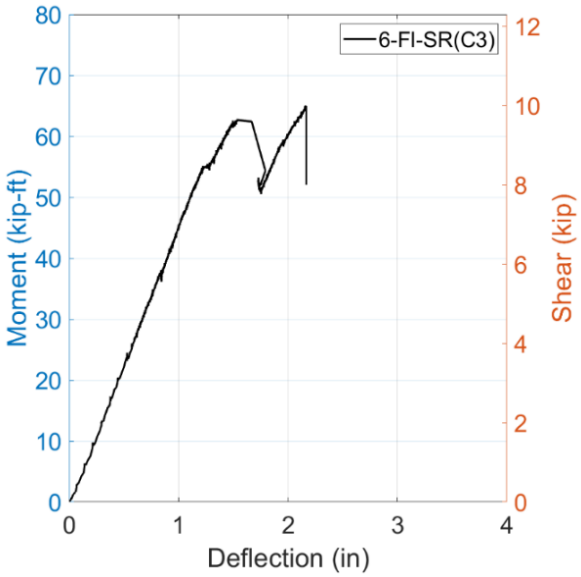

Figure 157: Moment vs deflection graph of 6-Fl-SR(C3)

(a) Crack started at mid-span (b) Split shifting (c) Mid-span cracked

Figure 158: Crack propagation of 6-Fl-SR(C3)

6-Fl-SR(C6)

The beam had a 12” long split at one end, which was repaired with 6’ long channels attached at the ends of each side of the beam. The actual dimensions of the beam were 5.75” x 17” with a length of 20’ 2” and the beam had notched ends. The moment vs deflection graph is presented in Figure 159. Creaking began at approximately 81.3 kip-ft, with compression failure initiating near the top, at around 84.5 kip-ft. At approximately 91 kip-ft, the entire load frame shifted. A compression crack (Figure 160-a) appeared near the load cell by the lateral support at 105.3 kip-ft. At a moment of 116.4 kip-ft, a mid-span crack occurred on both sides, accompanied by a loud pop, causing the moment to drop to 103.4 kip-ft. At 123.5 kip-ft, a flexure crack (Figure 160-b) developed with another loud pop, resulting in a 1.3 kip-ft moment drop. As the moment increased to 136.5 kip-ft, creaking noises were heard throughout the structure. At 139.8 kip-ft, a puff of dust emerged from the bottom near the load cell, leading to a sudden drop to 131.9 kip-ft. When the moment was increased again, the final crack at the bottom split open, indicating complete failure. The beam ultimately carried a moment of 141.1 kip-ft, at a mid-span deflection of 2.77”.

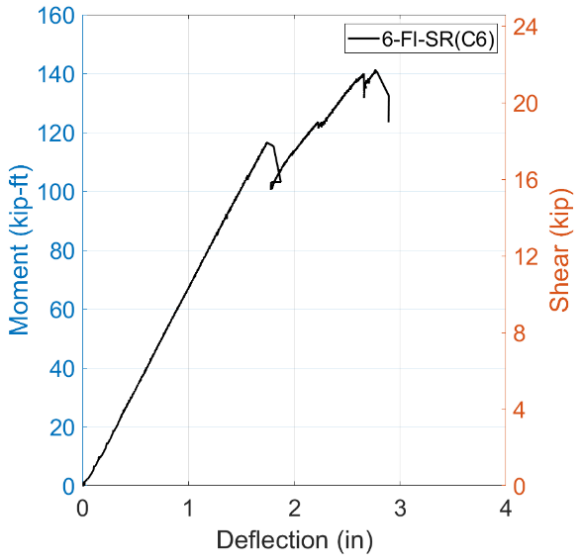

Figure 159: Moment vs deflection graph of 6-Fl-SR(C6)

(a) Compression crack at top (b) Flexure crack mid-span

Figure 160: Failure propagation of 6-Fl-SR(C6)

6-Sh-St(C)

The beam's actual dimensions were 5.75" x 17" and 10’ 0.5” long. It was cut in half for the shear test setup and strengthened by attaching channels in the middle of each side. Due to the uneven top surface, the beam was tested upside down. The shear vs deflection graph is shown in Figure 161. At 17.9 kip, a loud pop was heard followed by a sudden drop of shear to 17.1 kips. As the shear increased to 30.4 kips, a split was noticed at the end with a lot of creaking noise. When the shear hit 33.1 kips, another loud pop occurred, and a crack was observed at the bottom near the end, causing a drop to 27.2 kips. The loading continued and a split (Figure 162) also developed at the end. The beam's ultimate shear was 33.2 kips, at a mid-span deflection of 1.1". Eccentricity began to develop on the load cell due to bearing failure, prompting the decision to unload. No bearing issues were noted at the supports.

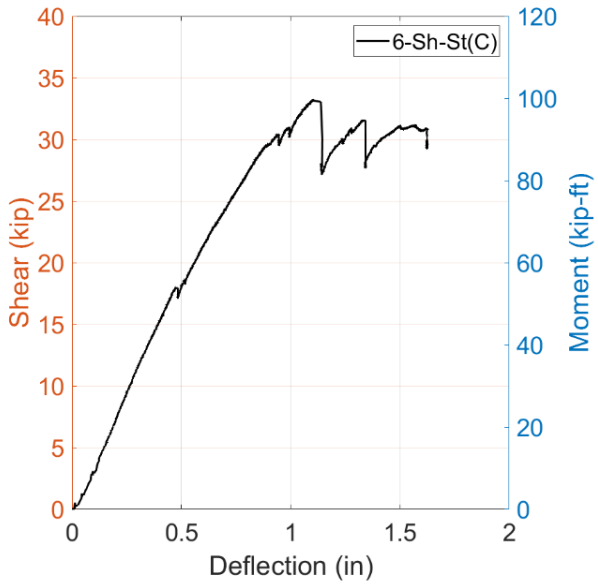

Figure 161: Shear vs deflection graph of 6-Sh-St(C)

Figure 162: Failure propagation of 6-Sh-St(C)

6-Fl-St(C-S)

This was a strengthened beam tested in a flexure setup. The strengthening was done by attaching two channels on the side and a strip at the bottom. It had dimensions of 5.75” x 17” and a length of 19’ 10”. There was an inclined cut on one end of the beam that added 3” to the total length of one side (Figure 163); however, the overall span length remained unaffected. A different size screw was mistakenly attached to the strip. The moment vs deflection graph is shown in Figure 164. During the load test, the first creaking was heard at around 58.5 kip-ft. At around 113.8 kip-ft, a small pop occurred on the end. At 136.5 kip-ft, a load pop occurred with no visible crack. When the moment was increased to 167.7 kip-ft, a crack emerged at the mid-span, accompanied by a distinct loud pop. At 176.2 kip-ft, creaking noises and a loud pop were heard as the crack in the mid-span expanded. The moment was then dropped to 170.9 kip-ft. At this point, one load cell was slightly eccentric, and creosote was oozing at the load cells (Figure 165-a). The crack propagated in the lower mid-span at around 182.0 kip-ft. The test was ultimately stopped at 189.2 kip-ft when the mid-span deflection was 2.77”, due to bearing failure at the load cell.

Figure 163: Inclined cut on one end

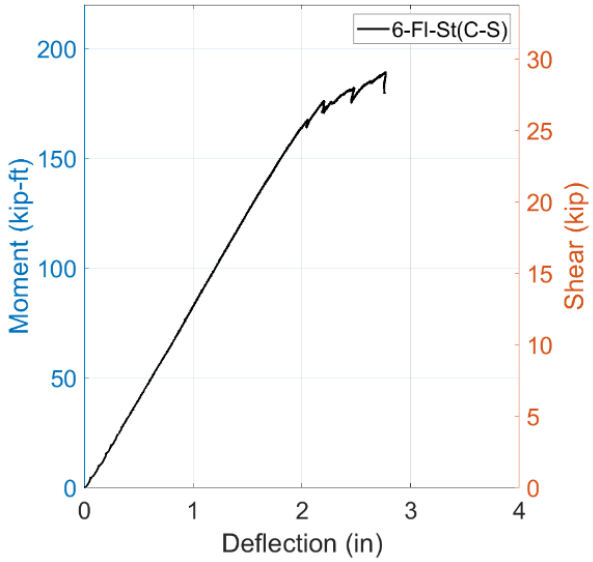

Figure 164: Moment vs deflection graph of 6-Fl-St(C-S)

(a) Creosote under load-bearing block

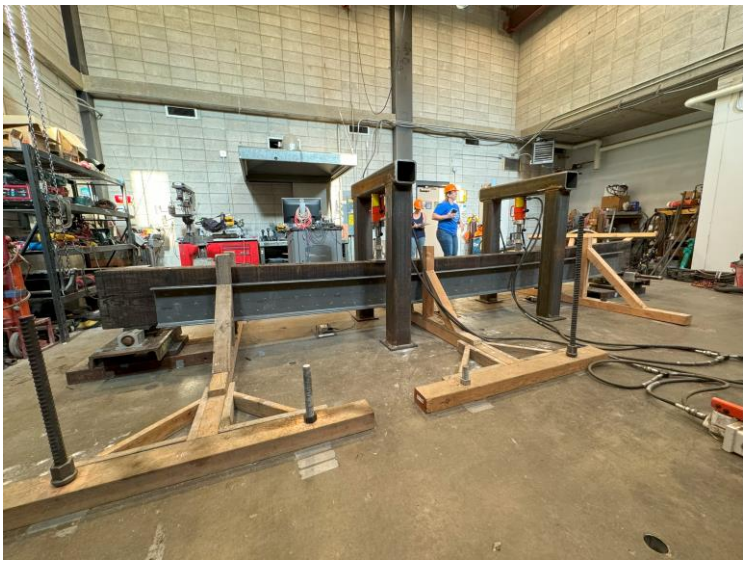

(b) Fully loaded beam

Figure 165: Failure propagation of 6-Fl-St(C-S)

6-Fl-St(S)

This was a strip-strengthened beam with three strips on the beam's sides and bottom. The beam's dimensions were 5.75" x 17" with a length of 19’ 0.75”. Like the 6-Fl-St(C-S) beam, there was an inclined cut on one end of the beam that added 3” to the total length of one side. The bottom of the beam was slightly uneven, so it was adjusted when loading, and then the deflection was re-zeroed after the beam was steady. The moment vs deflection is shown in Figure 166. Initially, a small pop occurred at approximately 65.0 kip-ft, followed by a slight creaking at midspan around 84.5 kip-ft. A distinct pop was heard when the moment reached 136.5 kip-ft, yet no visible damage was seen. At 144.3 kip-ft, a loud pop was heard, shaking the strip on the east side of the beam, and the first signs of cracking appeared under it. As the moment increased to 146.3 kip-ft, the beam experienced a 2.4" deflection, another loud pop occurred, and flexure cracking continued without a dramatic drop in moment. By 156.0 kip-ft, midspan cracking was observed in the beam, with a noticeable compression failure under one load cell, causing the moment to drop slightly to 152.1 kip-ft. At 165.1 kip-ft, the beam split with a loud popping sound from a knot at the end, leading to a 53" long visible opening on the east side and causing the moment to drop to 113.1 kip-ft. A slight recovery followed, with the moment rising back up to 126.8 kip-ft, but another loud pop was accompanied by a puff of dust from the top due to compression, further opening the split and causing shifts. Ultimately, the beam failed in shear at the end. The failure propagation of the beam is shown in Figure 167. The ultimate moment carried by the beam was 165.1 kip-ft, at a mid-span deflection of 2.81".

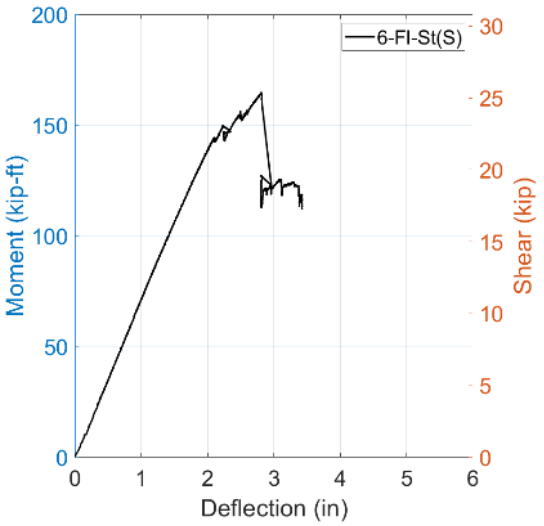

Figure 166: Moment vs deflection graph of 6-Fl-St(S)

(a) Crack at the middle

(b) Compression failure under load cell

(c) Split at the end

Figure 167: Failure propagation of 6-Fl-St(S)

8-Sh(1)

The actual dimensions of the beam were 7.75” x 17.5” and 26’ long with no noticeable damage. The beam was cut in 10’ 1’ for having a span length of 9’ with a 6.5” overhang on each side. Figure 168 shows the shear vs deflection of the beam. Bearing failure started forming at around 25.0 kips at the load-bearing blocks. The flexural crack started at the middle of the beam at around 34.0 kips when the mid-span deflection was 0.67”. The crack was opening up with increased loading. The beam failed by splitting at the end. The failure propagation of the beam is presented in Figure 169. The ultimate shear carried by the beam was 37.9 kips at a mid-span deflection of 0.98”.

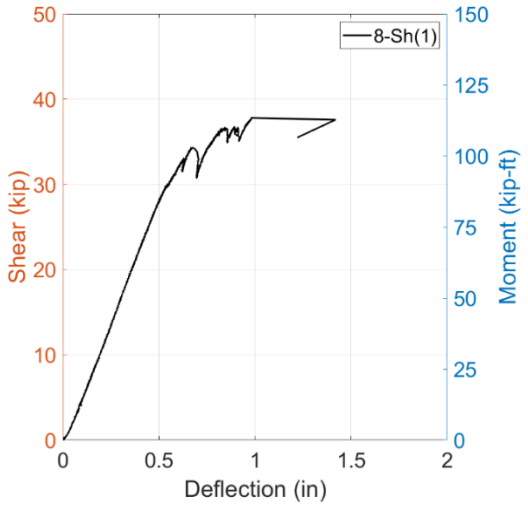

Figure 168: Shear vs deflection graph of 8-Sh(1)

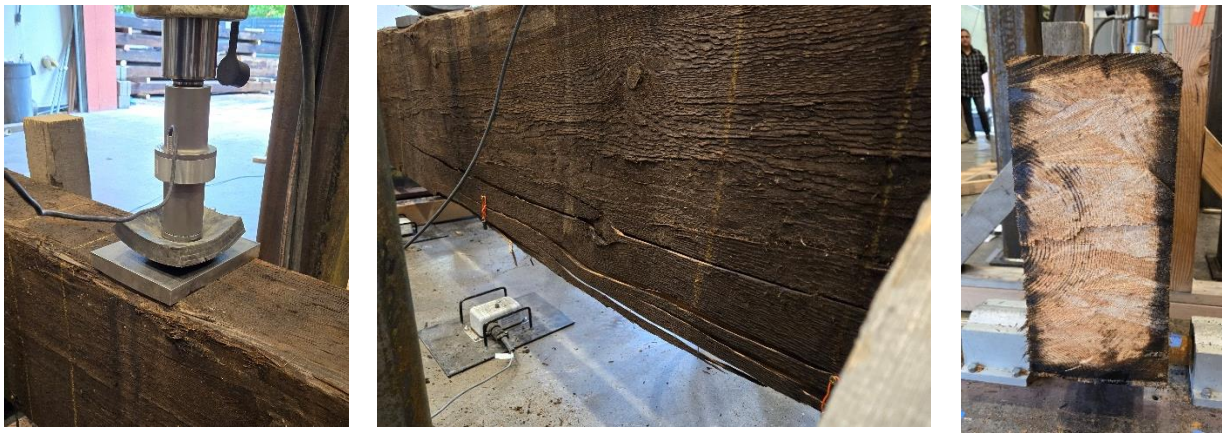

(a) Bearing failure started (b) Flexure crack at the mid-span (c) Split at the end

Figure 169: Failure propagation of 8-Sh(1)

8-Fl(1)

The beam's actual dimensions were 7.5” x 17” and 25’ 9” long. Its span length was 25’, with a 4.5” overhang on each side. The beam had no significant damage. Figure 170 presents the moment vs deflection of the beam. A flexural crack (Figure 171) started at around 132.0 kip-ft at the midspan of the beam and continued to open with higher load. The ultimate moment carried by the beam was 176.0 kip-ft at a midspan deflection of 3.28”. The beam failed due to flexure, with the crack initiating 66” from the right end and extending to 84” from the left end. The crack was located approximately 4” from the bottom of the beam.

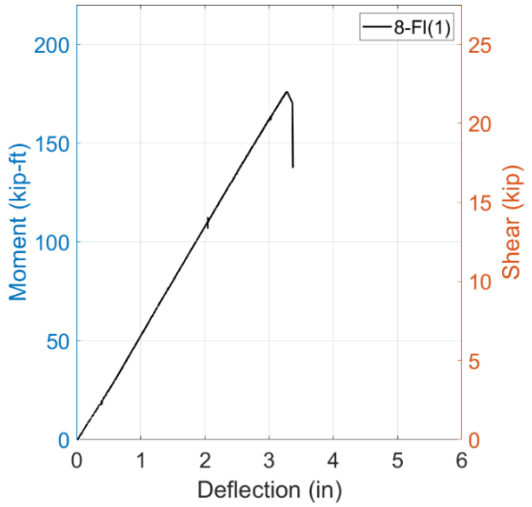

Figure 170: Moment vs deflection graph of 8-Fl(1)

(a) Flexure crack starting at mid-span (b) Cracked beam

Figure 171: Failure propagation of 8-Fl(1)

8-Fl(2)

The beam had some minor checks and wane defects. Its actual dimensions were 7.75" x 17", and it was 26' long. The moment vs deflection graph is shown in Figure 172. The creaking sound at mid-span started at around 84.0 kip-ft. At 94.4 kip-ft, a split propagated, and compression failure (Figure 173-a) occurred, resulting in a moment drop to 78.4 kip-ft. The beam failed at cracking in mid-span (Figure 173-b). The ultimate moment carried by the beam was 96.0 kip-ft when the deflection was 2.56". Two holes were drilled to see the beam's core, and it was confirmed that there was no rot.

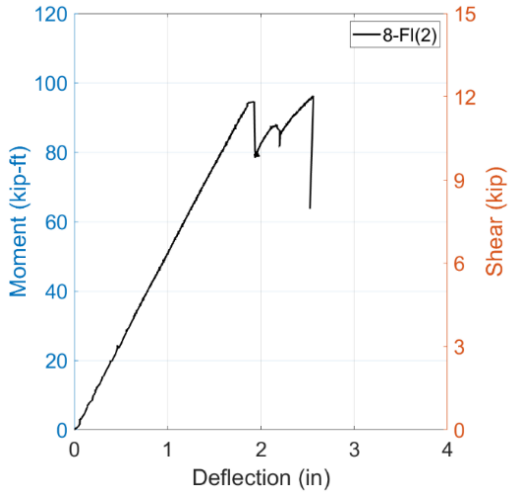

Figure 172: Moment vs deflection graph of 8-Fl(2)

(a) Compression failure at top

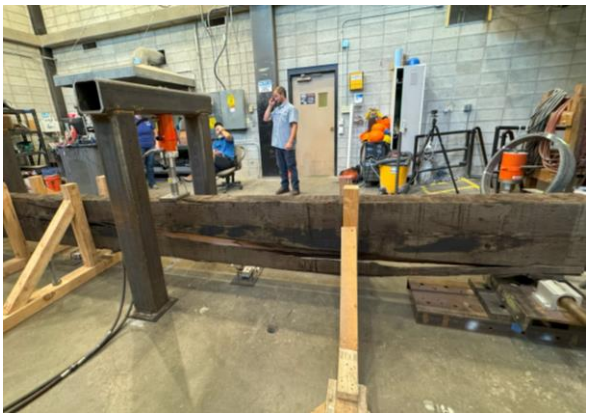

(b) Cracking in the mid-span

Figure 173: Failure propagation of 8-Fl(2)

8-Fl(1)-CR(C-S)

This was the crack-repair beam for flexural control 1 (8-Fl(1)). The repair process involved attaching channels on the sides and a strip on the bottom, and the detailed repairing processes are discussed in chapter three. The moment-deflection graph (Figure 174) showed a plateau at around 60 kip-ft, likely due to the screws engaging. There was a loud pop at around 242.4 kip-ft and a compression crack (Figure 175-a) near the load cell at 253.6 kip-ft. The test was stopped because the stroke limit was reached. The beam ultimately carried a moment of 264.8 kip-ft when the mid-span deflection was 5.28".

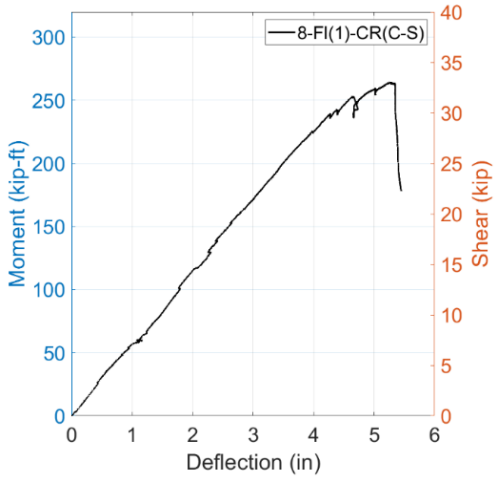

Figure 174: Moment vs deflection graph of 8-Fl(1)-CR(C-S)

(a) Compression failure at top

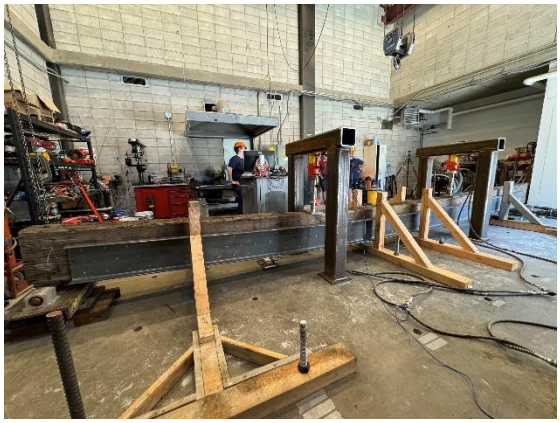

(b) Fully loaded beam

Figure 175: Failure propagation of 8-Fl(1)-CR(C-S)

8-Fl(2)-CR(S)

This was the Flexure Control 2 (8-Fl(2)) beam with crack repairs. Four strips were attached to the sides, and one was attached to the bottom. The detailed repair method is discussed in chapter three. The string potentiometers were anchored in the middle of two strips on the side. The moment vs deflection graph is shown in Figure 176. Creaking started in the midspan at around 104.0 kip-ft and continued with higher moment. At 160.0 kip-ft, a crack was opening up at the top middle through a knot (Figure 177-a), leading to a drop in the moment to 156.8 kip-ft. At 183.2 kip-ft, a poof of dust emerged from the top middle of the beam. When the moment reached 184.0 kip-ft, the beam started contacting the two lateral bracings. The loading was paused to take pictures at around 188 kip-ft. The beam cracked a lot while holding the load and eventually failed compression through a knot at the top face middle (Figure 177-b). The ultimate moment carried by the beam was 188.8 kip-ft when the mid-span deflection was 5.08".

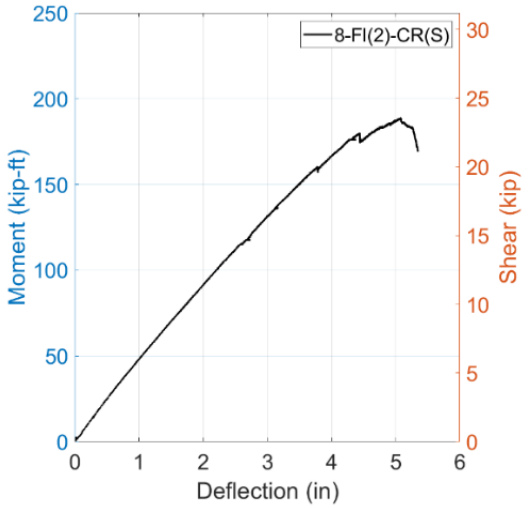

Figure 176: Load vs deflection graph of 8-Fl(2)-CR(S)

(a) Crack at mid-span through a knot

(b) Failure in compression

Figure 177: Failure propagation of 8-Fl(2)-CR(S)

8–Sh(1)-SR(C)

This was the split-repair beam of shear control 1 (8-Sh(1)), which was repaired following the steps outlined in chapter three, including attaching channels on the sides. There is an existing split on the end from the control test. The shear vs deflection graph is presented in Figure 178. Bearing failure began under the load block and support at approximately 26.0 kips. The beam started making contact with lateral bracings at around 36.0 kips. The existing split shifted at 36.8 kips. At 38.9 kips, a crack at the bottom midspan occurred, causing the shear to drop to 36.4 kips, with a screw on the channel shearing off. The load continued to increase, and shear failure was controlled on the end. The failure propagation of the beam is presented in Figure 179. The ultimate shear carried by the beam was 42.3 kips when the deflection was 1.58".

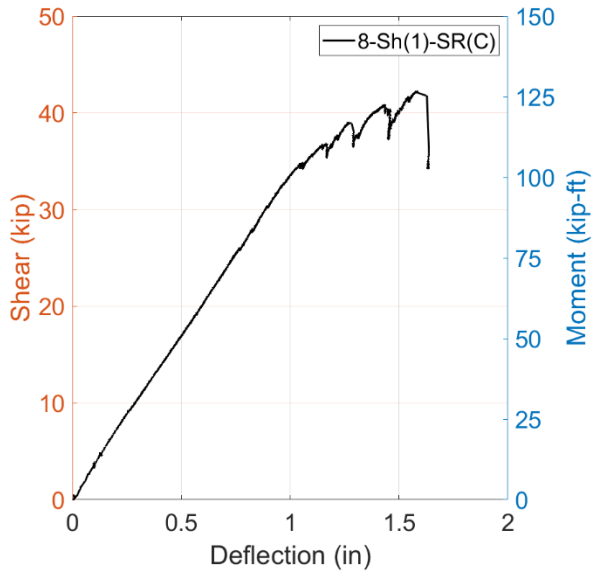

Figure 178: Moment vs deflection graph of 8-Sh(1)-SR(C)

(a) Bearing failure (b) Screw sheared off (c) Split at the end

Figure 179: Failure propagation of 8-Sh(1)-SR(C)

8-Fl-SR(C-S)

The beam's actual dimensions were 7.5" x 17" with a length of 26’ 0.75”. It had moderate checking along its length and was a split repaired beam with channels on the sides and a strip on the bottom. The beam had tapered ends and a through bolt was removed from one end. Figure 180 presents the moment vs deflection graphs. The first creaking occurred at around 94.4 kip-ft, and a small pop happened at around 112.0 kip-ft. A crack started forming in the bottom middle at around 133.6 kip-ft. Creaking continued with higher loading, and at a moment of 163.2 kip-ft, a crack formed under the channel, approximately 2” from the bottom on the east side, with a loud pop. As the moment increased to 175.2 kip-ft, a compression crack began to form near the top in the center of the beam. At 184.8 kip-ft, another loud pop was heard as the top middle of the beam buckled at the compression crack, causing the moment to drop to 143.2 kip-ft and then rebuild. At 167.2 kip-ft, a crack formation started near the D2 string potentiometer, about 12” from the load frame, followed by another crack at the bottom-mid, causing a slight load drop. As the moment reached 184.8 kip-ft, the beginning of a compression crack was observed near the center. At 187.2 kip-ft with 4.4” of deflection, a crack near the center began to open up. Finally, at 188.8 kip-ft with 4.7” of deflection, the bottom crack between the D1 and D2 string potentiometers started to widen, and a large crack formed near the D3 string potentiometer with a loud pop. The test was stopped after reaching the maximum stroke of the load cell. Figure 181 shows the failure propagation of the beam. The ultimate moment carried by the beam was 198.4 kip-ft at a mid-span deflection of 5.22”.

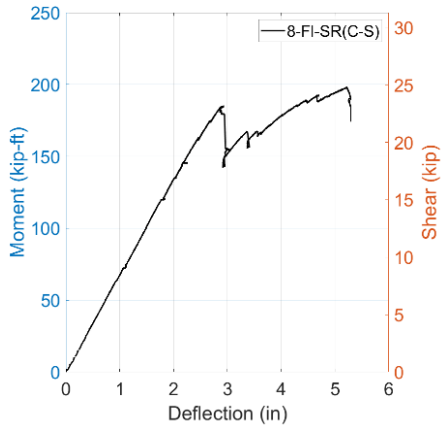

Figure 180: Moment vs deflection graph of 8-Fl-SR(S-C)

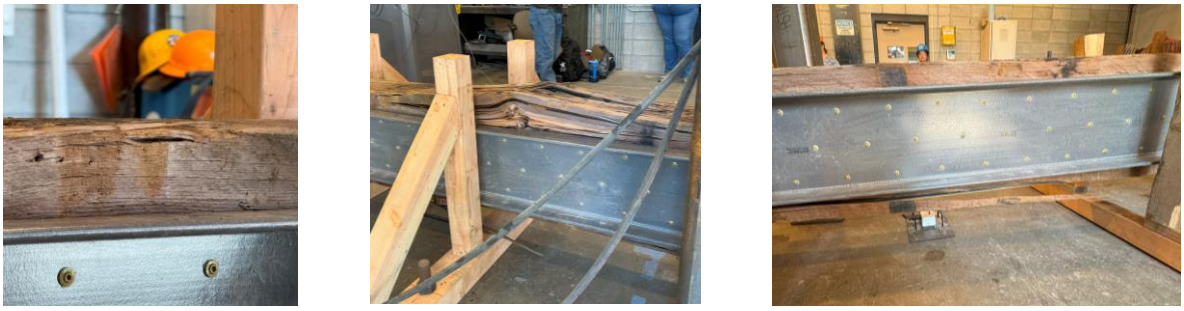

(a) Compression crack at top (b) Beam buckled at top middle (c) Flexure crack at bottom middle

Figure 181: Failure propagation of 8-Fl-SR(C-S)

8-Sh-St(C)

The actual dimensions of the beam were 7.5" x 17.5" with a length of 10'. It was a shear-strengthened beam cut into 10' section for the shear test setup. The strengthening process involved attaching channels on the sides, and more detailed information on the strengthening can be found in chapter three. String potentiometers were attached to the bottom flange of the channel. The bottom surface of the beam was not flat, so it was necessary to hold the beam in place before starting the loading. Figure 182 shows the shear vs deflection graph of the beam. The first creaking noise was heard at around 35.0 kips, and bearing failure occurred at both supports at around 43.0 kips (Figure 183-a). Creaking continued with higher loading, and a tension crack occurred at the bottom midspan at 52.5 kips, causing a slight load drop. The beam was continuously loaded and ultimately failed due to shear at one end, which caused split propagation and a shift (Figure 183-b). The ultimate shear carried by the beam was 56.3 kips at a mid-span deflection of 1.45".

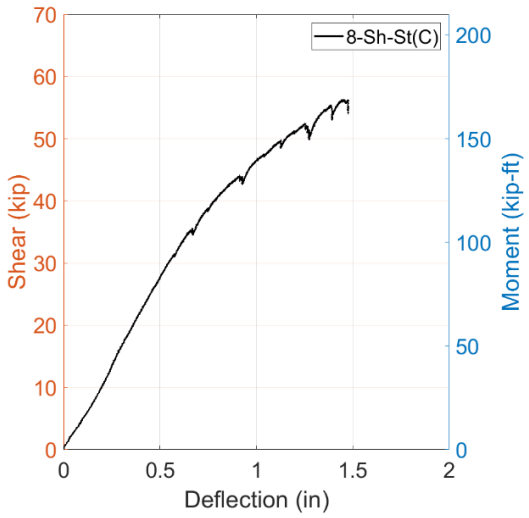

Figure 182: Load vs deflection graph of 8-Sh-St(C)

(a) Bearing failure at load block

(b) Split at the end

Figure 183: Failure propagation of 8-Sh-St(C)

8-Fl-St(C-S)

The beam was a strengthened beam with channels on the sides and a strip on the bottom. Its dimensions were 7.5" x 17" with a length of 26’ 1.5”. The moment vs deflection graph is shown in Figure 184. The first creaking noise was heard at around 128.0 kip-ft. At 144.0 kip-ft, there was a creak and a small pop from one end. As the moment increased to 172 kip-ft, crackling sounds accompanied by a small pop were heard from the end. When the moment reached 228.0 kip-ft, a loud pop was heard as a large compression crack began to form, causing a change in slope. At around 232.0 kip-ft, with a 4” mid-span deflection, the beam cracked just below the D2 string potentiometer with a loud pop (Figure 185-a), although the strip remained intact. At 252 kip-ft, with 5” of deflection, flange buckling was observed. Finally, at 255.2 kip-ft and 5.36” of deflection, a loud pop was heard as a small fragment flew off. The beam ultimately carried a moment of 255.2 kip-ft at a mid-span deflection of 5.32”.

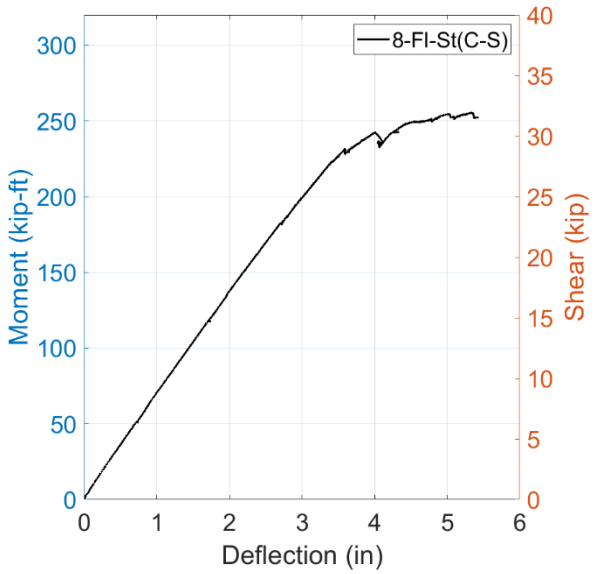

Figure 184: Moment vs deflection graph of 8-Fl-St(S-C)

(a) Crack at the bottom

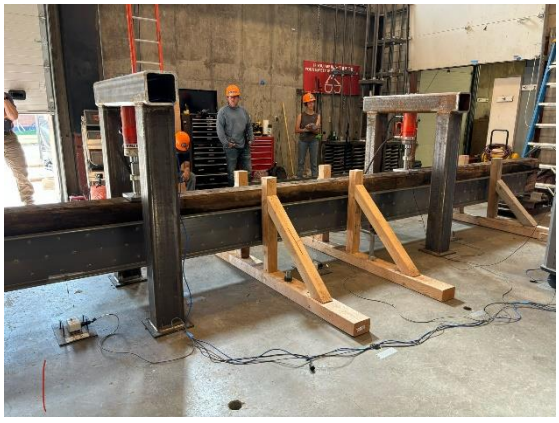

(b) Fully loaded beam

Figure 185: Failure propagation of 8-Fl-St(C-S)

8-Fl-St(S)

This was a beam reinforced with strips, with three strips attached to the sides and bottom. The beam's actual dimensions were 7.75" x 17.5" with a length of 26’ 6.75”. There was some significant checking and a large notch on one end, causing the strips to hang over. The string potentiometers were anchored above the strip on the side. The moment vs deflection is shown in Figure 186. Creaking began at around 112.0 kip-ft throughout the beam and continued with higher loading. Loud pops were heard at 168.0 kip-ft and 181.6 kip-ft with no significant drop in load. A crack (Figure 187-a) began propagating at 230.4 kip-ft on the bottom through a knot with a loud pop, causing the moment to drop to 214.4 kip-ft. The beam started touching the middle lateral bracing. Ultimately, the beam failed with a crack propagating to the midspan and compression failure under the load block (Figure 187-b) at around 200.0 kip-ft with a loud pop. The ultimate moment carried by the beam was 230.4 kip-ft when the deflection was 3.76”.

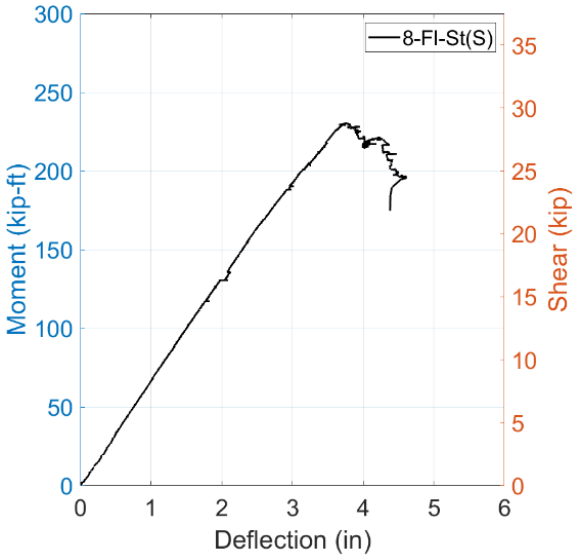

Figure 186: Moment vs deflection graph of 8-Fl-St(S)

(a) Crack starting (b) Compression at top

Figure 187: Failure propagation of 8-Fl-St(S)